©2020
Tianyi Li

ALL RIGHTS RESERVED

Predictive Performance of Loss-in-weight Feeders for Continuous Powder-Based Manufacturing

by

Tianyi Li

A dissertation submitted to the
School of Graduate Studies
Rutgers, The State University of New Jersey
In partial fulfillment of the requirements
For the degree of
Doctor of Philosophy
Graduate Program in Chemical and Biochemical Engineering

Written under the direction of
Professors Fernando J. Muzzio and Benjamin J. Glasser

Approved by:

_____

_____

_____

_____

New Brunswick, New Jersey
October 2020

ABSTRACT OF THE DISSERTATION

Predictive Performance of Loss-in-weight Feeders for Continuous Powder-Based Manufacturing

By Tianyi Li

Dissertation Directors:

Fernando J. Muzzio and Benjamin J. Glasser

Continuous manufacturing for pharmaceutical solid dosage forms has reached a significant milestone over the past decade due to efforts from academia, industry, and regulatory agencies. Advancement in the development of equipment design, process analytical technology, control systems, and modeling tools has facilitated the growing interest in implementation of continuous manufacturing methods in major pharmaceutical companies around the world. The US Food and Drug Administration has also provided regulatory support for the implementation of continuous manufacturing using science- and risk-based approaches. As the pharmaceutical industry modernizes its manufacturing practices and implements more efficient and precise approaches, a more comprehensive evaluation of the process, including unit operations, is needed.

Loss-in-weight feeders, as the first unit operations in a continuous manufacturing design, are responsible for dispensing a given weight of material per unit of time to downstream unit operations accurately and constantly. Disturbances on a given feeder may travel downstream through the process and consequently impact critical quality attributes of the final products, such as potency and content uniformity. Therefore, it is essential to understand the potential aspects that could impact the feeder's performance and how

feeders and downstream unit operations would react in response to the different levels of disturbances and perturbations.

In this work, the effect on feeder performance in a direct compaction (DC) continuous manufacturing line was studied. Studies included the performance of feeders operating in normal gravimetric mode and the effects of feeder refills. Feeder tooling and material properties were both considered to determine their effect on feeder performance. Principal component analysis, a multivariate statistical analysis method, was utilized in order to build up a material library with 30 material flow properties. Partial least squares regression is used to correlate process performance to material flow properties. Multiple near infrared spectroscopy methods were applied to monitor the content uniformity exiting blend uniformity or content uniformity in the final product.

The results obtained from these studies were used to determine the design space for a commercially available loss-in-weight K-Tron KT20 feeder and its dependency on the conditioned bulk density of the powder. Additionally, a methodology was developed to correlate feed rate deviation caused by hopper refill to material flow properties and to create a predictive model.

To understand variations in drug concentration in a continuous direct compaction line, experiments were conducted on how perturbations on the mass flow rate from the feeders transfer down the continuous line, and how much dampening the downstream unit operations can provide to the variability in the mass flow rate. Controlled step changes in concentration and hopper refill operations were performed over short intervals with different blender speeds and total throughputs and the drug concentration in the blend and

the tablets was characterized to determine residence time distribution and deviation in concentration.

The results from this work can be applied to the design of a continuous line, the development of a manufacturing plant, and the evaluation of process risks associated with the continuous manufacturing of solid dosage forms. Using the predictive methods enabled by the results discussed here, operators will be able to identify potential failure modes of the feeding operations and facilitate risk assessment for regulatory reporting.

Acknowledgements

Throughout the course of this project, I have been fortunate to have the guidance, support and encouragement from many individuals. I would like to thank my thesis advisors, Prof. Fernando Muzzio and Prof. Benjamin Glasser for their support, mentoring and dedication to reviewing my manuscripts and also improving my communication and presentation abilities. I would also like to thank my committee members, Dr. Gerardo Callegari and Dr. Sarang Oka, for their continued suggestions and feedback.

I would also like to thank the National Science Foundation's Engineering Research Center for Structured Organic Particulate Systems (ERC-SOPS) and the Rutgers Catalyst Manufacturing Consortium for the opportunities to interact with industrial partners and experts in the relevant fields. The students and faculty members working in these organizations have provided invaluable insight into my research.

Throughout my time at Rutgers, I was privileged to have met so many skilled individuals who have shared their knowledge and encouragement. My special thanks go to Yifan Wang and James Scicolone for their enthusiastic mentoring and support. I would also like to acknowledge Savitha Panikar, Sarang Oka, Wei Meng, Sebastian Escotet, Pallavi Pawar, Thamer Omer, Golshid Keyvan, Andres Roman, Sara Moghtadernejad, Yi Tao, Zhanjie Liu, Jingzhe Li, Qiushi Zhou, Alexis Venere, Pedro Martinez and all the students who have spent many hours aiding me in the lab: Kien Chau, Nikita Soni, Glinka Pereira, Lan Le, Yasaswini Potla and Catrina Jou.

I would particularly like to thank my family for being selflessly supporting me throughout this special journey: my wife, Jie Jiang and my parents, Xueping Fei and Huasheng Li. Your endless love, patience and encouragement have been invaluable.

Table of Contents

List of Tables

List of Figures

Chapter 1. Introduction

1.1. Background

Continuous manufacturing of pharmaceutical solid dosage forms has received a significant amount of interest over the past decade due to efforts from academia, industry and regulatory agencies [1-4]. Major pharmaceutical and equipment companies around the world are quickly embracing this novel manufacturing method by adding it to their technology portfolios for both legacy and new drug products [5]. Continuous manufacturing offers a number of economic and quality advantages over batch processing [6-9] including higher production capacity, smaller equipment, and the capability of implementing process analytical technology (PAT) and control systems to monitor the critical quality attributes (CAQs) and critical process parameters (CPPs) in real time [10, 11]. Advancement in the development of equipment design, process analytical technology, control systems, and modeling tools has facilitated the growing interest in implementation of continuous manufacturing methods in major pharmaceutical companies around the world.

Regulatory perspectives on pharmaceutical manufacturing have evolved significantly in the last two decades as well. A draft guidance for industry has been provided by FDA on the quality considerations for continuous manufacturing in 2019 [12], and there are several FDA-and EMA-approved products on the market which are being produced using continuous manufacturing. As the pharmaceutical industry modernizes its manufacturing practices and implements more efficient and precise approaches, a more comprehensive evaluation of the process, including unit operations, is needed [13-19].

In continuous manufacturing, loss-in-weight feeders play a vital role to introduce accurately controlled amount of powder per unit of time. Compared to volumetric feeders, loss-in-weight feeders have improved the ability to control feed rate and minimize flow variability caused by density changes associated with the emptying of the feeder hoppers. They are as the key unit operation in continuous manufacturing required to maintain the target concentration of the Active Pharmaceutical Ingredient (API) within acceptable variability. However, the intrinsic nature of powder flow and the operational conditions used to make pharmaceutical products, which use cohesive ingredients and low mas flow rates, make the delivery of a consistent flow rate of all ingredients a challenge; therefore, loss-in-weight feeders are also at a high potential risk to be the first unit operation to introduce variability into the line, which will impact the content uniformity of final products. Consequently, a comprehensive knowledge on loss-in-weight feeders and the downstream effect on feeding variabilities are essential to achieve good continuous manufacturing practice.

1.2. Motivation

Loss-in-weight feeders work on the principle of monitoring weight changes in a hopper as powder is dispensed by a connected conveying system. There are several factors that affect a feeder's performance, including material flow properties, feeder hopper design, feeding operating condition, feeder refill strategy, and feeder control algorithm. For example, cohesive materials that tend to agglomerate, or to entrap air within the powder bed, will have lower ranges in feed rate than easy flowing, well-packing material for a given equipment set up. Irregularity in bed density, due to entrapped air, can result in unstable flow rate and variability. Another issue with powders is electrostatic effects, such as

charge buildup, which can lead to material sticking to the exit of feeders or to any exposed surface. Feeder tooling selection plays a major role in feeder characterization. Concave screws are considered as self-cleaning screws, which are designed for adhesive materials that will attach to the screw surface, and auger screws are normally used for free flowing or compacting powders. Periodic hopper refill of the feeders can also lead to inconsistent and poor feeding performance[20]. These effects cause variation in feed rates that can then be transferred down to succeeding unit operations and affect the quality of the final products.

For loss-in-weight feeders, existing knowledge includes 1) a method for loss-in-weight feeder's feeding and refilling characterization [20-22], 2) the effect of powder properties on tooling selection and flow rate intermittence [23, 24], 3) the effect of feeder design and operation on discharged powder properties (which resides with the equipment manufacturer)[25, 26], 4) the evaluation of the baseline performance that could be expected from loss-in-weight feeders when operated without any significant external disturbance, 5) flow sheet models of gravimetric and volumetric feeding, 6) residence time distribution studies on a loss-in-weight feeder with a horizontal flow aid system [27-29].

The work presented in this dissertation is motivated by the fact that loss-in-weight feeder characterization has normally been performed using a trial by error approach, which requires large amounts of materials, labor, and time. Therefore, a method on how to identify the optimal tooling selection and the ideal design space of a loss-in-weight feeder for a target material, based on material flow properties, is needed. Specifically, raw material flow properties characterization and how to use it to predict feeder's feeding capacity and the ideal design space of a target material are discussed in specific Aim I.

In Specific Aim II, a multivariate analysis method is introduced and applied to the correlation between material flow properties and feeder's performance during hopper refill. As powder flow behavior is typically complex and there is no unifying index to describe powder's flowability, the multivariate analysis is established based on 30 material flow properties. Results are used to establish a material library and to identify the similarities and differences between materials with respect to their performance in a gravimetric feeder. As a result, a correlation between feeder's performance during hopper refill and material properties was established using a regression model.

Specific Aim III addresses the lack of knowledge on how a feeder's feed rate deviation would transfer in the downstream unit operations, specifically in a continuous blender and feed frame in the tablet press where feeders are integrated into continuous manufacturing platform and where the API concentration in final products would be affected by the inevitable feed rate variation. The Aim also examines the effect of the back-mixing zones existing in the continuous line. This aim involves two different formulations where high and low dosage of API are used. An inline NIR model is set up for each formulation to monitor the API concentration after the blender in real time. An offline NIR model is set up to measure the API concentration in the produced tablet samples and to compare it with the variation in feed rates.

1.3. Scope of this dissertation

Given the preceding discussion, this dissertation focuses on three specific aims, which are summarized as follows:

- Specific Aim I: Developing an ideal design space for loss-in-weight feeders

- Specific Aim II: Predicting feed rate deviation caused by hopper refill as a function of powder material flow properties
- Specific Aim III: Dampening effect on feed rate variation by downstream units in pharmaceutical continuous manufacturing as a function of line back-mixing capacity.

This dissertation is divided into 5 chapters. The effort started with the discussion on material flow properties and feeder characterization (Chapter 2) and then moved forward to a method for developing an ideal design space for loss-in-weight feeders based on material properties and feeder performance (Chapter 3). The developed predictive model could help save a great amount of time and labor from preliminary loss-in-weight feeder characterization and tooling selection. Then, the effort moved on to using statistical analysis to correlate the feed rate deviation during hopper refill to the material flow properties, which could be applied to the design of the refill strategy for different levels of specifications feeding variation during hopper refill (Chapter 4). Chapter 5 focuses on the impact on variation in feed rate in a continuous manufacturing design of direct compaction. Different levels and durations of designated disturbances on feed rates and hopper refilling operations of API and major excipient are performed on feeders during continuous production. Impact from different blender speed and total throughputs of production are also discussed in this chapter. Content uniformity of the blend is monitored inline (after the blender) and offline (after the press) by scanning collected tablets. The dampening effect by back-mixing in downstream unit operations on feeding variation is characterized.

The work presented in this dissertation can be applied to the design, development and evaluation of continuous manufacturing of solid dosage forms and can also be used to

identify potential failure modes of the feeding process and facilitate risk assessment for regulatory purposes.

Chapter 2. Overview of Powder Flow Properties, Powder Feeding Characterization and Multivariate Analysis

2.1. Introduction

Powders and granular materials are encountered frequently during processing in many powder-based industries[30, 31]. They exhibit a variety of flow patterns, and behavior differs with application[32, 33]. Due to the lack of fundamental understanding of powder behavior, multiple problems are encountered during manufacturing, such as jamming of hoppers, sub-standard blending performance, and weight variability of final products due to segregation and/or agglomeration[34-39]. Scale-up of processes is also a challenge since there is a lack of constitutive equations for granular materials, limiting the development of scaling theories (e.g., the use of dimensionless numbers to describe powder processes)[40, 41].

Powder characterization can be used as a distinguishing method for choosing the best-fit material, as well as a predictive tool to analyze process performance[42-44]. As a result, powder characterization has a central role in both product and process development. There are numerous methods to characterize the flow properties of granular materials: avalanching testers, fluidizers, shear cells, “indicizers”, density methods, angle of repose testers, etc[45-52]. However, most of these methods were designed for a specific application; therefore, it is not clear how various methods correlate with each other or with process performance[53, 54]. In the pharmaceutical industry, the processing of powder and granular materials, like many other processes, is done through a series of unit operations. Some examples are feeding, mixing, granulation, drying and compaction. Since the application of the methods outside of their intended use frequently results in process

failures, relating powder characterization measurements to fundamental material properties is critical.

In the pharmaceutical industry, during the early stages of development, only a relatively small amount of the Active Pharmaceutical Ingredient is typically available, so companies would like to measure powder material properties and their effects on process performance using laboratory scale tests, to predict behavior in production-scale processing and develop the manufacturing plan based on the prediction results[34, 35, 55].

There are several characterization techniques available with each one measuring powder flow behavior from a slightly different aspect. These tests also test powder under different states: from fully aerated to varying degrees of consolidation, from confined to unconfined, from incipient flow to steady state flow. The tests can be classified as the measurement of one of more of the following properties: compressibility, permeability, bulk density, cohesion, etc. In addition, other testing methods focus on hydrophobicity, electrostatics, friability, which are related to flow properties and which incorporate also the effects of particle size and particle shape[56-60]. These properties are not independent from each other; they are typically partially correlated. For example, as the particle size increases, there is an accompanying decrease in cohesion due to the Van der Waals forces[61]. The mechanism of particle shape affecting the flowability of a material is through the mechanical interlocking between particles. Several studies have been conducted to investigate the correlation between raw material properties as well as how material flow properties affect process performance. Studies include how to improve the powder flowability [62-66] and the impact of powder properties on process performance [23, 56, 67-75].

Loss-in-weight feeders have been designed to achieve accurate and consistent delivery of materials to ensure overall process stability. They control material dispensing by weight at a precise rate and minimize the mass flow rate variability caused by the change of hopper level and material bulk density[76]. Research has found that material flow properties have major impact on loss-in-weight feeders' performance [23, 26, 77-79]. Moreover, periodic hopper refill of the feeders, which is needed for continuous operation, can lead to inconsistent and poor feeding performance[20, 80]. Difference in performance are easily detected among materials with different flow properties.

This chapter describes the methods that are used in this dissertation to characterize (i) material flow properties, (ii) feeder performance under gravimetric feeding and (iii) feeder performance during hopper refill. In addition, a multivariate analysis method which can identify the relationship between raw material properties and process performance is introduced.

2.2. Powder flow property characterization

As mentioned above, there is no unifying framework to describe powder flow behavior; therefore, materials were characterized by multiple flow property measurements so that each reflects a different aspect of flow behavior. Multiple material characterizations were used to test powder's flow behavior in terms of different material properties from different aspects.

2.2.1. Compressibility

The compressibility test is part of the Freeman Technology Powder Rheometer suite (Freeman Technology Inc., Worcestershire, UK). It is a measure of how density changes as a function of applied normal stress[81]. The powder is first conditioned by a helical

blade moving downwards and moving upwards three times with a tip speed of 60 mm/s in order to create a uniform and reproducible packing state without changing particle properties[82]. A normal force is then slowly applied to the powder using a vented piston, ranging from 0.5 kPa to 15 kPa and is applied over 10 intervals, holding each load for 60 seconds. The change in volume due to compression is measured and the compressibility is calculated as the percent change in volume after compression.

$$\mathrm{CPS\%} = 100 * \frac{V_c - V_p}{V_c} \qquad \text{Equation 2-1}$$

where V_c is bulk volume after the conditioning step and V_p is powder volume after compression. The schematic of the test is shown in Figure 2-1.

2.2.2. Permeability

The permeability test, which is also achieved by the FT4 Powder Rheometer, is a measure of how easily a material can transmit a fluid (in this case - air) through its bulk[83]. For powders, it is influenced by many physical properties such as particle size distribution, cohesion, particle shape, surface texture, and bulk density. After a similar conditioning step as described in the compressibility test, an upward air with a velocity of 2 mm/s is introduced from the bottom of the powder bed. At the same time, a normal stress is applied by the vented piston over a range of 0.5 to 15 kPa. The pressure drop of the air is measured and recorded under each normal stress. The schematic of the test is shown in Figure **2-2.**

2.2.3. Dynamic flow test

The dynamic flow test measures the flow energy E of the powder bulk, which is defined as the energy required to move a helical blade through a bulk of powder. The FT4 dynamic

flow test measures this energy as a function of time and shear rate[84]. A similar conditioning process as in the previous two tests is first performed on the bulk of powder in the vessel. Then, the blade moves downward and upward, to test the energy consumed to induce the powder to flow, followed by a testing cycle which is repeated seven times with measured flow energy E_1 – E_7. The flow energy required on the seventh downward blade passing is recorded as the basic flow energy (BFE). The energy consumed during the seventh upward passing is recorded as specific energy (SE). The stability index (SI) reflects the change in flow energy over time:

$$SI = \frac{E_7}{E_1} \qquad \text{Equation 2-2}$$

where E_1 is the flow energy required on the first downward blade pass, and E_7 is the energy required on the seventh downward blade pass. An SI value of 1 indicates that the material is stable and non-friable. If SI is larger than 1, it indicates that the material being tested requires more energy to flow over time, possibly due to de-aeration, agglomeration, moisture uptake, or electrostatic charges. If SI is smaller than 1, it indicates that the material may have de-agglomerated during the tests.

Four additional repetitions are performed using different shear rates, with a tip speed ranging from 10 to 100 mm/s. The flow rate index (FRI) represents the ratio between the required flow energy at 100 mm/s and 10 mm/s.

$$FRI = \frac{E_{11}}{E_8} \qquad \text{Equation 2-3}$$

where E_{11} is the basic flow energy at a blade tip speed of 100 mm/s, and E_8 is the basic flow energy at 10 mm/s. If a material is sensitive to changes in shear rate, such as a cohesive

material with high porosity, the FRI value are typically higher than a compacting or good flowing material[85].

2.2.4. Shear cell test

The shear cell test is also performed with FT4 Powder Rheometer. The original shear cell test measures how easily a consolidated powder previously at rest will begin to flow[86-90]. Modern systems such as the FT4 Freemen flow rheometer measure the force required to maintain flow once it reaches steady state. This characterization technique has become prevalent and international standards detailing the procedure have been defined [86]. Some studies have been conducted to compare the measurements of a particular shear cell parameter between different types of shear testers as well as the correlation between the resulting properties within one tester [91, 92].

The standard shear cell test involves three steps: pre-conditioning of the powder bed, pre-shearing of the powder at a given consolidation stress bed until steady state flow is achieved, and subsequent shearing (typically at a lower normal load) until the powder yields. The pre-shearing process is repeated 4-5 times using normal stresses at 20 – 80% of the consolidation stress, which results in a series of measurements of corresponding normal and shear stresses, the so called the ‘yield locus’. The yield locus is fit with a straight line that is extrapolated to y-axis, which is defined as the cohesion of the powder.

In addition, Mohr circle analysis is performed on the yield locus, which is a geometric representation of a coordinate transformation to identify the principal stresses. Two circles are used, where the first one goes through the origin and is tangent to the best-fit line through the yield locus, which represents the conditions presented at the free surface of an

arch. The second circle is tangent to the yield locus and passes through the pre-shear point, which represents the conditions for the critical state. The principal stresses extracted from these analyses is called the unconfined yield stress and the major principal stress. The yield locus is measured at several consolidation stresses, and the unconfined yield stress and compacting stress are extracted from each yield locus. The unconfined yield stress – major principal stress pairs are plotted from each yield locus to give the 'flow function'. The flow function coefficient (ff_c), which is often correlated to the arching phenomenon in hoppers, is defined as the ratio between the major principal stress (σ_1) and the unconfined yield strength (σ_c):

$$\text{ffc} = {}^{\sigma_1}/_{\sigma_c} \qquad \text{Equation 2-3}$$

The slope of the flow function indicates how well a powder flows; the steeper the slope, the worse the powder flows. A schematic of shear cell test is shown in Figure 2-3.

2.3. Feeder characterization

Loss-in-weight feeders are one of the most commonly observed unit operations in continuous powder-based manufacturing process. Compared to volumetric feeders, loss-in-weight feeders can control the angular speed of screws by monitoring the rate of weight loss from the system, which enables loss-in-weight feeder to perform good flow rate accuracy by maintain a tight control over the screw speed. However, besides the feeder control system, a loss-in-weigh feeder's performance is highly dependent on material flow properties[23, 77, 93-95]. A poorly flowing powder can create jamming in the hopper can does not flow out of the feeder and adhesive powders can attach to the pitches of the feeding

screws which causes changes in screw feeding volume thus create inconsistency of mass flow rate[96-98].

In Chapter 3 and Chapter 4 of this dissertation, a commercially available twin screw loss-in-weight feeder, the feeding performance of the K-Tron KT20's (Coperion K-Tron Pitman, INC. Sewell, NJ, USA) will be discussed. A KT20 loss-in-weight feeder consists of a volumetric feeder, a weighing platform, and a gravimetric controller. The weighing platform measures the material's mass in the feeder hopper, and the controller adjusts the screw speed based on the calculation of weight loss over time to ensure that the feeder is feeding at the target feed rate. The offline setup of the KT20 feeder is shown in **Figure 2-4.** The feeder is placed on a plane lab bench. A gain-in-weight catch scale (OHAUS adventurer, OHAUS Corporation, Parsippany, NJ, USA) is used to record the weight of powder dispensed by the feeder every 1 second. A bucket is placed on the scale to collect the sample. The feeder is connected to an external laptop, which allows the experimental operator to record several process parameters during feeding, such as feed factor, net weight, mass flow, setpoint, screw speed, perturbation value, drive command, etc.

To characterize a loss-in-weight feeder performance, volumetric studies need to be performed first to determine feeder capability, followed by gravimetric studies to evaluate overall performance. The feeder is first tared with all the feeder parts assembled, and then the feeder is first filled up to 80% (weight percent) of the hopper capacity with the material to be tested. A feed rate calibration is then performed to obtain the initial feed factor, which is also considered as the feeder's maximum feed rate with the tested powder and tooling used. Subsequently, a target setpoint is input and then the feeder starts to run.

Loss-in-weight feeders need to be refilled in order to maintain an efficient feeding performance. Since the hopper size of the loss-in-weight feeders are often constrained by the weight capacity of the load cell, a refill system was set up independently to the load cell and will dispense a given mass of material to the feeder hopper. Based on the experimental design, a hopper refill operation is needed when the hopper level reaches a designated refill minimum level, which can be set in the control system. During hopper refill, the feeder runs in volumetric mode with a constant screw speed. After refill is completed, and a brief delay, which can be set normally at 5 or 10 second, the feeder will switch back to gravimetric mode. The feeder's gravimetric feeding performance analysis is based on the recorded mass from the catch scale. The analysis of the feeder's performance during hopper refill is based on the contribution from both the catch scale and the process parameters recorded by the feeder's control box. William et al has compared the difference in feeder performance caused by hopper due to different refill levels [20]. However, there is a lack of study on how material properties would impact hopper refill performance. In Chapter 4 of this dissertation, a predictive model will be introduced to correlated feeder refill performance to material flow properties based on a KT20 loss-in-weight feeder.

2.4. Multivariate analysis

Multivariate data analysis is a set of statistical models that examine patterns in multidimensional data by considering, at once, multiple data variables. It is an expansion of bivariate data analysis, which considers only two variables in its models. Typically, multivariate analysis is used to address the situations where multiple measurements are made on each experimental unit and the relations among these measurements and their

structures are important [99, 100]. The aim of using multivariate analysis in the work of this dissertation is to find the hidden structure and correlation between variables, in this case, feeder performance and material flow properties.

2.4.1 Principal component analysis (PCA)

Principle component analysis is a clustering technique which transforms several possibly correlated variables into a smaller number of orthogonal (i.e., linearly independent) variables that are defined as principal components. It uses vector space transformation to reduce the dimensions of a large data set. Principle component analysis followed by similarity scoring (PCA-SS) is a method to calculate the similarity between different objects, in this case, materials. In the PCA-SS approach, a PCA model was used to represent the material property data set (X) in a reduced dimension (principal component space) such that the major axes of variability are identified. The data set X can be decomposed, based on the equation below, into a set of scores (T) and loadings (P), while the remaining variability is modeled as random error (ε):

$$X = TP^T + \varepsilon \qquad \text{Equation 2-4}$$

The columns T represent principal component (PC) scores of each material in the projected space. Loading P represent the significance of each material property in each principal component. Both T and P are obtained from eigenvectors and eigenvalues of the covariance matrix of X. The number of components should be chosen based on the type of analysis required for each case study. In some cases, the small number of principal components are able to capture most of the variability while in other cases, more than 10 principal components have to be used to fully explain the data set.

A Bartlett's test of sphericity needs to be done prior to PCA for factor analysis, to verify that a data reduction technique can actually compress the data in a meaningful way. It is used to test the hypothesis that the correlation matrix is an identity matrix, which would indicate that the variables are unrelated and therefore unsuitable for structure detection, which is to make sure that the correlation matrix of the variables in the dataset diverges significantly from the identity matrix, so a reduction technique is suitable to use. A small values P-value of significance level (less than 0.05) indicates the statistical significance of each principal component [101-104].

2.4.2 Partial least squares regression

Partial least squares regression is also known as projection to latent structure regression, which is used to reduce the predictors to a smaller set of uncorrelated components and performs least squares regression on these components instead of on the original data. It correlates a number of independent variables X with response variables Y by finding the latent variables in the data set. The calculation of latent variables in the PLSR method takes the response variables into account so that the linear combinations have maximum covariance. PLSR is especially useful when predictors are highly collinear or there are more predictors than observations and ordinary least-squares regression either produces coefficients with high standard errors or fails completely.

In the Chapter 4 of this dissertation, the collected material properties data was firstly preprocessed using Z-score normalization. The z scores were calculated as follows:

$$z = \frac{x-\mu}{\sigma} \qquad \text{Equation 2-5}$$

where μ is the average of each property and σ is the standard deviation from the average. The data after z-score normalization are centered around 0 with a standard deviation of 1, which is a common requirement for most machine learning estimators, especially for clustering analysis, such as PCA, when comparing similarities between samples is needed based on certain distance measures.

Then, principal component analysis was first used to project materials into reduced dimensions. Predictive capability was implemented by calculating similarity scores to find materials with similar flow behavior. Alternatively, Partial Least Squares Regression (PLSR) was used to predict feeder performance directly during hopper refill, as quantified by maximum deviation, deviation time, and total deviation% based on material property inputs. The method was demonstrated by using a commercially available feeder, K-Tron KT20 loss-in-weight feeder, with a type C gear box for seven powder materials that have been characterized by four flow testing techniques, represented by 30 flow indices and one process variable.

2.5. Figures for Chapter 2

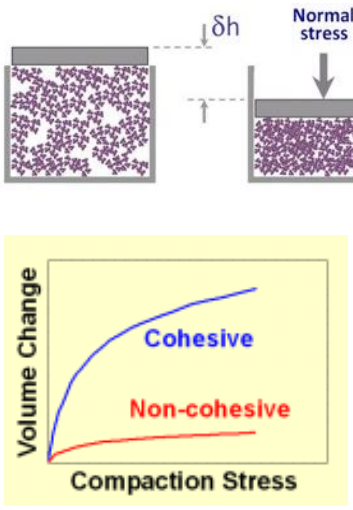

Figure 2. 1: Schematic of compressibility test (up) and comparison of compressibility between cohesive and non-cohesive powders (down). Image source from Freeman Technology [84].

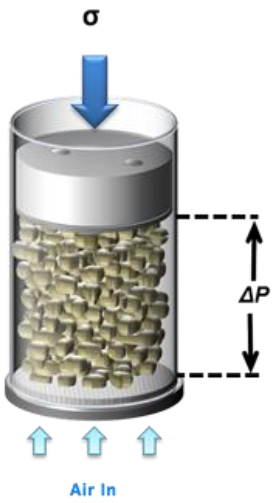

Figure 2. 2: Schematic of permeability test by Freeman Technology FT4 Powder Rheometer. Image source from Freeman Technology [84].

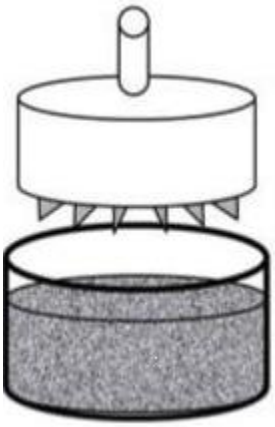

Figure 2.3: Schematic of shear cell test by Freeman Technology FT4 Powder Rheometer.

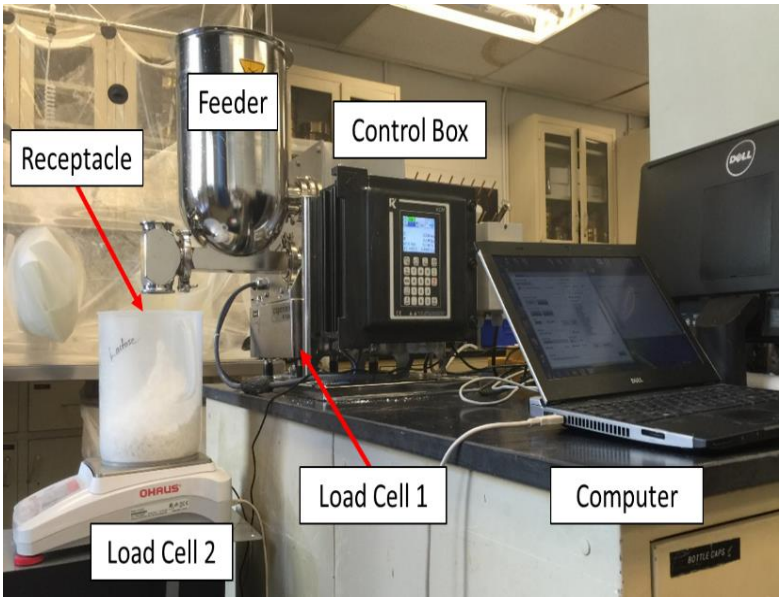

Figure 2.4: Experimental setup of twin screw loss-in-weight feeder Coperion KT20.

Chapter 3. Identifying a Loss-in-Weight Feeder Design Space Based on Performance and Material Properties

Acknowledgement of publication status:
Full sections of this chapter were published in a scientific article written by the author of this thesis under the title: Identifying a loss-in-weight feeder design space based on performance and material properties. The article was published on June 3rd, 2019 in the Journal of Pharmaceutical Innovation. This work was done in collaboration with:

James V. Scicolone[1], Eric Sanchez[2] and Fernando J. Muzzio[1]
[1] Department of Chemical and Biochemical Engineering, Rutgers, The State University of New Jersey, Piscataway, NJ, 08854, USA
[2] Advanced Technologies Center of Excellence, Janssen Supply Chain, Gurabo, PR, USA

3.1. Introduction

Loss-in-weight (LIW) feeders are vital components in powder-based manufacturing in general, and continuous pharmaceutical solid dose manufacturing in particular. Gravimetric feeders are used to accurately meter a given weight of material per unit of time. The range in operation of loss-in-weight feeders depends on the feeder size, feeder tooling, and the properties of the material. Per a given set-up, cohesive materials, which tend to agglomerate or entrap air within the powder bed, will have narrower feed rate ranges than well flowing material. Irregularity in bed density can result in unstable flow rate[24, 105]. Another issue with powder flow is electrostatic effects, which can lead to material sticking to the exit of the feeders or to any exposed surface in the line. The variability introduced by these types of erratic flow behaviors can be transferred down to successive unit operations downstream of the feeders[106, 107], where inaccurate dosing of pharmaceutical constituents can lead to sub-potent or super-potent product.

Pharmaceutical manufacturing has long been performed in batch production mode [4, 108-110]. While many other manufacturing industries have shifted from batch to continuous processing decades ago, the pharmaceutical industry lagged behind, staying within the confines of familiar and approved methods. The FDA has indicated that modernizing and improving pharmaceutical manufacturing technology would be desirable, launching a regulatory modernization initiative meant to encourage companies to adopt newer methods, such as continuous manufacturing[111]. Guidance documents have also been published to promote the modernization of pharmaceutical manufacturing. A framework for process analytical technologies (PAT)[112] was published in 2004 to monitor in-line powder content uniformity and to determine if the final product within specified potency. Next, guidance dpcuments were issued on the use of quality by design (QbD) approaches for product and process design[113, 114]. Companies such as Vertex and Janssen have led the charge and gained approval from the FDA for manufacturing drugs continuously[9, 115, 116]. The Product Quality Lifecycle Implementation, which has been in creation by the International Society of Pharmaceutical Engineering, launched a CM initiative that set out best practices and expectations when developing and manufacturing products via CM. The cumulative result of these efforts places an increasing emphasis on accuracy of dispensing materials in manufacturing[117].

Loss-in-weight feeders work on the principle of monitoring weight changes in a hopper equipped with a powder conveying system. The hopper designs come in various shapes and sizes and can be extended to increase capacity within the limit of the weighing platform. For typical screw-conveying systems, motors are used to control an agitation, or distribution, unit (also called “bridge breaking” device) along with the feeding screws. The

screws come in various shapes and sizes, normally selected for a given situation based on previous knowledge in mind or via a trial and error approach. The motor speed, adjusted by a feedback control loop, is used to control the mass feed rate and to minimize flow rate variability[105, 118-120]. By monitoring the mass change, an instantaneous feed rate can be calculated and compared with the setpoint. If the feed rate differs from the setpoint, the controller adjusts the speed of the motor in order to match the mass flow with the setpoint.

Recent work has shown ways of optimizing feeders by understanding how uniformly material flows out of a feeder, dependent on a feeder size and screw type[21, 121]. This technique requires a full hopper of material to be dispensed. As the density of the material can change based on the degree of compression of powder in the hopper, as the powder level drops, so too can the bulk density. Engisch et al. [21] proposed a method for evaluating the steady state performance of loss-in-weight powder feeding equipment and demonstrated the use of the method in evaluating the performance of a K-Tron KT-35. The authors compared the performance of various tooling to optimize feeder performance through analysis of variance (ANOVA). In other studies, methods for measuring the feeding performance during hopper refill have been proposed[20]. Kehlenbeck et al. [120] showed improved feeder dosing consistency by using a single proportioning device at the discharge. Tardos et al. used a vibratory agitator on the hopper to improve overall flow and feeding precision[121]. However, once the ideal screw and feeder type have been determined, significant feeder experiments would still need to be carried out.

A method to select a suitable screw *a priori* would save companies significant amounts of material, effort, and developmental time. Wang et al. [83] proposed the methodology to correlate feeder performance with the material bulk and flow properties by using principal

component analysis (PCA) coupled with a statistical model to quantitatively predict a feeder's feeding consistency and accuracy. To fully understand how the feeder and material behave, an ideal range of operation needed to be selected, which would help in determining the design space of the feeder.

In this work, the mass flow rate of multiple pharmaceutical powders using various screws was characterized in a K-Tron KT-20 C-gearbox pharma loss-in-weight feeder. Four screws were used in this analysis: coarse auger, fine auger, coarse concave, and fine concave, and six feed rates were studied for 14 materials, which result with 336 experiments. The results show an effective range in motor operation, to be between 20 and 90% of the drive command, which is represented by the motor speed in a percentage scale from zero to 100%. Another substantial discovery from this study was that a correlation exists between material packing (conditioned bulk density) and the feed factor. The feed factor is the maximum mass flow rate of a given material, feeder, and screw type combination, i.e. when the screws are spinning at maximum screw speed (i.e., at 100% drive command). By obtaining the conditioned bulk density for a given material, the maximum flow of a material can be calculated for each screw type, and with an effective range in drive command identified to be between 20 and 90%, the effective range on mass flow rates can be quickly calculated. This correlation can be used to select a feeder and a screw type based only on material characterization without needing to run the feeder, except for case validation.

3.2. Materials and Methods

3.2.1. Materials

To obtain a broad understanding of feeder behavior, the material chosen for this work had a wide range in particle sizes and densities. Multiple PH grades of Avicel (FMC Corporation) were used, including 101, 102, 105, 301, and 200. Additional excipients include Foremost(R) lactose 310 monohydrate (Kerry Inc.), croscarmellose sodium (FMC Corporation), magnesium stearate (FMC Corporation), Prosolv HD 90, HD200, and 50 (JRS Pharma), Ceolus KG-802 (Asahi Kasei Corporation). Two APIs are used in this study; first was a powder grade acetaminophen/paracetamol (Powder Grade APAP, Mallinckrodt Pharmaceuticals) and the second was a granulated API (Janssen Ortho LLC-Gurabo). Additionally, non-pharmaceutical materials typically used in ceramic applications, coarse grade alumina (Albermarle, Netherlands), and molybdenum oxide (Albermarle, Netherlands), were chosen to add to the study because both had significantly higher densities than common pharmaceutical powders. Particle sizes for all components were obtained by a Beckman-Coulter LS 13-320 laser diffraction particle size analyzer with a tornado dry powder attachment, Table 3-1.

3.2.2. Material Characterization

All materials were characterized in terms of particle size, packing, and flow properties. The Freeman FT4 powder rheometer (Freeman Technology Ltd., Worcestershire, UK) was used in this work to obtain powder properties under static and flowing regimes[81-83]. Conditioned bulk density (cBD) is a good indicator of packing behavior and is easily obtained and was therefore used for all the powders considered here.

The FT4 compressibility test was used to measure the change of powder bulk density versus increasing normal consolidation stress. To perform the test, the powders were added to a standard Freeman Technology vessel with a 25mm diameter cylindrical vessel that has a testing volume of 10 mL. A helical blade was used to condition the powder by removing any effect that may have developed by pouring the material into the vessel. The blade moved downward at a constant rate with a constant tip speed to remove any voids or lumps. The vessel was then split, and the remaining mass of material, occupying 10 mL volume, was recorded. After the device calculates the bulk density, a porous piston was used to compress the powder bed to a pre-set normal force. The device measures the bed height at each normal force and calculates the changes in density[122]. The test measured the change in volume of the powder as the normal stress was applied to a known powder bed, of recorded mass and a fixed 10mL volume. The percent change in volume and the resultant density was recorded up to 15kPa normal stress.

The second test performed on the material was to use a cylindrical shear cell, which also used the 25 mm, 10mL vessel, to characterize powder flow when the powder was in a confined, static state. After the material was loaded into the vessel, a helical blade and a piston was used to condition and then compress the powder to a predetermined normal stress, with which the user can choose one of the four the pre-shear stress to be 3, 6, 9, or 15 kPa. Each stress point represents a completely different test; therefore, the user can distinguish how the properties change with increasing normal stresses. After the material was compressed to the specified normal stress, the vessel was split, with the remaining material occupying a 10mL volume. The shear cell then compresses the powder bed to the specified normal stress and rotates at a constant rate, inducing a shear stress until a shear

plane was established. Once the bed shears, the shear stress required to maintain motion at constant speed was recorded (yield point). Five yield points are obtained at five decreasing levels of normal stress, for each pre-shear test. The yield locus plot is then obtained by plotting the yield points versus the normal stresses from which they were obtained. With this graph, a number of parameters were determined including unconfined yield strength (UYS), major principal stress (MPS), minor consolidation stress (MCS), cohesion (τ_c), angle of internal friction (AIF), and flow function coefficients (FFc and Re*l*(p))[86, 92, 123-128]. A representative yield loci plot and the resultant data obtained from the plot appear in Figure 3-1. The flow function coefficients are calculated based on Equations 1 and 2. FFc, a ratio of the major principal stress to unconfined yield strength, has commonly been used to rate powder flow from a confined static state to a confined moving state. The Jenike flow function, Re*l*(p), has been defined as the difference between MPS and MCS divided by the UYS[126].

$$FFc = {}^{MPS}/_{UYS} \qquad \text{Equation 3-1.}$$

$$Rel(p) = \frac{(MPS-MCS)}{UYS} \qquad \text{Equation 3-2.}$$

Materials that have a high cohesion tend to have lower values for the flow functions (FFc and Re*l*(p)). These values can be obtained at each of the four chosen pre-shear values. For this research, shear cell tests were performed at pre-shear tests of 3 and 6 kPa.

Tapped density measurement was also performed on the materials using a Quantachrome Dual Autotapper. The tapped density was followed according to the US Pharmacopeia <616> standardized procedure. A 250mL graduated cylinder was filled approximately to 75% of capacity, the weight of the powder recorded, and the initial density was calculated

as the aerated bulk density. The powder was repeatedly tapped until a change in volume of less than 2mL was observed, normally between 1250 and 1500 taps. The final density was recorded as the tapped density. The ratio between the tapped density and the initial (aerated) density was referred to as the Hausner Ratio.

3.2.3. K-Tron KT-20 Pharma Loss-in-Weight Feeder Characterization

3.2.3.1. Experimental Setup

A K-Tron KT20 twin screw loss-in-weight feeder with a type C gearbox (with a gear reduction ratio of 12.9:1) was tested in this study. The K-Tron KT20 loss-in-weight feeder's design consists of three parts: volumetric feeder, weighing platform (load cell), and gravimetric controller (Figure 3-2). The volumetric feeder was mounted on top of the weighing platform with a 10-liter hopper containing a horizontal agitator which helps break powder bridges and arches in order to allow the powder to flow to the flight of the feeder screws. The agitation speed was set to 17% of the screw speed; therefore, the speed of the agitator changes with the changes in screw speed. The KT20 with a type C gearbox used in this study has a maximum processing screw speed of 154 RPM and a maximum motor speed of 2000 RPM. (170 RPM @ 110% was also achievable by over-speeding). Four commonly used 20 mm diameter screws, shown in, Figure 3-3, were tested in this study: coarse auger screws (CAS), fine auger screws (FAS), coarse concave screws (CCS), fine concave screws (FCS). The feeder delivers powder materials in gravimetric mode, by using a gravimetric controller that acquires signals from the weighing platform as a function of time and screw speed. By calculating the weight loss reported by the weighing platform, the controller can determine the instantaneous feed rate, compare the calculated results to

the target setpoint, and then adjust the speed of the screw that dispenses the powder from the feeder to make the mass flow achieve the target setpoint.

The feeder control box was connected to a laptop, which was used to record multiple feeding performance parameters. Values recorded include time, setpoint, mass flow (the instantaneous feed rate calculated by the feeder's controlling system), initial feed factor (kg/h), average feed factor (kg/h), screw speed, drive command (the percentage of instantaneous screw speed compared to the maximum screw speed), net weight, and perturbation value. In addition to recording the feeder parameters from the loss-in-weight control box of the KT20 feeder, a gain-in-weight catch scale was also used to monitor the discharge performance. A collection bucket was placed on an Ohaus laboratory scale, underneath the outlet of the feeder, to collect the material as it was discharged. The mass was recorded every 1 second by the catch scale and recorded by the same laptop that was recording the feeder parameters.

3.2.3.2. Methods and analysis

The general procedure for the feeder characterization experiments was as follows:

1. Calibrate the feeder's scale platform and the catch scale by using standard weights.
2. Fill the feeder (100% hopper level).
3. Perform the feeder and material calibration 3 times and get the average of the initial feed factor, which was considered as the maximum feed rate with the combination of certain material and type of screws.
4. Calculate 10%, 30%, 50%, 70%, 90%, and 110% of the initial feed factor and make these results the target set points.

5. Run the feeder under Gravimetric mode for 20 minutes at all the target set points separately with the same initial fill level of 80 % of the hopper by refilling after each setpoint.

The maximum controllable feed rate was achieved by initial feeder calibration rather than running volumetric capacity tests. This approach returns the value of the initial feed factor with a unit of kilogram per hour, which was the estimated feed rate at 100% of the screw speed. From the initial feed factor, the desired feed rates to target 10%, 30%, 50%, 70%, 90%, and 110% of the drive command. As the purpose of this work was to figure out the feeding range of materials with different flow properties under the gravimetric mode (most commonly used across the industry for research and development of powder-based manufacturing methods), it should be noted that the actual recorded drive command would not be a one-one-one match with the experimental design. Specifically, while the designed experiments are to be performed at drive command values of 10%, 30%, 50%, 70%, 90%, and 110%, the feed factor changes slightly for different flow rates. At high screw speeds, screw filling may be less than 100%, resulting in a lower calculated feed factor, and therefore a higher drive command. Taking this into consideration, the real time screw speed would not stay constant, causing fluctuations of the average feed factor, which was the maximum feed rate being calculated every 0.1 second during the running process. In this case, the average of the real drive command would be used as the tested range instead of the designed ones.

For each material with each type of screws, each setpoint was run from an initial fill level of 80%, the ending hopper level differs with different setpoint from approximately 40% to 70%. Each experiment was run for 20 min to obtain enough data points for data analysis.

Defining the target mass feed rate as ṁ, the actual mass feed rate, $\dot{m}_i$, at the ith time point can be calculated by:

$$\dot{m}_i = \frac{\Delta m_i}{\Delta t} \quad \text{Equation 3-3.}$$

Since the set point for each material may not be the same, the relative standard deviation (RSD) and relative deviation between the set point and the mean (RDM) were used as criteria for feeder performance:

$$\sigma = \sqrt{\frac{\sum_{i=1}^{n}(\dot{m}_i - \bar{\dot{m}})^2}{n-1}} \quad \text{Equation 3-4.}$$

$$\text{RSD} = \frac{\sigma}{\bar{\dot{m}}} \quad \text{Equation 3-5.}$$

$$\text{RDM} = \frac{|\dot{m} - \bar{\dot{m}}|}{\bar{\dot{m}}} \quad \text{Equation 3-6.}$$

3.3. Results and Discussion

The initial point of this study was to characterize the properties of the various materials to understand the effects of bulk density and flow properties on performance. Next, the various materials were fed from the feeder at multiple flow rates to understand the operational ranges for each material. Finally, a correlation between material properties, and screw type, on the operational flow rate range was determined.

3.3.1. Material Properties

The first test run on the material was the FT4 compressibility test, detailed in Section 2.2. As the piston compressed the material, changes in density were recorded. Additionally, the tapped density test was performed on the material. The conditioned bulk density, compressed density at 15kPa normal stress, compressibility at 15kPa normal stress, aerated

bulk density, tapped density, and Hausner Ratio obtained for the different materials are shown in Table 3-2. From this data, molybdenum powder had the highest density and magnesium stearate (MgSt) had the lowest density. The densities of the granular materials change very little with the increasing normal stress, while the fine powders (powder acetaminophen, Avicel 105, MgSt) show a significant change in density. In most cases, the tapped density test resulted in an improved packing and higher densities than the density obtained at a normal stress of 15kPa. The only cases where this was not true were for MgSt and Avicel 105. These powders had the smallest particle sizes of all the materials tested; therefore, the resultant weight of the individual particles is much lower and do not apply enough force to change the structure of the bed as efficiently as the piston from the FT4 compressibility test.

The results for the shear cell results appear in Tables 3-3 (3 kPa) and Table 3-4 (6 kPa). The results show that, as expected, the materials that have the highest values of cohesion, Avicel 105 and powder APAP, also had the lowest values for flow functions. Avicel 200 and Prosolv HD90 had the lowest values for cohesion. MgSt had the most significant change in flow properties between the two tests. From the 3 kPa results, MgSt would be considered a cohesive material that does not flow well; however, the results at 6 kPa shows that MgSt was a freely flowing material. This significant change in flow was due to the material, as the same flow changes did not occur for other cohesive materials, i.e. Avicel 105 or Ceolus KG-802. MgSt has been known to be a soft material that deforms easily due to shear stresses. In general the higher the normal stress, the higher the shear stress required to maintain a given powder flow. For consolidation stresses up to 3 kPa, the shear stress was not sufficient to deform the material; however, the higher shear stresses observed

for the consolidation stress of 6 kPa were likely high enough to affect the particle structure. Shear cell results were performed at a preconditioning normal stresses of 3kPa and 6kPa.

3.3.2. Characterizing the Operational Range of a Loss-in-Weight Feeder

3.3.2.1. Determination of volumetric capacity

The first step, when characterizing a feeder, was to determine the feed factor, defined as the flow rate at 100% drive command. The feeder control has a program that will run the feeder for 30 seconds at 50% drive command, and then calculates the feed factor based on the mass change for the 30 seconds. This process was conducted 3 times for each screw and material combination. The initial feed factor was defined as the average of the 3 feed factors calculated by this process.

3.3.2.2. Operational range of gravimetric feeding

To determine the operational range of gravimetric feeding, each combination of material and tooling was fed by multiple set-points, selected as 10%, 30%, 50%, 70%, 90% and 110% of the initial feed factor. The feeder could reach a screw speed with a drive command of 110% due to the design of K-Tron KT20. The feeder was filled to 80% of the feeder hopper capacity and was run for 20 minutes. The catch scale's data was recorded to calculate the relative standard deviation (RSD) and the deviation from mean of the actual feeding (RDM). The results are plotted in Figure 3-4 as a function of the percent drive command of the motor for Prosolv HD 90, Avicel 101, Avicel 102, Avicel 105, Avicel 200, Avicel 301, powder APAP, magnesium stearate and lactose monohydrate 310 appear. These results show that the RSD was the highest at low drive command levels, < 20% drive command. From 40% drive command up to 90% drive command, the RSD was

very similar for all materials and screw types. High RSD at drive command greater than 90% may be caused by reduced screw fill efficiency.

Between 20% and 40% drive command, we see the same general results in RSD for three of the four screws. Within the range of 20% and 40% drive command, the fine concave, coarse concave, and coarse auger screws all have RSD values similar to RSD values found in the 40% to 90% drive command range. The fine auger screw had higher RSD values between 20% and 40% than the other three screws, resulting in a smaller operational region.

A similar trend was found for the RDM. High deviation was observed below 10% and above 100% drive command. The largest deviation from the mean occurs at the highest drive command, for the same reason as for the RSD. The maximum limit in the acceptable variation of the feed rate (RSD) was dependent on the different standard required. For this work, the target was to have an RSD value below 5%. The maximum limit of RDM depends on the design of the manufacturing line and was not covered further in this work.

The next step was to combine all the data into a single plot. When examining all the RSD data in a single plot, shown in Figure 3-5, a similar trend was identified across all materials and screws. The RSD was high for low screw speeds, then at higher values of the drive command, the RSD plateaus at a consistent value. When looking at all the RDM data in a single plot, Figure 3-5, again a similar trend was observed for all materials and screws. At low drive command, the RDM was low, meaning the feeder was achieving the target set point; however, at high drive command, the feeder can no longer reach the desired set point, reaching a steady flow rate below the desired set point. Using the information from these two figures, a suitable range in operation of the K-Tron KT20 C-gearbox feeder was

between 40% and 90% of the drive command for all tested screws. This range was not an absolute range of operation because it was possible to obtain low RSD and low RDM below 40%, down to 20% drive command, using fine concave, coarse concave, and coarse auger screws.

3.3.2.3. Ideal design space of gravimetric feeding based on material properties

An ideal design space for a gravimetric feeder would be defined by the range of feed rates in which the feeder will perform accurate gravimetric feeding at the required target mass flow rate with acceptable relative standard deviation (RSD) and acceptable relative deviation between the mean and the setpoint (RDM). In principle, the design space boundaries will depend on the tooling selection for a given material. On the other hand, a good gravimetric feeding performance will not be guaranteed if a loss-in-weight feeder was not operated within the ideal design space (between 40% and 90%). If the selction to the best performing screw could be correlated to specific material properties, it would save a large amount of materials and effort. This would save material and time because a blind, wide ranging, experimental list, varying all screw types and multiple feed rates can be avoided and replaced with a targeted experimental list focused on a single screw.

In order to identify a correlation between one of the material properties and the feed factor, values of the feed factor obtained from all the materials were analyzed and correlated to values of the material properties introduced in Section 3.1. Most of the properties, such as particle size, flow function coefficient, and cohesion, did not result in any identifiable trend. Statistically significant correlation was observed between the feed factor and the density of the materials. The conditioned bulk density (cBD), when plotted versus the feed factor, resulted in the lowestR-squared values; however, similar trendlines were observed for

aerated bulk density and tapped density. The R-squared values for cBD were above 0.9, for all screw types with P-values much less than 0.05, while the R-squared values for aerated bulk density and tapped density were between 0.9 and 0.75. Figure 3-6 shows a linear relationship between feed factor and the conditioned bulk density, obtained from the FT4, of the material for all four screw times. Coarse auger screws had the largest slope, representing the largest throughput, followed by coarse concave screws. Fine auger and fine concave screws have similar feed factors for low density materials; however, as the density of the material increases, the fine auger screw has a slightly higher throughput value than the fine concave screws. While cBD showed a linear relationship to feed factor, it should be noted that none of the other density properties, particle size, cohesion, nor the compressed densities from 1kPa to 15kPa, showed the same correlation, with R-squared values above 0.9. Therefore, by analyzing 10mL of material, the necessary amount to obtain cBD, the maximum flow rate of a particular material and screw combination can be approximated.

Based on the results from feeder's operational range, which identified a drive command between 40 – 90% for Fine Auger Screws and 20 – 90% for the other three types of screws,and the feed factor correlation to cBD, an effective design space for the four different screw types can be determined (Figure 3-7). The graphs in Figure 3-7 show the linear equation relating cBD to the feed factor for each of the four screws. Additionally, the equation to calculate feed rate at 90% screw speed (the upper desired limit for each of the screws, as shown in Figure 3-5) has been shown on all four graphs. The lower acceptable limit was also determined and plotted for each of the four graphs. For the coarse auger, coarse concave, and the fine concave screws, the lower line represents the

throughput at 20% of the screw speed, and for the fine auger screws, the lower line represents the throughput at 40% screw speed. Using the subsequent equations, derived in Figure 3-7, when a new material was identified, the cBD value of that material can be input into the equations to identify the effective range of operation for each of the four screws. It should be noted that this was specific for the K-Tron KT-20 C-gearbox feeder.

By knowing the target throughput and cBD of a material, a proper screw and feeder type can be identified. If it was determined that the desired throughput was too low or too high for the four identified screws, the recommendation would be to switch feeder types from a KT-20 C-gearbox, studied here, to a higher gearbox, which has a higher maximum screw speed for larger throughputs, or a smaller feeder with lower feeding capacity.

Feeder characterization has been performed for over a decade by research groups in academia and in industry, and over time, streamlined characterization procedures have been established that save significant amounts of time and materials. Early on, characterization was performed by trial and error. For this example, the formulation had five components (API, two excipients, disintegrant, and lubricant) and two doses of interest. To characterize the feeders, a range in throughputs were tested: a high, low, and the target throughput. Given that the formulation had two doses of interest, five throughputs were tested for the API since the two target conditions were far enough apart that a midpoint was required. For the API and the two excipients, all four screws were tested, while only the two fine screws were used for the lubricant and disintegrant, as both were low weight percentages in the formulation. An example of the effort required for a trial by error approach to characterize feeders for this product is presented in Table 3-4. The

characterization required over 30 hours and 255 kg of material to determine the optimal screw type for each material. The same feeder characterization, based on the method described in this manuscript, would only require 2 screw types for the API (one for each dose) and 1 screw type for the remaining materials. If three set points for each screw type were kept for validation, the characterization would result in a total 9 hours of work and 70 kg of material, Table 3-4. Both calculations did not include the time required for set up and cleaning, both of which would be significantly longer for the trial by error approach. By using the design space and correlated feed factor to bulk density method proposed in this manuscript, the characterization time would have been decreased by 70%, and requiring 75% less material.

3.4. Conclusions

Feeder characterization has been performed in the past using a trial and error approach to determine optimal feeder and screw selection for a given material and formulation. The trial and error approach commonly resulted in delays in product and process development. In this work, a QbD approach has been identified that identifies a maximum powder and screw throughput (feed factor) from conditioned bulk density. Coupling the correlation to feed factor with the identified ideal design space for a K-Tron feeder, the operational throughput for a given material and screw can be determined by obtaining the conditioned bulk density. In order to identify the ranges of operation, 10 materials with a wide range of particle sizes, densities, and flow properties were tested to understand and develop the design space of a K-Tron KT20 loss-in-weight feeder, with a C-gear box. By feeding all of these materials at six different levels of drive commands, the effective range of operation was located by calculating the relative standard deviation and the relative deviation from

the mean and identifying a region of minimum values in both calculations. Values of 20% and 90% were determined as the lower and upper limit of drive command for suitable operational range for fine concave, coarse concave, and coarse auger screws with KT20 C-gear box, while the acceptable range for fine auger screws was between 40% and 90% drive command. These observations were confirmed for several types of materials ranging from freely flowing to cohesive. In addition to the operational range for the feeder, a linear correlation between the conditioned bulk density and the feed factor was identified. With these two design criteria, the K-Tron KT-20 C-gearbox feeding capacity can be predicted for each of the different types of screws by the conditioned bulk density of the material. Specifically, this means that by characterizing on a small amount of material, i.e.,10 mL, enough information would be obtained to determine the feeder's feed factor, and with the suitable feeding range established in this work, for each screw, a feeder's design space can be determined. While this method quickly identifies the optimal screw required for a target throughput, it should be noted that the material and screw combination should be validated experimentally. The validation process would confirm that the RSD was at a low acceptable value (i.e., below 5%), and also identify any electrostatic issues that the material may experience while feeding. Using the feeder design space method, a large amount of time, effort, and material can be saved during the process development stage.

3.5. Tables for Chapter 3

Table 3. 1: Particle sizes of pharmaceutical material

Material	d10 (microns)	d(3,2) (microns)	d50 (microns)	d90 (microns)	Span
API Granules	96.6	143.7	215.7	405.7	1.4
Avicel 101	24.1	48.9	73.5	167.3	1.9
Avicel 102	37.8	74.6	124.7	245.3	1.7
Avicel 105	6.6	12.8	18.6	36.4	1.6
Avicel 200	45.3	74.0	143.7	195.1	1.0
Avicel 301	17.6	36.5	61.9	133.0	1.9
Avicel 302	32.9	64.1	105.3	170.8	1.3
Ceolus KG 802	21.5	44.1	66.4	140.7	1.8
Coarse Alumina	11.2	32.0	59.4	122.2	1.9
Croscarmellose Sodium	18.9	32.6	45.1	118.7	2.2
Lactose Monohydrate 310	18.6	34.9	82.7	176.3	1.9
Magnesium Stearate	4.5	8.8	12.1	23.5	1.6
Molybdenum Oxide	0.8	2.0	3.7	10.3	2.6
Powder APAP	9.9	23.5	57.4	166.0	2.7
Prosolv HD 50	20.1	28.3	60.4	118.0	1.6
Prosolv HD 90	26.7	56.9	127.0	241.0	1.7
Prosolv HD 200	61.2	103.8	176.7	243.0	1.0

Table 3. 2: **Density Results from the FT4 Compressibility and Tapped Density Tests**

Material	Conditioned Bulk Density (g/cc)	Compressibility @ 15.0kPa (%)	Bulk Density @ 15.0kPa (g/cc)	Aerated Bulk Density (g/cc)	Tapped Density (g/cc)	Hausner Ratio
API Granules	0.340	7.07	0.368	0.350	0.460	1.30
Avicel 101	0.340	16.92	0.420	0.320	0.460	1.40
Avicel 102	0.340	15.18	0.400	0.320	0.440	1.38
Avicel 105	0.375	28.23	0.521	0.354	0.545	1.54
Avicel 200	0.361	10.03	0.401	0.331	0.417	1.26
Avicel 301	0.451	15.59	0.534	0.429	0.573	1.34
Avicel 302	0.461	11.44	0.521	0.463	0.596	1.29
Ceolus KG 802	0.250	22.82	0.320	0.260	0.360	1.37
Coarse Alumina	0.965	3.90	1.003	0.850	1.056	1.24
Croscarmellose Sodium	0.490	12.67	0.570	0.520	0.680	1.30
Lactose Monohydrate 310	0.691	19.61	0.859	0.685	0.885	1.29

Magnesium Stearate	0.195	45.70	0.359	0.160	0.230	1.44
Molybdenum Oxide	1.395	25.00	1.743	1.200	1.906	0.59
Powder APAP	0.280	50.63	0.560	0.350	0.580	1.67
Prosolv 50	0.337	11.40	0.381	0.340	0.443	1.30
Prosolv HD 90	0.480	7.38	0.520	0.460	0.560	1.22
Prosolv HD200	0.507	5.10	0.534	0.461	0.560	1.22

Table 3. 3: **Shear Cell resulted obtained using the 3 kPa test with the Freeman FT4**

Material	Cohesion, kPa	UYS, kPa	MCS, kPa	MPS, kPa	FFc	Rel (p)	AIF, º
API Granules	0.110	0.49	1.22	6.14	12.67	10.15	40.17
Avicel 101	0.289	1.14	1.27	6.12	5.37	4.25	36.32
Avicel 102	0.163	0.63	1.30	5.46	10.28	7.79	35.16
Avicel 105	0.707	2.69	1.02	6.35	2.36	1.99	34.46
Avicel 200	0.077	0.27	1.51	4.93	26.27	18.23	30.73
Avicel 301	0.203	0.80	1.24	5.63	7.02	5.48	36.33
Avicel 302	0.137	0.48	1.41	4.91	10.32	7.36	31.19
Ceolus KG 802	0.328	1.34	1.27	6.67	5.03	4.07	38.04
Coarse Alumina	0.120	0.42	1.58	4.70	11.29	9.59	30.39
Croscarmellose Sodium	0.176	0.87	1.17	7.99	9.26	7.90	45.85
Lactose Monohydrate 310	0.220	0.82	1.31	5.33	6.60	4.98	33.33
Magnesium Stearate	0.363	1.21	1.49	5.35	4.43	3.19	28.04
Molybdenum Oxide	1.020	4.27	0.79	7.23	1.69	1.78	38.89
Powder APAP	0.670	2.57	1.11	6.64	2.59	2.16	34.94
Prosolv 50	0.989	3.34	2.74	11.16	3.34	2.52	28.73
Prosolv HD 90	0.096	0.32	1.60	4.69	14.84	9.76	27.61
Prosolv HD200	0.542	1.85	2.97	10.53	5.68	4.08	29.36

Table 3. 4: **Shear Cell resulted obtained using the 6 kPa test with the Freeman FT4**

Material	Cohesion, kPa	UYS, kPa	MCS, kPa	MPS, kPa	FFc	Rel (p)	AIF, º
API Granules	0.11	0.47	2.52	11.72	25.00	19.65	39.35
Avicel 101	0.47	1.84	2.58	11.83	6.71	5.24	36.13
Avicel 102	0.22	0.78	2.73	9.93	13.03	9.46	32.70
Avicel 105	1.08	4.23	2.14	12.38	2.93	2.42	35.75
Avicel 200	0.04	0.15	2.95	9.44	61.81	42.52	31.22
Avicel 301	0.32	1.26	2.63	11.32	8.99	6.90	35.86
Avicel 302	0.15	0.57	2.61	10.18	17.92	13.32	34.95
Ceolus KG 802	0.56	2.38	2.49	13.60	5.74	4.69	39.52
Coarse Alumina	0.07	0.26	3.02	9.23	35.85	39.43	32.51
Croscarmellose Sodium	0.37	1.84	2.44	16.92	9.44	8.08	46.16
Lactose Monohydrate 310	0.39	1.44	2.63	10.41	7.20	5.39	33.15
Magnesium Stearate	0.2	0.62	3.63	9.09	15.04	9.03	23.60
Molybdenum Oxide	1.48	6.30	1.95	13.57	2.16	2.25	39.58
Powder APAP	1.11	4.16	2.30	12.28	2.95	2.40	33.91
Prosolv 50	0.99	3.34	2.74	11.16	3.34	2.52	28.73
Prosolv HD 90	0.07	0.24	2.96	9.32	38.37	26.17	30.52
Prosolv HD200	0.54	1.85	2.97	10.53	5.68	4.08	29.36

3.6. Figures for Chapter 3

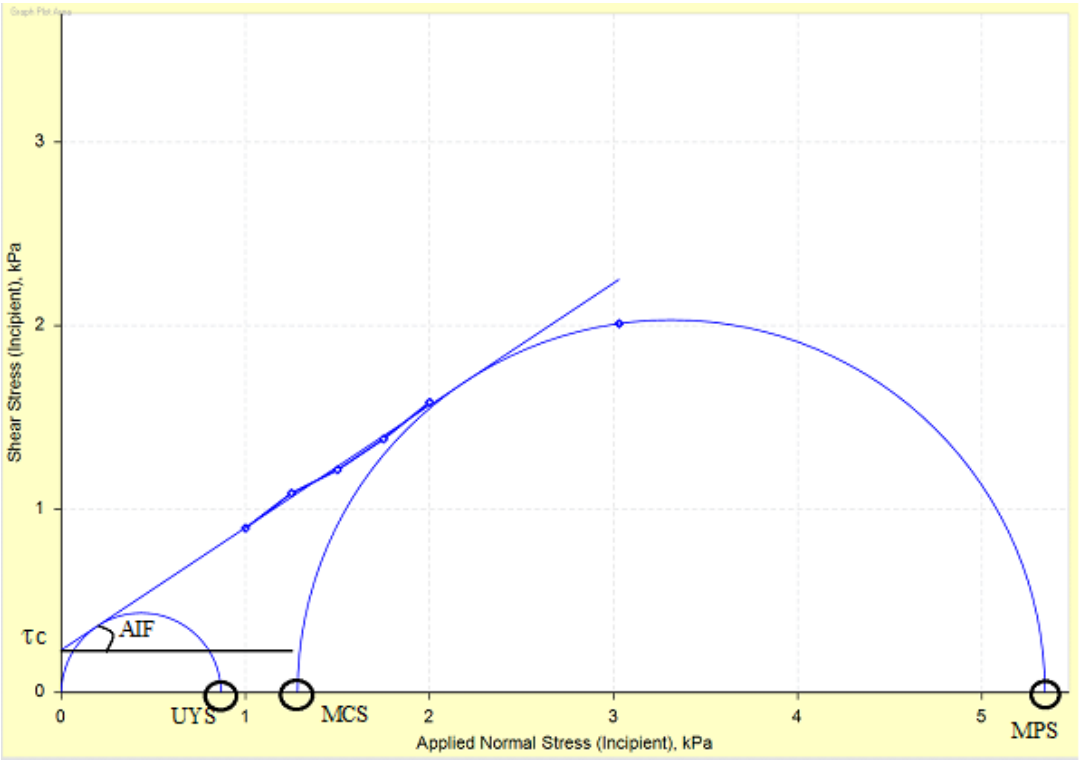

Figure 3. 1: Yield locus plot with the specific data obtained from the plot. τ_c is the cohesion, AIF is the angle of internal friction, UYS is the unconfined yield stress, MCS is the minor consolidation stress, and MPS is the major principal stress [84].

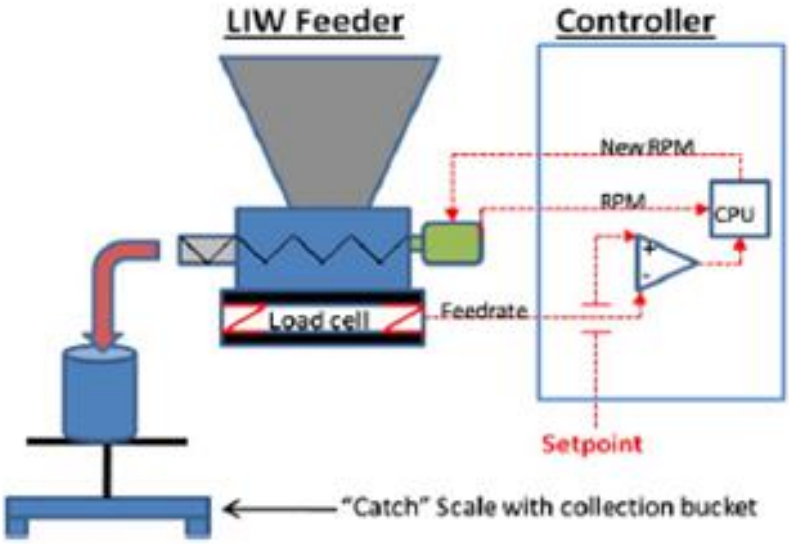

Figure 3. 2: A schematic illustration of a loss-in-weight feeder. (W. Engisch, F. Muzzio[11])

Figure 3. 3: K-Tron KT20 feeder tooling. From left to right: fine concave screws (FCS), coarse concave screws (CCS), fine auger screws (FAS), coarse auger screws (CAS)[21]

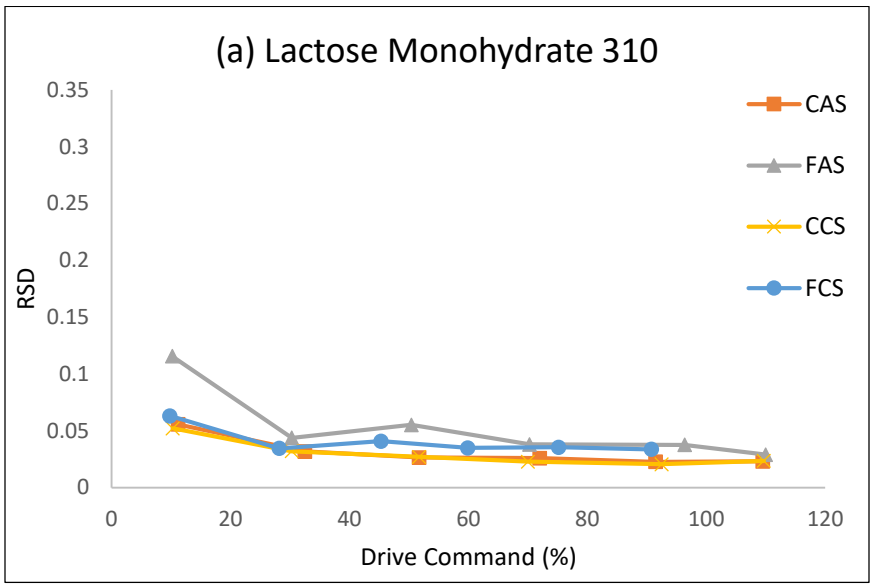
(a) Lactose Monohydrate 310
RSD
0.35
0.3
0.25
0.2
0.15
0.1
0.05
0
0
20
40
60
80
100
120
Drive Command (%)
CAS
FAS
CCS
FCS

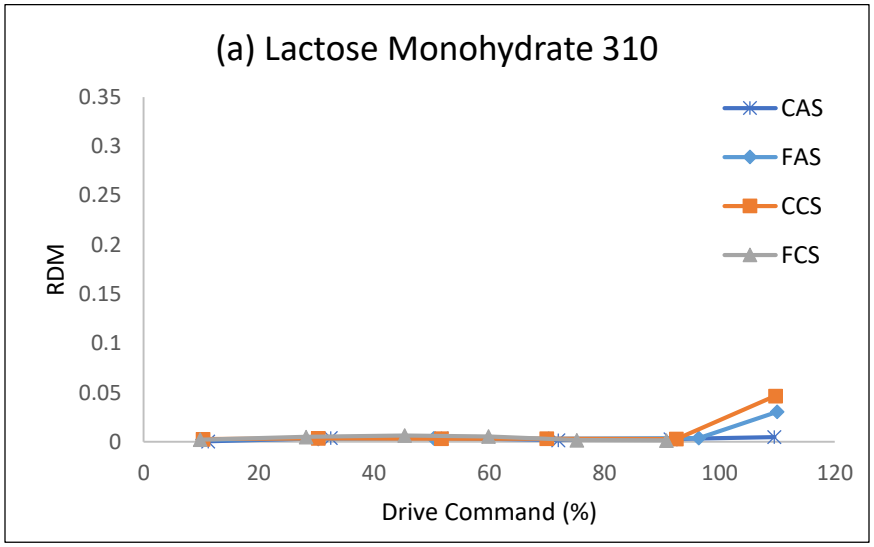
(a) Lactose Monohydrate 310
RDM
0.35
0.3
0.25
0.2
0.15
0.1
0.05
0
0
20
40
60
80
100
120
Drive Command (%)
CAS
FAS
CCS
FCS

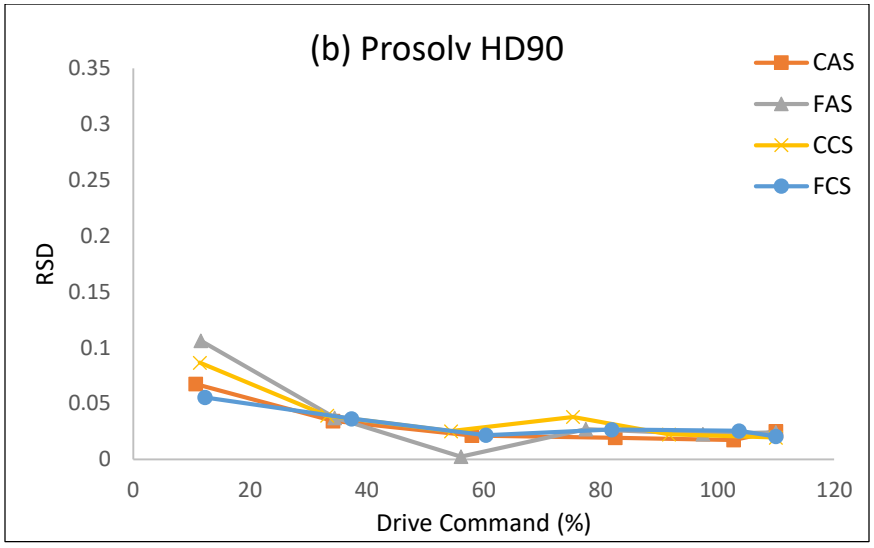
(b) Prosolv HD90
RSD
0.35
0.3
0.25
0.2
0.15
0.1
0.05
0
0
20
40
60
80
100
120
Drive Command (%)
CAS
FAS
CCS
FCS

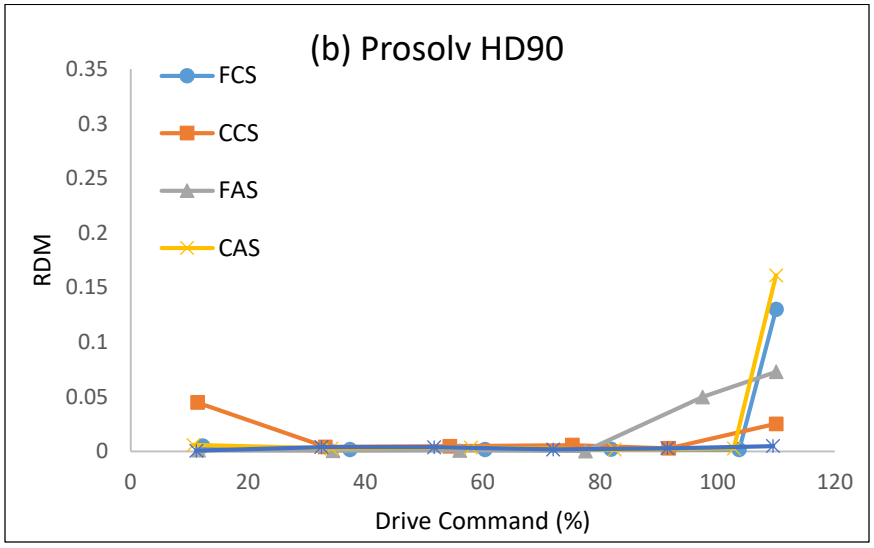
(b) Prosolv HD90
FCS
CCS
FAS
CAS
RDM
0.35
0.3
0.25
0.2
0.15
0.1
0.05
0
0
20
40
60
80
100
120
Drive Command (%)

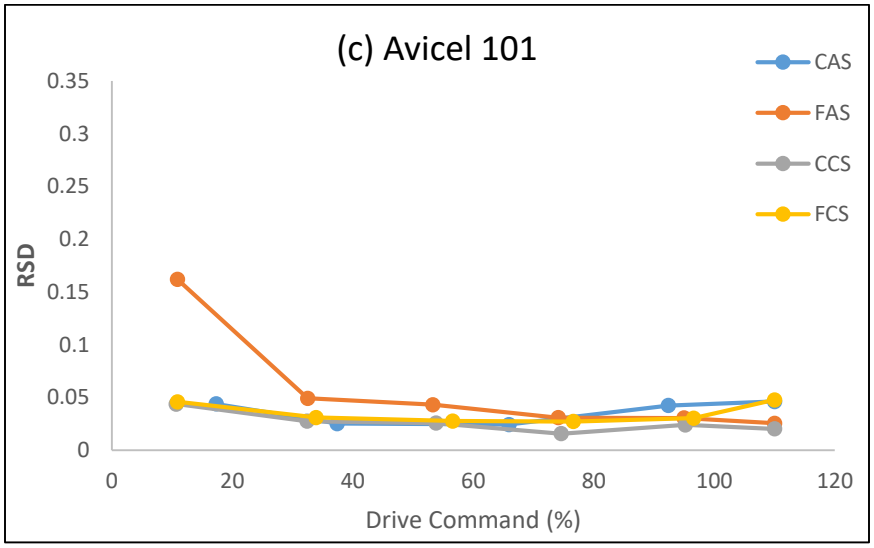
(c) Avicel 101
CAS
FAS
CCS
FCS
RSD
0.35
0.3
0.25
0.2
0.15
0.1
0.05
0
0
20
40
60
80
100
120
Drive Command (%)

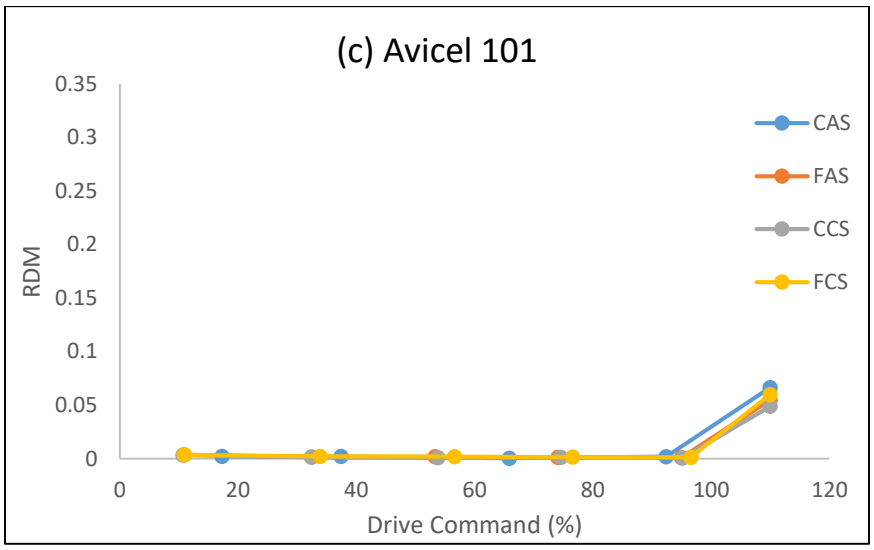
(c) Avicel 101
CAS
FAS
CCS
FCS
RDM
0.35
0.3
0.25
0.2
0.15
0.1
0.05
0
0
20
40
60
80
100
120
Drive Command (%)

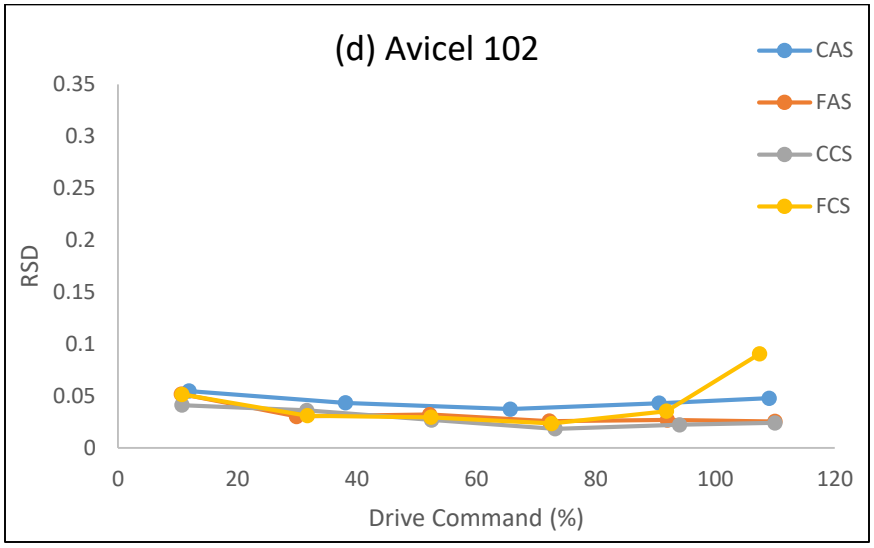
(d) Avicel 102
CAS
FAS
CCS
FCS
RSD
0.35
0.3
0.25
0.2
0.15
0.1
0.05
0
0
20
40
60
80
100
120
Drive Command (%)

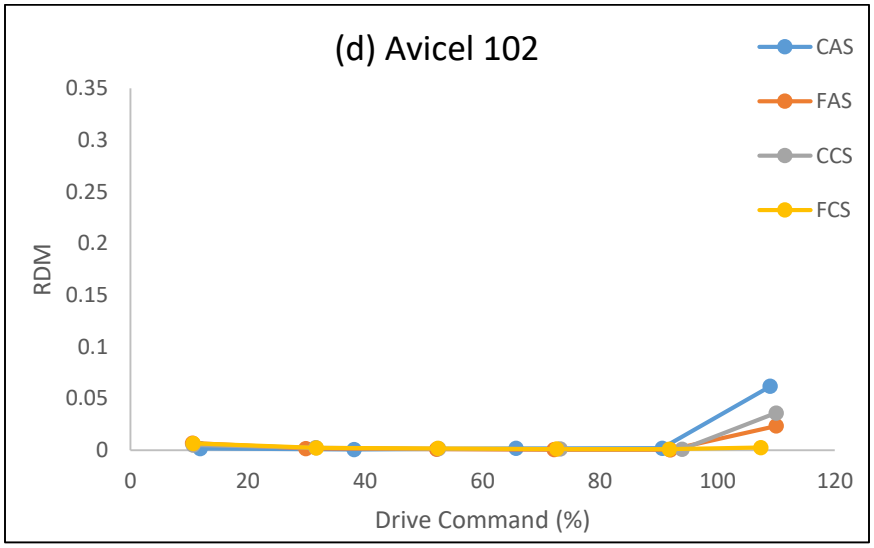
(d) Avicel 102
CAS
FAS
CCS
FCS
RDM
0.35
0.3
0.25
0.2
0.15
0.1
0.05
0
0
20
40
60
80
100
120
Drive Command (%)

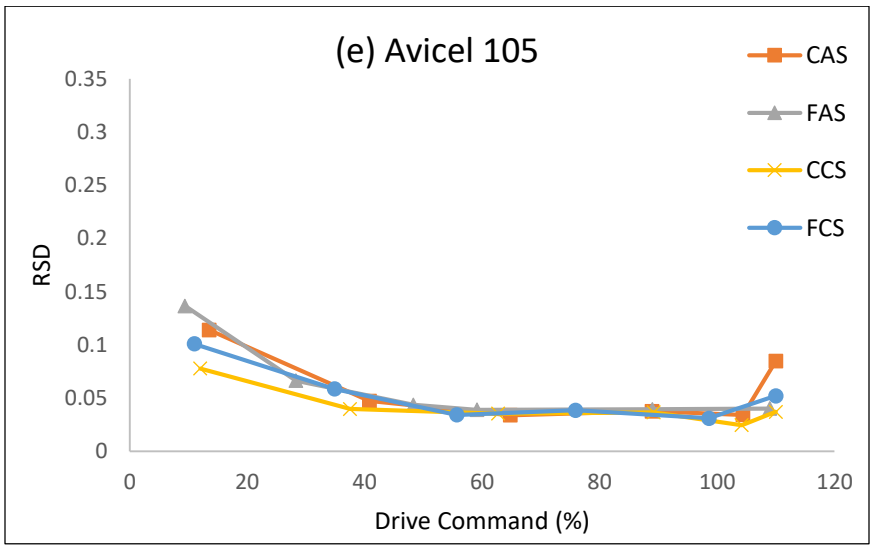
(e) Avicel 105
CAS
FAS
CCS
FCS
RSD
0.35
0.3
0.25
0.2
0.15
0.1
0.05
0
0
20
40
60
80
100
120
Drive Command (%)

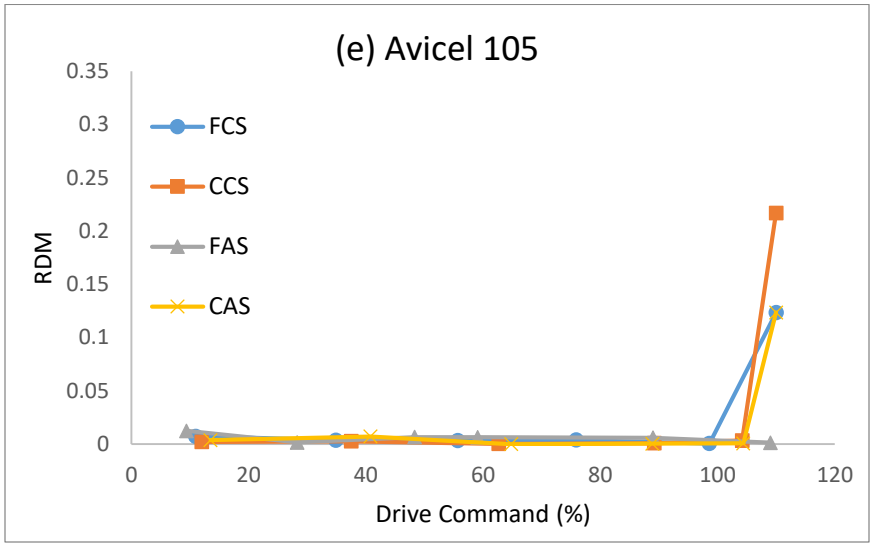
(e) Avicel 105
RDM
0.35
0.3
0.25
0.2
0.15
0.1
0.05
0
FCS
CCS
FAS
CAS
0
20
40
60
80
100
120
Drive Command (%)

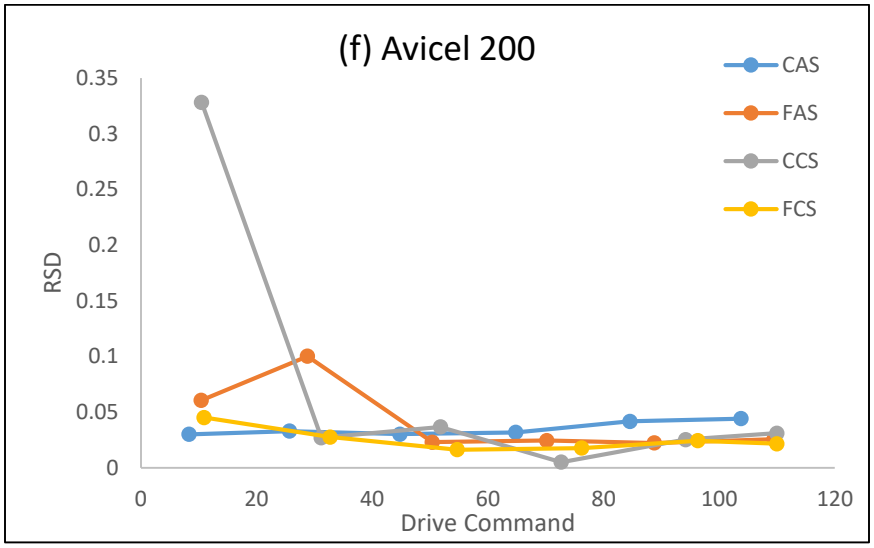
(f) Avicel 200
RSD
0.35
0.3
0.25
0.2
0.15
0.1
0.05
0
CAS
FAS
CCS
FCS
0
20
40
60
80
100
120
Drive Command

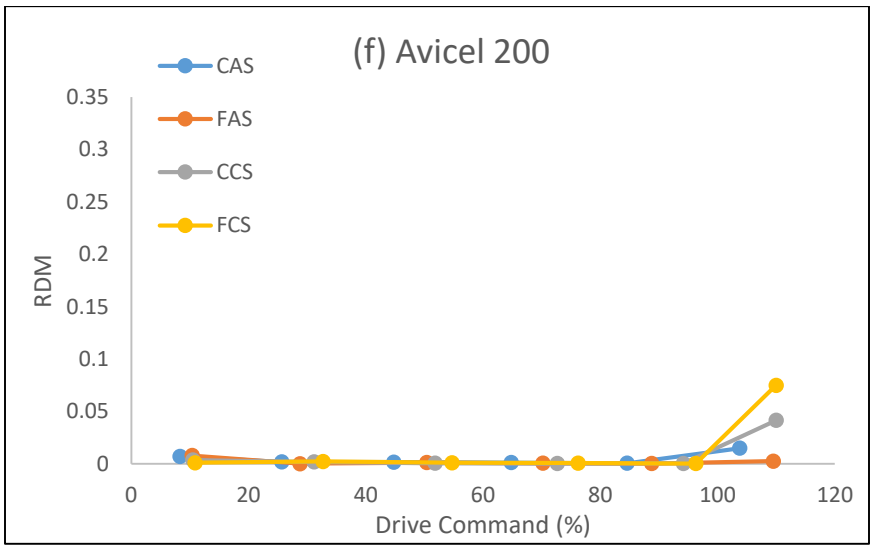
(f) Avicel 200
RDM
0.35
0.3
0.25
0.2
0.15
0.1
0.05
0
CAS
FAS
CCS
FCS
0
20
40
60
80
100
120
Drive Command (%)

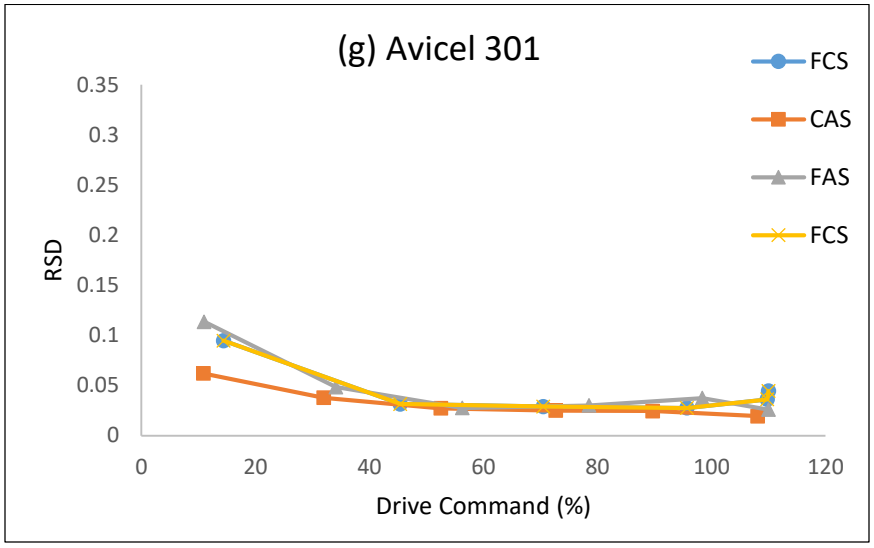
(g) Avicel 301
FCS
CAS
FAS
FCS
RSD
0.35
0.3
0.25
0.2
0.15
0.1
0.05
0
0
20
40
60
80
100
120
Drive Command (%)

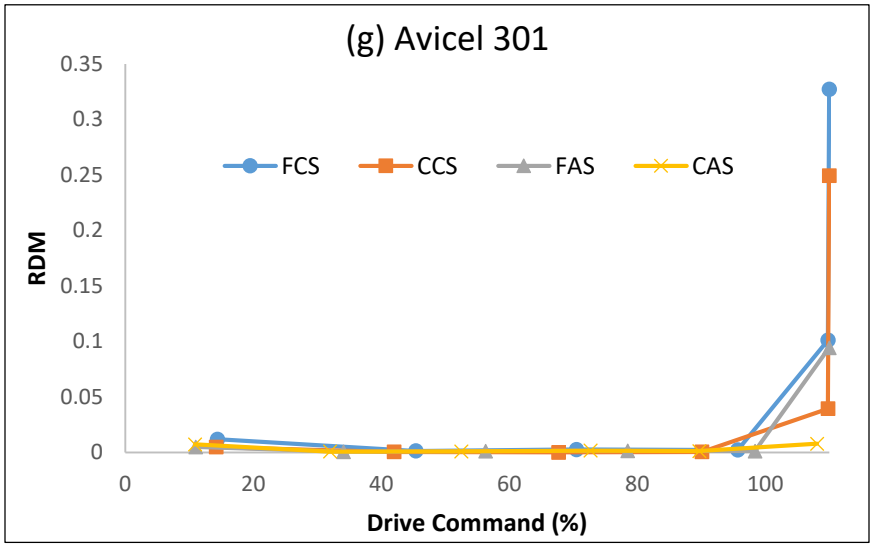
(g) Avicel 301
FCS
CCS
FAS
CAS
RDM
0.35
0.3
0.25
0.2
0.15
0.1
0.05
0
0
20
40
60
80
100
Drive Command (%)

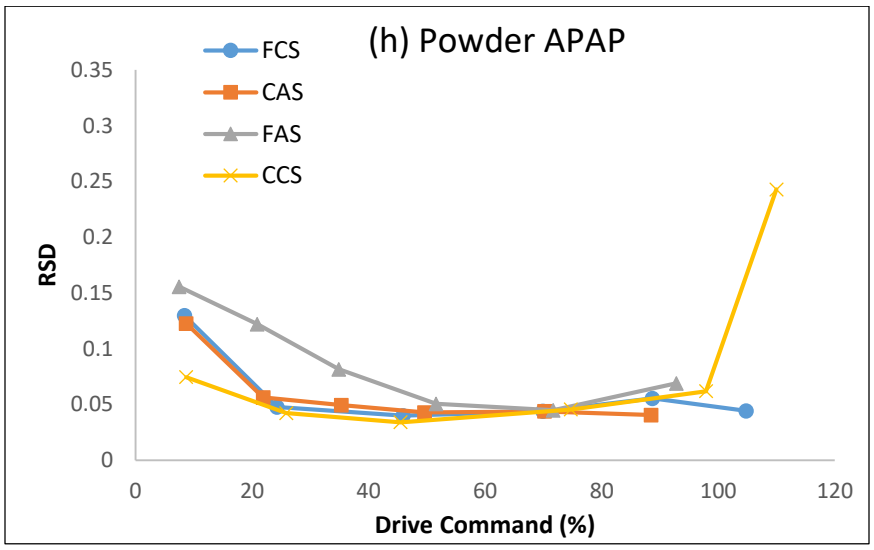
(h) Powder APAP
FCS
CAS
FAS
CCS
RSD
0.35
0.3
0.25
0.2
0.15
0.1
0.05
0
0
20
40
60
80
100
120
Drive Command (%)

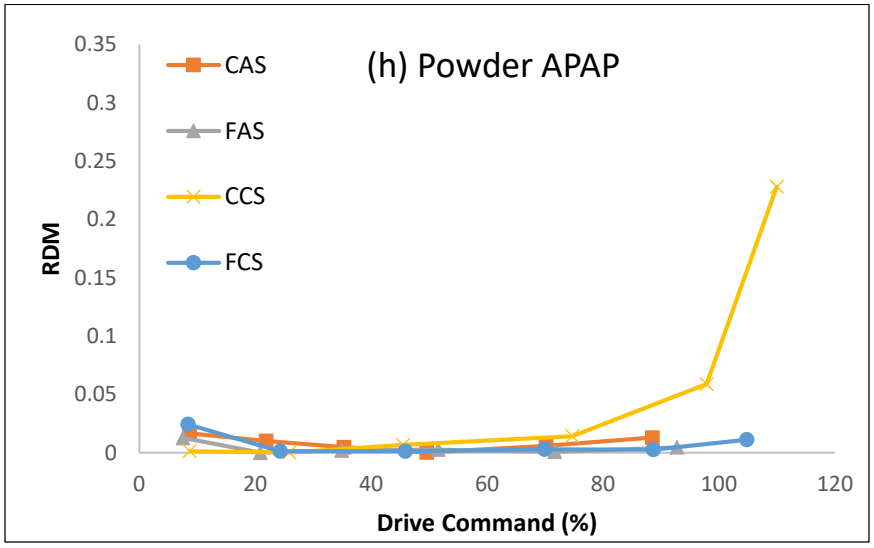
(h) Powder APAP
CAS
FAS
CCS
FCS
RDM
0.35
0.3
0.25
0.2
0.15
0.1
0.05
0
0
20
40
60
80
100
120
Drive Command (%)

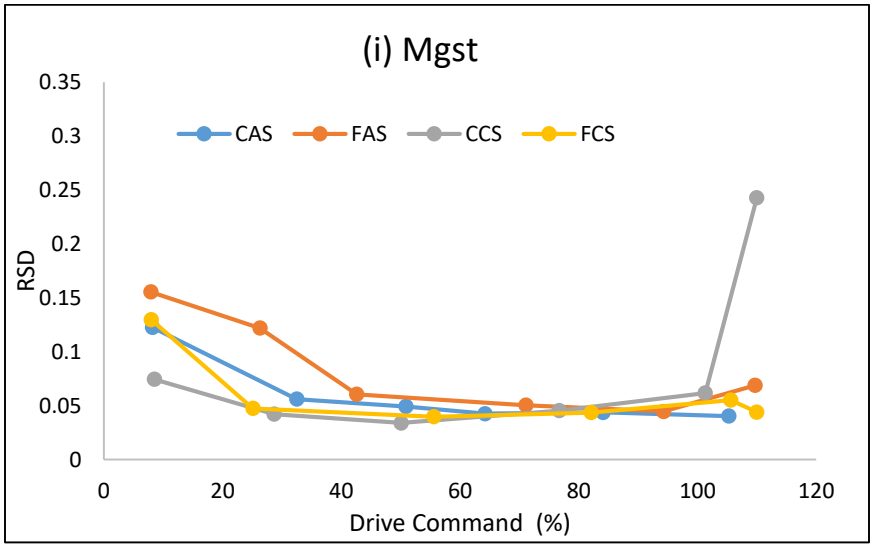
(i) Mgst
CAS
FAS
CCS
FCS
RSD
0.35
0.3
0.25
0.2
0.15
0.1
0.05
0
0
20
40
60
80
100
120
Drive Command (%)

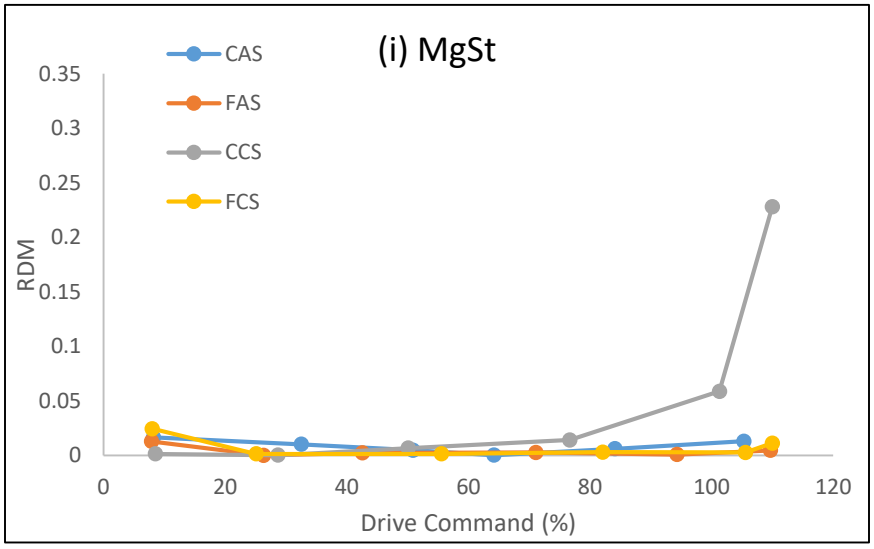
(i) MgSt
CAS
FAS
CCS
FCS
RDM
0.35
0.3
0.25
0.2
0.15
0.1
0.05
0
0
20
40
60
80
100
120
Drive Command (%)

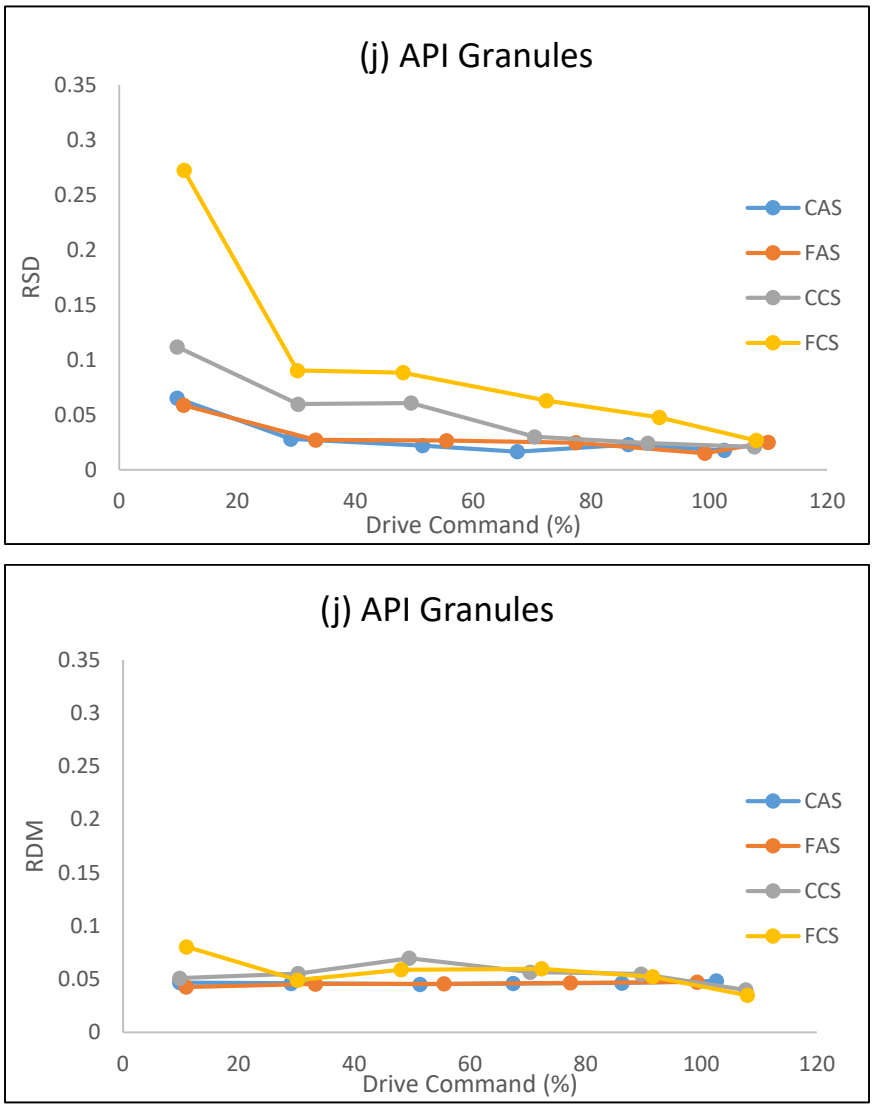

Figure 3. 4: **The relative standard deviation and relative deviation from mean versus drive command (%), and screw type, for Lactose Monohydrate 310 (a), Prosolv HD90 (b), Avicel 101 (c), Avicel 102 (d), Avicel 105 (e), Avicel 200 (f), Avicel 301 (g), powder grade APAP (h), MgSt (i), and Lactose Granules (j).**

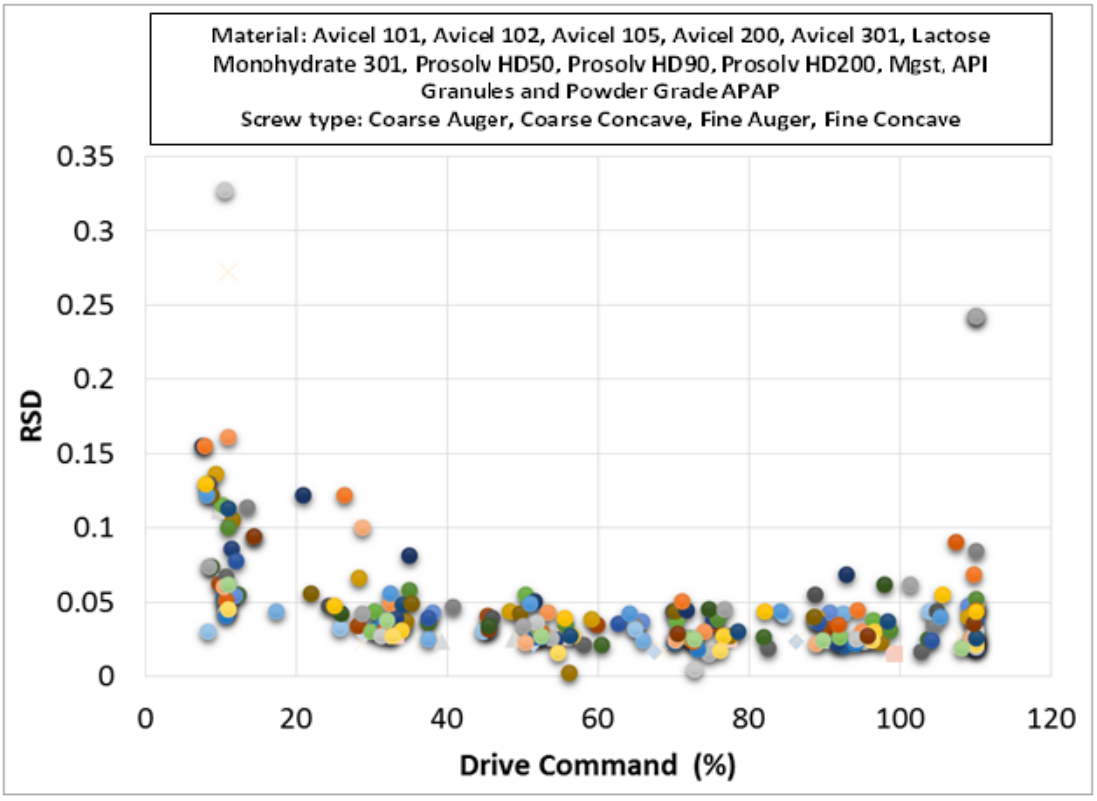
Material: Avicel 101, Avicel 102, Avicel 105, Avicel 200, Avicel 301, Lactose Monohydrate 301, Prosolv HD50, Prosolv HD90, Prosolv HD200, Mgst, API Granules and Powder Grade APAP
Screw type: Coarse Auger, Coarse Concave, Fine Auger, Fine Concave
RSD
0.35
0.3
0.25
0.2
0.15
0.1
0.05
0
0
20
40
60
80
100
120
Drive Command (%)

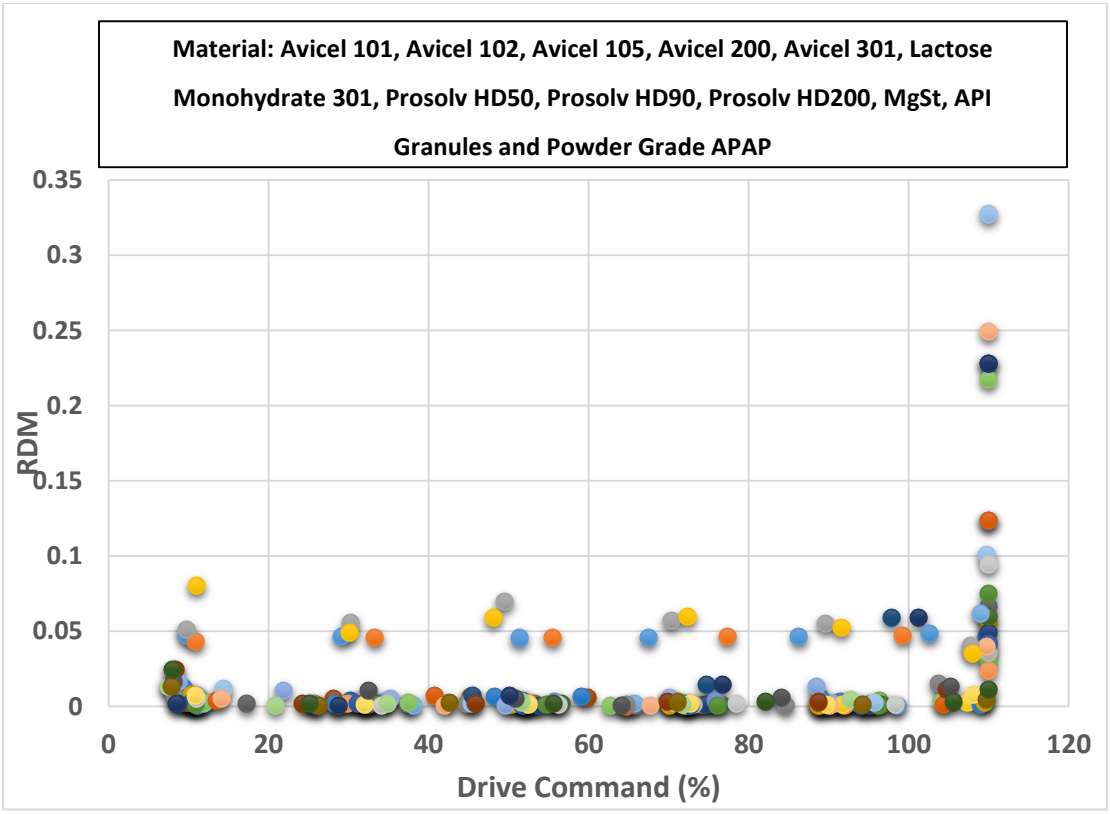
Material: Avicel 101, Avicel 102, Avicel 105, Avicel 200, Avicel 301, Lactose Monohydrate 301, Prosolv HD50, Prosolv HD90, Prosolv HD200, MgSt, API Granules and Powder Grade APAP
RDM
0.35
0.3
0.25
0.2
0.15
0.1
0.05
0
0
20
40
60
80
100
120
Drive Command (%)

Figure 3. 5: Combined RSD (top) and RDM (bottom) vs Drive command (%) of Avicel 101, Avicel 102, Avicel 105, Avicel 200, Avicel 301, Lactose Monohydrate 310, Prosolv HD50, Prosolv HD90, Prosolv HD200, Magnesium Stearate, API Granules, and Powder grade APAP.

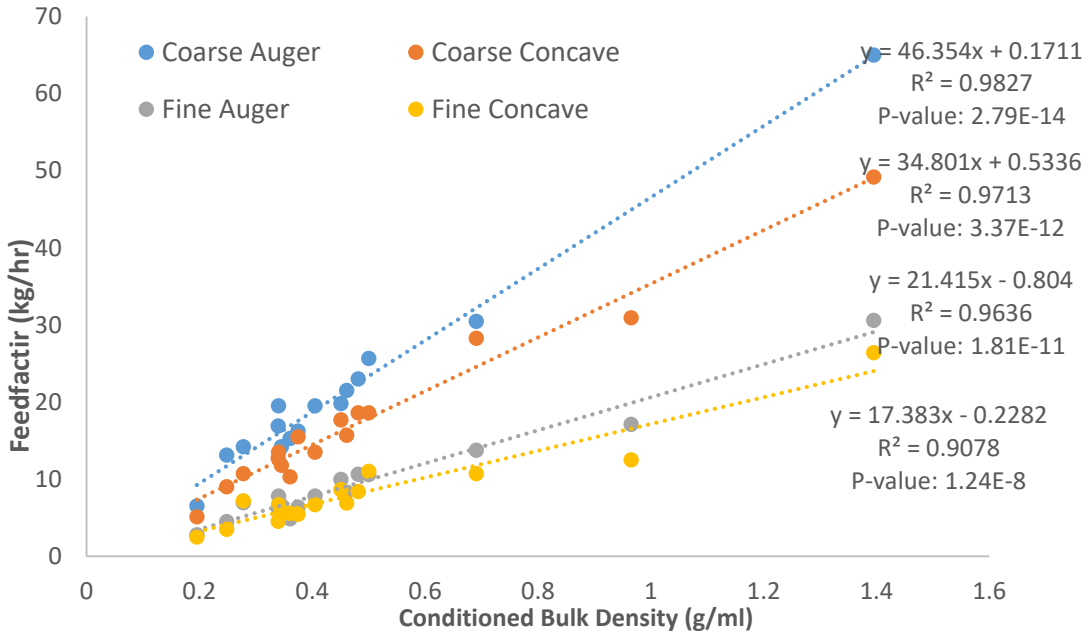

Figure 3. 6: The relationship between feed factor and material conditioned bulk density, for the various material listed, over a wide bulk density range, and for the four screw types.

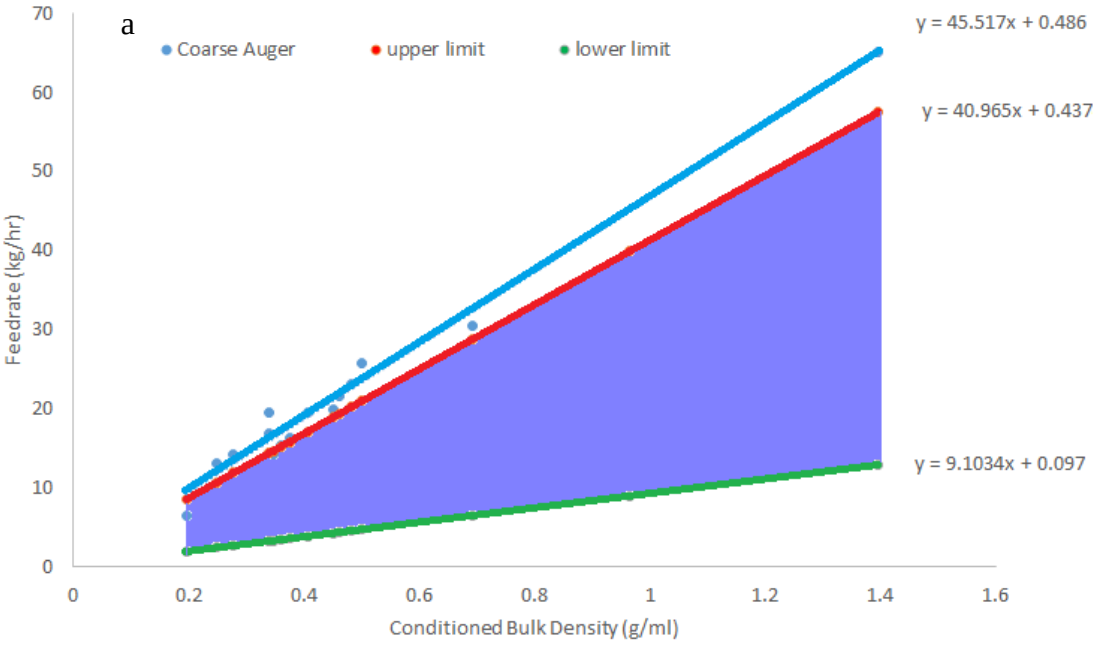
a
Coarse Auger
upper limit
lower limit
y = 45.517x + 0.486
y = 40.965x + 0.437
y = 9.1034x + 0.097
Feedrate (kg/hr)
Conditioned Bulk Density (g/ml)
0
10
20
30
40
50
60
70
0
0.2
0.4
0.6
0.8
1
1.2
1.4
1.6

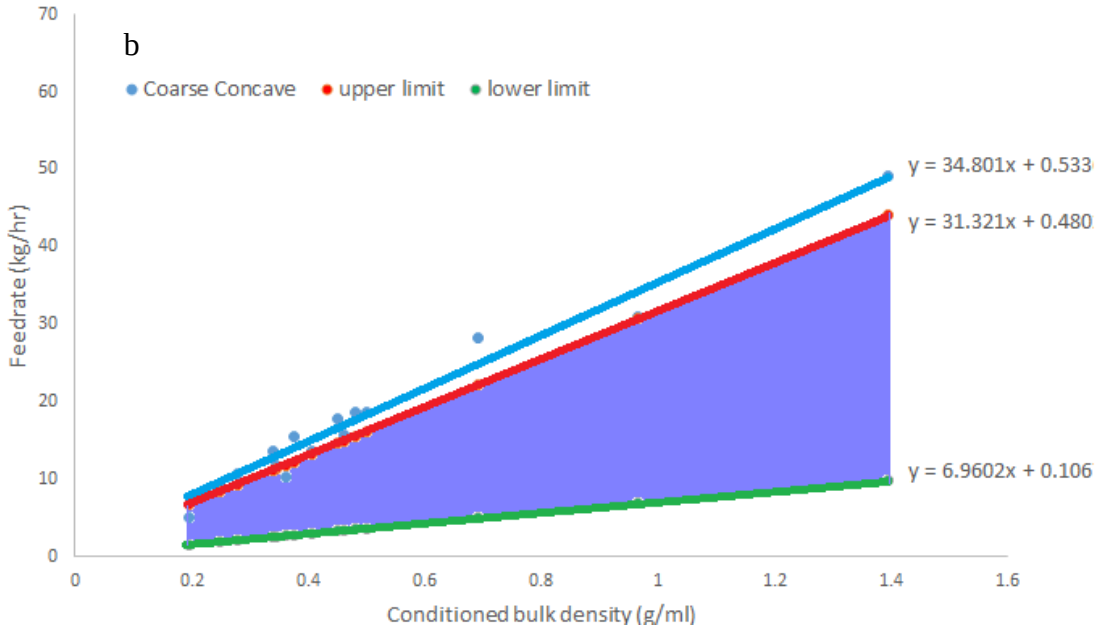
b
Coarse Concave
upper limit
lower limit
y = 34.801x + 0.533
y = 31.321x + 0.480
y = 6.9602x + 0.106
Feedrate (kg/hr)
Conditioned bulk density (g/ml)
0
10
20
30
40
50
60
70
0
0.2
0.4
0.6
0.8
1
1.2
1.4
1.6

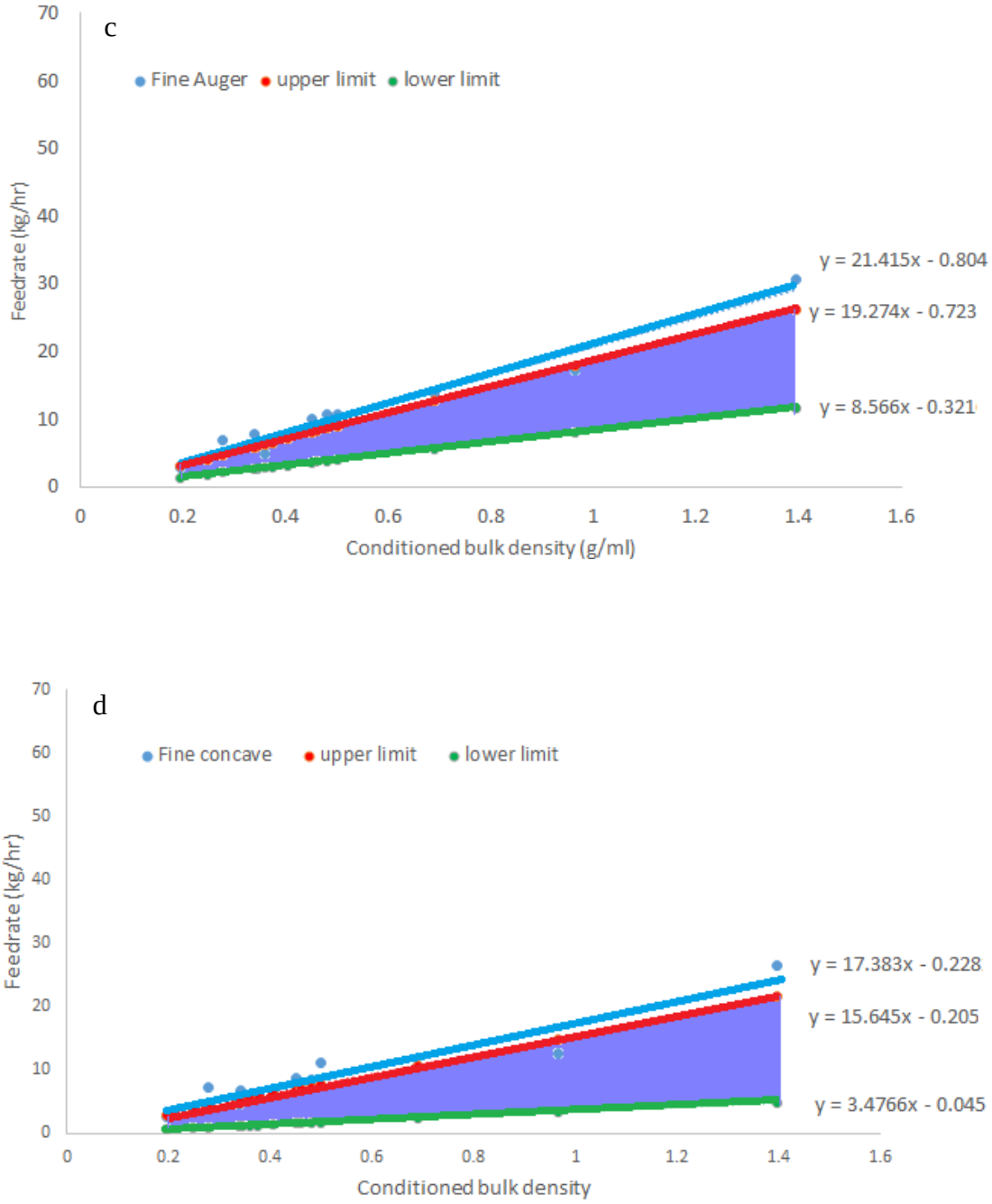

Figure 3. 7: **The KT-20 feeder design space (flow rate range for a given density) for the Coarse Auger (a), Coarse Concave (b), Fine Auger (c), and Fine Concave (d) screws.**

Chapter 4. Predicting Feed Rate Deviation Caused by Hopper Refill Based on Material Flow Properties

4.1. Introduction

The pharmaceutical industry is steadily moving away from traditional batch manufacturing towards the implementation of continuous manufacturing, which aims to optimize supply chain logistics. This has increased the need for in-depth knowledge of the relevant material properties in terms of manufacturability and process understanding. The US Food and Drug Administration has also provided regulatory support for the implementation of continuous manufacturing using science and risk-based approaches[129]. In addition, continuous manufacturing has been widely adopted across many industries, such as bulk chemical production, driven by the advantages of its smaller scale equipment, higher flexibility, enhanced controllability and reduced labor requirements.

Loss-in-weight feeders, as the first unit operation and the primary control tool for content uniformity in a continuous manufacturing system, are responsible to dispense a given mass of material per unit of time into the downstream unit operations. Inconsistency in mass flow on a given feeder will travel downstream through the process and can consequently impact the quality attributes of the final products, such as potency (assay) and content uniformity. To establish a continuous and uninterrupted process, periodic refill of the feeder hopper is required due to the limitation on a loss-in-weight feeder's hopper capacity. Because gravimetric control is based on a differential weight measurement, loss-in-weight feeders have to be operated in volumetric mode during the refill process as the load cell cannot calculate the loss in mass with the positive influx of material. Therefore, during hopper refill process and a short post refill delay (typically about 10 -15 seconds), the screw

speed remains constant (or follows a pre-defined algorithm) and the controller does not monitor the feed rate[24, 130]. If the density of the material at the entrance of the screws (bottom of the feeder hopper) or the screw filling fraction changes during the refill process, the feed rate can deviate from the setpoint as the incoming material compresses the powder bed in the hopper, and pushes powder into the screw channel more efficiently, both effects causing an increase in density of the powder at the feeder screws, which results in over-feeding[131]. Additionally, the powder can become aerated by the refill process, which will lead to an uncontrollable flow[132].

Feeder refill has been a popular study topic among feeder manufacturers and researchers for years. In US Patent 4535886[133], values stored during powder dispensing of the feeder hopper were used to select the screw speed during refill[131], and this is the method that most manufacturers, including Coperion K-Tron used to build the refilling algorithm of loss-in-weight feeders. In US Patent 4579252[134], Wilson and Bullivant have also discussed and implemented a method which uses a second feeder to feed the feeder that needs to be refilled. By using this method, a better feeding performance with lower feed rate during the refill process were achieved; however, this approach may double the expense in terms of feeders and require additional space for the equipment setup. Engisch et al. 2015 had defined 3 types of quantitative deviations (maximum deviation, deviation time, and total deviation) during hopper refill and has also compared the difference in deviations between refilling at three refill points in terms of percentage of feeder hopper volume [20]. Wang et al. 2017 had built up a predictive correlation between material bulk properties and both the feed rate variation and deviation under gravimetric control [23]. Other researchers have also proved that loss-in-weight feeders' feeding performance is

highly dependent on material properties[72, 77, 79, 80, 135, 136]; however, there was a lack of work on demonstrating how materials with varied flow properties impact the performance of loss-in-weight feeders when running in volumetric mode without control, let alone a predictive model that identifies the major material properties that contribute to the refill performance.

The work discussed in this chapter focuses on a way to identify similarity between materials using principal component analysis followed by similarity scores (PCA-SS) and then moves on to correlating the three types of feed rate deviations with material flow properties using partial least squares regression (PLSR). A benefit of using PLSR is that it allows the identification of the relative contribution of each of the different material properties on each type of deviation. After the model was built using the initial material, feeder refill experiments were performed to validate the model and prediction results, which proved that the developed model could successfully predict the feed rate deviation caused by hopper refill.

With this developed frame work, once a material is characterized, the bulk properties could be used to predict the potential disturbance to the mass flow of the feeder caused by hopper refill operations. By having the potential deviations predicted beforehand, massive materials and effort can be saved. In addition, this work can be applied to the development of a more efficient control and alert system that can be developed based the formulation in process. Moreover, a more efficient refilling strategy can be derived based on specific criteria of the whole integrated continuous process, all with an acceptable disturbance and fewer total number of refills to be performed.

4.2. Materials and Methods

4.2.1. Materials

The materials that were studied in this work include: Fine alumina (Albermarle Inc., Amsterdam, the Netherlands), Fine zeolite (Albermarle Inc., Amsterdam, the Netherlands), Molybdenum dioxide (fine, sublimed type, Albemarle Inc., Amsterdam, the Netherlands), Satintone (calcined kaolin SP-33, BASF Corporation, NJ, USA), Lactose monohydrate (Foremost Farms, WI, USA) and Zeolite (Y-type CBV100, BASF Corporation, NJ, USA). In addition, calcined zeolite (Albermarle Inc., Amsterdam, the Netherlands) was named as 'Material A' in the material library to validate the predictive model. 'Material A' was chosen due to its relevant poor flow properties, including a high cohesion value that could potentially lead to failure in processing

4.2.2. Material properties measurements

The following tests were performed: permeability, compressibility, dynamic flow, and shear cell (Testing methods see Chapter 2). Particle size distribution in terms of d_{10}, d_{50} and d_{90}, for all components, were obtained by a Beckman-Coulter LS 13-320 laser diffraction particle size analyzer. All the material properties obtained and applied to the predictive model are shown in Table 4-1.

4.2.3. Loss-in-weight feeder setup and refill characterization

A K-Tron KT20 twin screw loss-in-weight feeder with a type C gearbox (with a gear reduction ratio of 12.9:1) was tested in this study. K-Tron KT20 loss-in-weight feeder's design consists of three parts: volumetric feeder, weighing platform (load cell), and gravimetric controller**.** The volumetric feeder is mounted on top of the weighing platform with a 10-liter hopper containing a horizontal agitator which helps break powder bridges

and arches in order to allow the powder to flow into the channel of the feeder screws. The agitation speed is set to 17% of the screw speed; therefore, the speed of the agitator changes with the changes in screw speed. The KT20 with a type C gearbox used in this study has a maximum processing screw speed of 154 RPM and a maximum motor speed of 2000 RPM (170 RPM @ 110% is also achievable by over-speeding). As the feeder delivers powder materials, the gravimetric controller acquires signals from the weighing platform as a function of time. By calculating the weight loss reported by the weighing platform, the controller can determine the instantaneous feed rate, compare the calculated results to the target setpoint, and then adjust the speed of the screw that dispenses the powder from the feeder to make the mass flow achieve the target setpoint. Coarse concave screws with 20 mm diameter were used in this study. The schematic of the KT20 feeder with a pre-refill hopper is shown in **Figure 4-1**. The feeder control box was connected to a laptop, which was used to record multiple feeding performance parameters. Values recorded include time, setpoint, mass flow (the instantaneous feed rate calculated by the feeder's controlling system), initial feed factor (kg/h), average feed factor (kg/h), screw speed, drive command (the percentage of instantaneous screw speed compared to the maximum screw speed), net weight, and perturbation value.

The feeder was first tared and filled up to 100% hopper level. The net weight of 100% hopper level was recorded. Then, the weights of 80% and 40% were calculated based on the weight achieved from 100% hopper level. Feeder calibration was then performed under volumetric throughput with 50% drive command, operated for 30 seconds, to obtain the initial feed factor. The mass fill of the feeder was then increased or decreased until the mass fill reached 80%, the starting fill level for all experiments. A feeder refill would occur

when the mass fill reached 40%, and powder would be added to the hopper until it was refilled up to 80% mass fill.

Each refill experiment first started from an 80% mass fill with a setpoint of 8 kg/h under gravimetric mode until the net weight reached refill min. The setpoint and screw was selected based on the previous experimental work which identified the optimal performance of the feeder[21, 135]. When the feeder reached a 40% mass fill, the control platform then switched the feeder from gravimetric to volumetric mode. A hopper refill was then performed to make the hopper level reach and get a bit over the refill max and after a few seconds of refill delay, the feeder changed back to gravimetric mode automatically. Each refill was performed twice to get an average result. A plot of feeder's operating principles in terms of 'net weight vs. time' is shown in **Figure 4-2**.

In addition to recording the feeder parameters from the loss-in-weight control box of KT20, a gain-in-weight catch scale was also used to monitor the discharge performance. A collection vessel was placed on an Ohaus laboratory scale, underneath the outlet of the feeder, to collect the material as it was discharged. The mass was recorded every 1 second by the catch scale and recorded by the same laptop that was recording the feeder parameters. The data recorded from the catch scale is used to determine the refill performance of the feeder.

Maximum deviation is the deviation between the maximum feed rate achieved during hopper refill and the target setpoint. Deviation time is the time gap between the change of feeder between volumetric and gravimetric mode, when the feeding process is out of specification. Percentage of total deviation (%Total) represents the total mass of powder

that fed in excess divided by the target feeding mass. An example plot to introduce the three quantified deviations is shown in **Figure 4-3**.

4.2.4. Multivariate analysis

In this work, multivariate analysis was conducted using The Unscrambler X 10.2 software (Camo, Oslo, Norway) and JMP Pro 15 (SAS Institute, NC, USA). Principle component analysis followed by the similarity scoring method was used to identify similarity between different materials, and then, the partial least squares regression method was used to build up a regression model between quantified deviation in mass flow caused by hopper refill and the correlation to material properties.

Principal component analysis followed by similarity scoring (PCA-SS) is a method to calculate the similarity between different objects, in this case, materials. In the PCA-SS approach, a PCA model was used to represent the material property data set (X) in a reduced dimension (Principal component space) such that the major axes of variability are identified. The data set X can be decomposed, based on the equation below, into a set of scores (T) and loadings (P), while the remaining variability is modeled as random error (ε):

$$X = TP^T + \varepsilon \qquad \text{Equation 4-1}$$

The columns T represent principal component (PC) scores of each material in the projected space. Loading P represent the significance of each material property in each principal component. Both T and P are obtained from eigenvectors and eigenvalues of the covariance matrix of X. A good indication of similarity between two materials is a measure of the Euclidean distance between them. Principal components are orthogonal to each other, and each is associated with the value that explains the proportion of variability in the data

set[137, 138]. Usually, only a few PCs are retained based on their statistical significance. The similarity scores between Material A and Material B can thus be calculated based on weighted Euclidean distance d_w:

$$d_{w(a,b)} = \sqrt{\sum_{i=1}^{n} w_i (a_i - b_i)^2} \qquad \text{Equation 4-2}$$

Where n is the total number of principal components selected in the model, a_i is the score of Material A in the i^{th} principal component, b_i is the score of material B in the i principal component, w_i is the weight of the i principal component, namely the relative variability explained by the it principal component:

$$0 < w_i < 1 \qquad \text{Equation 4-3}$$

The similarity score is based on the concept of distance between objects, which quantifies the similarity, or dissimilarity, between observations in the data set. A relatively small value of d_w indicates similarity between materials.

Since there are limitations for predicting process performance by using PCA-SS, namely the undefined sufficient size of material library, a regression model is needed by setting the process performance as the response variable into the predictive model. Partial least squares regression, also known as projection to latent structure regression, was used also to correlate a number of predictor variables X with response variables Y by finding the latent variables in the data set. The calculation of latent variables in the PLSR approach takes into account the response variables so that the linear combinations have maximal covariance[139].

Since the experiment was designed to maintain the same feed rate, 8 kg/h, for each of the different powders, the screw speeds will be different for each material due to the differences in material properties. To take this variable into consideration, drive command (percentage screw speed of the maximum screw speed) of each material was added into the material properties library. Hence, the PLSR model was built up from 30 material flow properties and one process parameter, drive command.

4.3. Results and discussion

Based on the material characterization results in Table 4-1, the material properties of calcined zeolite (Material A) were found to be in-between the maximum values and the minimum values of the other six test materials, which indicates that calcined zeolite's flow behavior is contained within the behavior studied and the model would not be used to extrapolate to an under represented area. A Bartlett's test of sphercity was first performed to test the feasibility of applying principal component analysis to the material properties dataset generated in this work. The P-value for the first four principal components are smaller than 0.001, which means a principal component analysis can be used for the reduction of this dataset.

To further illustrate the correlation and difference between materials and material properties, principle component analysis was then performed on all seven materials. **Figure 4-4a** shows a 2D scores plot with the first principal component (PC-1) versus the second principal component (PC-2), obtained from the principle component analysis. PC-1 and PC-2 each capture 54% and 26% of the variance in material flow properties. **Figure 4-4b** displays a 3D scores plot to visualize how different materials are distributed in projected spaces, which adds PC-3 to the plot in Figure 4a.

Refill experiments on all the materials were done first to obtain the results of three types of deviations. **Figure 4-5** shows the refill performance of each material in terms of 'feed rate vs time', from which differences in all three types of deviations among seven materials can be obtained and **Figure 4-6** shows the quantified deviations of a) maximum deviation, b) deviation time and c) % total deviation.

4.3.1. PCA followed by similarity scores (PCA-SS)

To identify the similarity/difference in material properties and potential refill performance between different materials in the library, the weighted Euclidean distances between materials in the scores plot of the PCA analysis were calculated based on the coordinates on the first four generated principal components together with their weights. As shown in **Figure 4-7**, taking Material A as the target material, the weighted Euclidean distance between the target and the six other materials were calculated and sorted from the smallest to biggest. Fine zeolite was found to be the closest material in distance to Material A.

To validate the results from PCA-SS, feeder refill experiments on fine zeolite and Material A were then performed using the set up described in section 2.3. **Figure 4-8** shows the comparison of refill performance between Material A and Fine Zeolite, including all the three types of deviations. Results show that Material A and Fine Zeolite have relatively similar deviations which indicates that they have similar refill performance and it proves the PCA-SS prediction.

4.3.2. Partial Least Squares Regression (PLSR)

To further evaluate the correlation between materials' refill performance and material flow properties, another multivariate analysis method, partial least squares regression, was used. By setting material properties as 'X' variables and each quantified deviation as a 'Y'

variable, three PLS regression models were developed based on the six calibration materials (excluding Material A). Then, Material A's material properties were input into the model and the three types of quantified deviation were predicted. **Figure 4-9** shows the comparison between the experimental values and PLSR-predicted values. Only minor differences were seen between the measured and predicted values, for all the three types of deviations, indicating that the predictive models had successfully built up the correlation between material properties and the performance of the feeder during a refill process.

To further validate the model, each of the six calibration materials were selected to be the new 'Material A', and the remaining six materials were used as the new calibration materials to build up new PLSR models. After all materials were modeled, a full comparison plot between measured values and predicted values was developed for all the seven materials involved in this work, **Figure 4-10**. The slope of the 'measured vs predicted' plots for maximum deviation was 0.9122, for deviation time it was 1.0242, and for the percentage of total deviation it was 1.0415. The slopes were all close to one with R squares higher than 0.9 and P-values much less than 0.05, which means that the predicted values are in good agreement with the measured values and this model is good to be used for prediction. This again proves that deviations in mass flow caused by hopper refill are highly correlated to the material flow properties and that it is possible to predict these behaviors.

Moreover, based on the PLSR model, the regression coefficient of each material property can be obtained. **Figure 4-11** shows the regression coefficient of each material property for a) maximum deviation, b) deviation time, and c) total deviation. Material properties with positive values indicate that they are positively related to the deviation, and *vice versa*.

The regression coefficient plots acquired from the model point out that permeability, conditioned bulk density, and shear cell properties were significantly correlated to maximum deviation and deviation time; however, permeability, shear cell properties, and particle size are the crucial properties to %total deviation. More materials and feeder conditions will require investigation on feeder mass flow performance during a refill event to further develop this regression model. A model with a more comprehensive material database will be more accurate for prediction.

4.4. Conclusion

Two methodologies, PCA and PLSR, were utilized to develop predictive correlations between material flow properties and the perturbations to mass flow experienced in loss-in-weight feeders due to hopper refill. The method includes characterization of material flow properties, characterization of feeder performance during hopper refill, and predictive multivariate analysis. Six calibration materials, with varying flow properties, were first characterized in terms of 30 specific material bulk property measurements. Two approaches were discussed and compared in this work. The first was PCA-SS; the approach was based on weighted Euclidean distances, calculated after performing the principal component analysis on the entire data set. The bulk properties of the material that had the shortest distance, in the PCA scores plot, to the material of interest, calcined zeolite, was compared to and confirmed to have similar flow behavior to each other. The PLSR approach further quantified the correlation between material properties and the deviations caused by hopper refill.

This study showed that the feed rate deviations caused by the refill of the feeder hopper were highly correlated with, and predictable from, bulk material properties. The predicted

mass flow deviation results were, in general, in good agreement with the experimental results. The work presented here has shown an efficient approach to correlate material properties with process performance using multivariate analysis. Moreover, this study also identifies the significant material flow properties for each type of deviation during hopper refill. Therefore, potential mass flow deviations due to feeder refills can be forecasted, based on the materials bulk properties, so that refills can be performed under selected conditions that lessen the impact on the mass flow.

The model developed from this study can be especially powerful when the amount of a given new material is limited, or if the new material is expensive or dangerous. This model can be easily updated with more materials and properties input into the database. This method can also be applied to process scale-up, validation and commercial manufacturing in order to capture process knowledge and identify predictability by adding additional performace measurements.

Future work should include testing of a wider range of material properties and include additional feeder process parameters. Additionally, broadening the study to additional feeders, both on different sizes and manufacturers, and performing the refill method on feeders with different control algorithm, is desirable. Finally, reducing the number of measurements by further identifying the essential properties for different processes would be a significant improvement to reduce the number of characterization tests required to perform the predictions.

4.5. Tables for Chapter 4

Table 4. 1: 30 material flow properties were tested for 7 materials including fine alumina, fine zeolite, molybdenum oxide, satintone, lactose monohydrate, calcined zeolite Y-655 (Material A) and zeolite.

	Fine alumina	Fine Zeolite	Molybdenum oxide	Satintone	Lactose	Y-655	Zeolite
Compressibility@15 kPa	29.6	14.7	25.0	36.4	0.7	25.9	35.0
Conditioned Bulk Density (g/ml)	0.3	0.9	1.4	0.5	21.0	0.3	0.3
Permeability	32.9	8.6	8.0	4.1	13.1	10.0	4.9
Cohesion @ 3kPa	0.4	0.5	1.0	0.9	0.5	0.8	0.8
Unconfined Yield Strength @ 3kPa	1.5	1.6	4.3	3.7	1.8	2.9	3.0
Major Principle Stress @ 3kPa	5.5	4.4	7.2	7.2	5.5	6.0	6.2
Flowability @ 3kPa	3.7	2.8	1.7	1.9	34.4	2.1	2.1
Angel of Internal Friction @ 3kPa	31.2	24.9	38.9	37.1	3.1	31.0	33.0
Cohesion @ 6kPa	0.8	0.5	1.5	1.2	0.8	1.2	1.8
Unconfined Yield Strength @ 6kPa	2.6	1.6	6.3	5.0	2.9	4.2	6.3
Major Principle Stress @ 6kPa	10.5	8.6	13.6	13.4	10.7	11.2	12.5
Flowability @ 6kPa	4.0	5.4	2.2	2.7	33.3	2.7	2.0
Angel of Internal Friction @ 6kPa	28.7	25.4	39.6	38.5	3.7	31.1	31.2
Cohesion @ 9kPa	1.0	0.6	2.2	1.3	0.9	1.5	1.8

Unconfined Yield Strength @ 9kPa	3.3	1.7	8.9	5.3	3.5	5.3	6.5
Major Principle Stress @ 9kPa	15.6	12.9	20.3	20.0	16.1	16.5	18.5
Flowability @ 9kPa	4.7	7.5	2.3	3.7	33.6	3.1	2.8
Angel of Internal Friction @ 9kPa	28.6	23.8	36.9	37.5	4.6	30.4	31.3
Cohesion @ 15kPa	1.4	0.5	2.5	1.0	1.1	1.8	1.7
Unconfined Yield Strength @ 15kPa	4.6	1.5	10.5	4.4	4.3	6.5	6.4
Major Principle Stress @ 15kPa	25.3	21.2	32.1	31.2	26.0	26.2	28.7
Flowability @ 15kPa	5.5	14.2	3.1	7.2	34.1	4.1	4.5
Angel of Internal Friction @ 15kPa	27.6	24.6	39.9	40.7	6.0	31.1	33.5
Basic Flow Energy (mJ)	212.4	574.0	4218.5	858.7	1338.5	234.5	401.4
Stability Index	1.2	1.4	1.1	1.1	1.0	1.1	1.0
Flow Rate Index	1.9	1.7	1.3	1.5	1.4	2.0	1.7
Specific Energy (mJ/g)	6.9	7.4	12.2	14.9	9.1	8.1	9.9
D10	1.0	0.9	0.8	0.9	10.3	0.8	0.8
D50	4.1	3.9	3.7	6.1	63.5	2.3	3.0
D90	11.5	5.8	10.3	21.1	150.3	7.6	10.4

4.6. Figures for Chapter 4

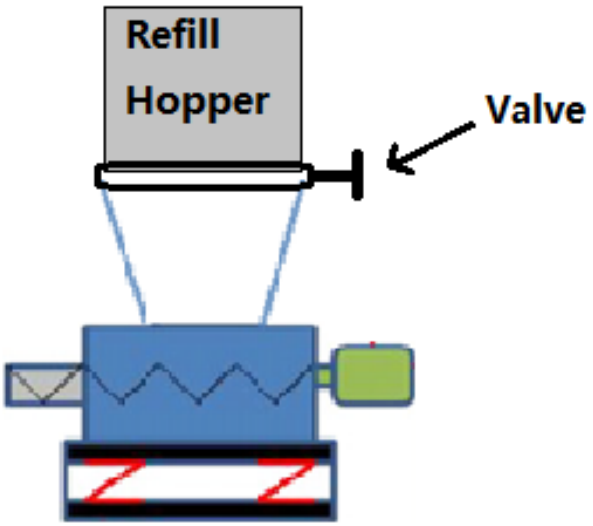

Figure 4. 1: **Schematic of feeder components and refill strategy.**

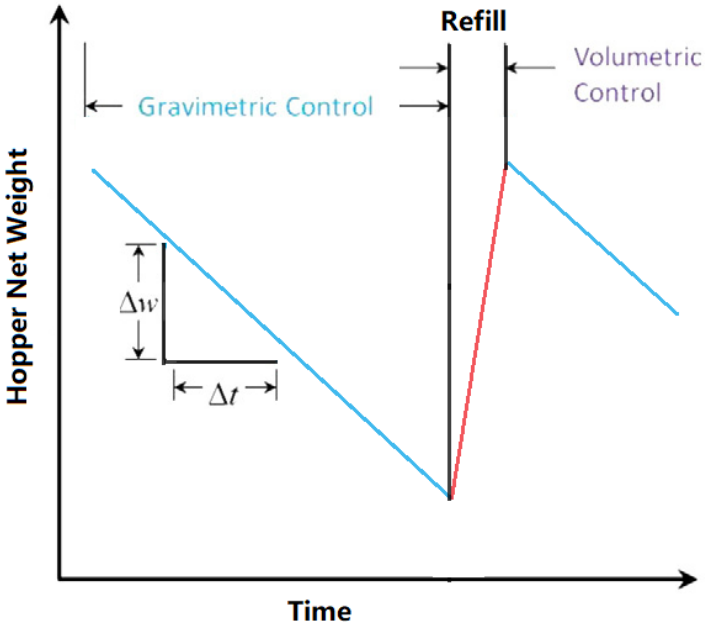

Figure 4. 2: **Loss-in-weight feeder operating principle depicting the loss-in-weight feeding cycle created by periodic hopper refill.**

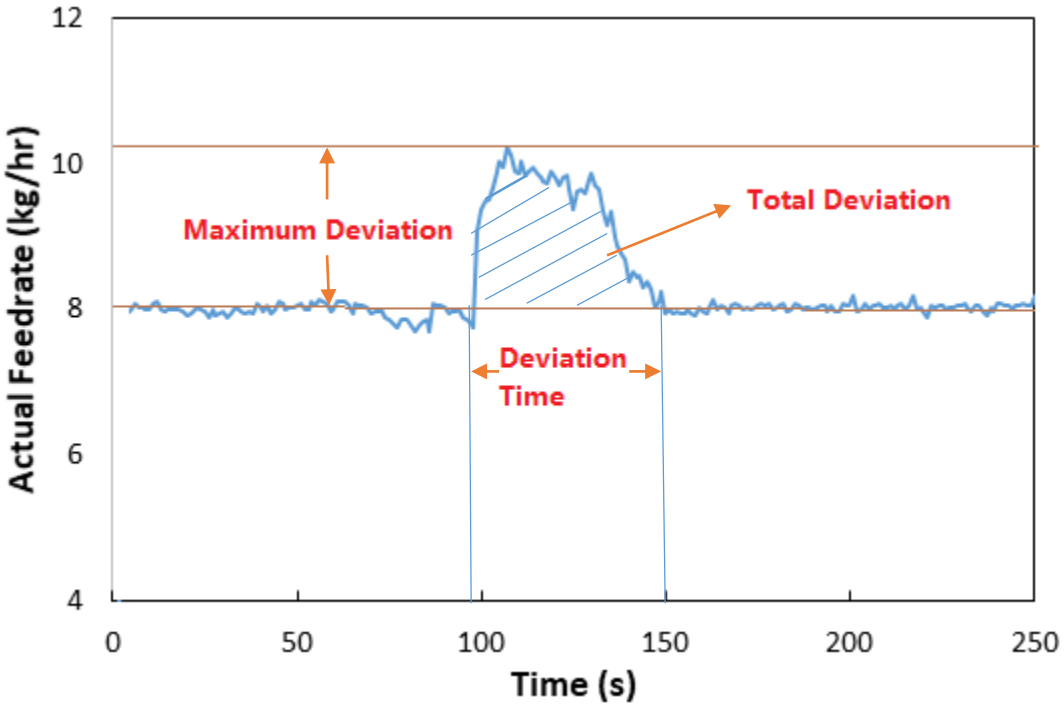

Figure 4. 3: Methods for quantifying the deviation from setpoint: a) magnitude of the maximum deviation, b) the time that the feed rate is out of specification, and c) the percentage of total deviation over set amount.

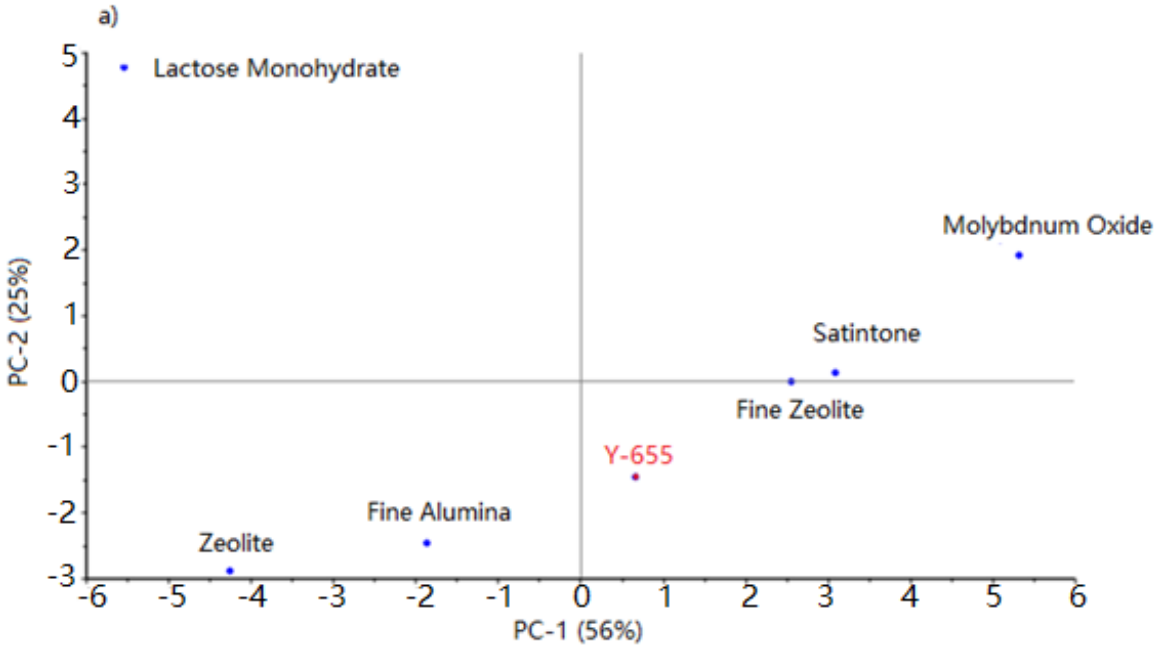

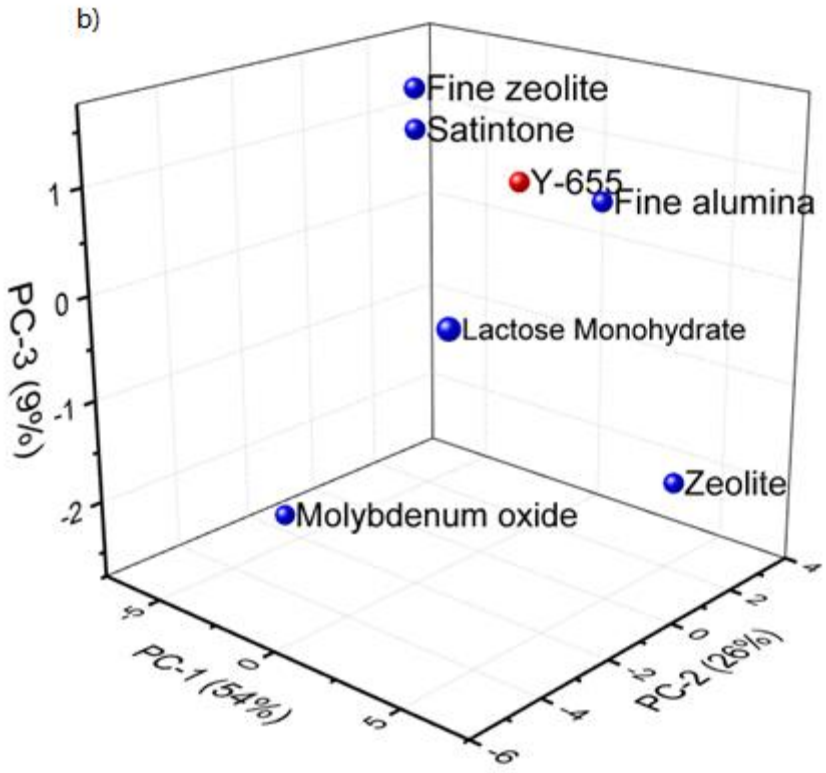

Figure 4. 4: **a) A 2D plot based on PC-1 and PC-2 and b) a cubic score plot was used to visualize how different materials are distributed in the projected spaces. The coordinates of each material are shown as the scores of each principal component.**

(a)

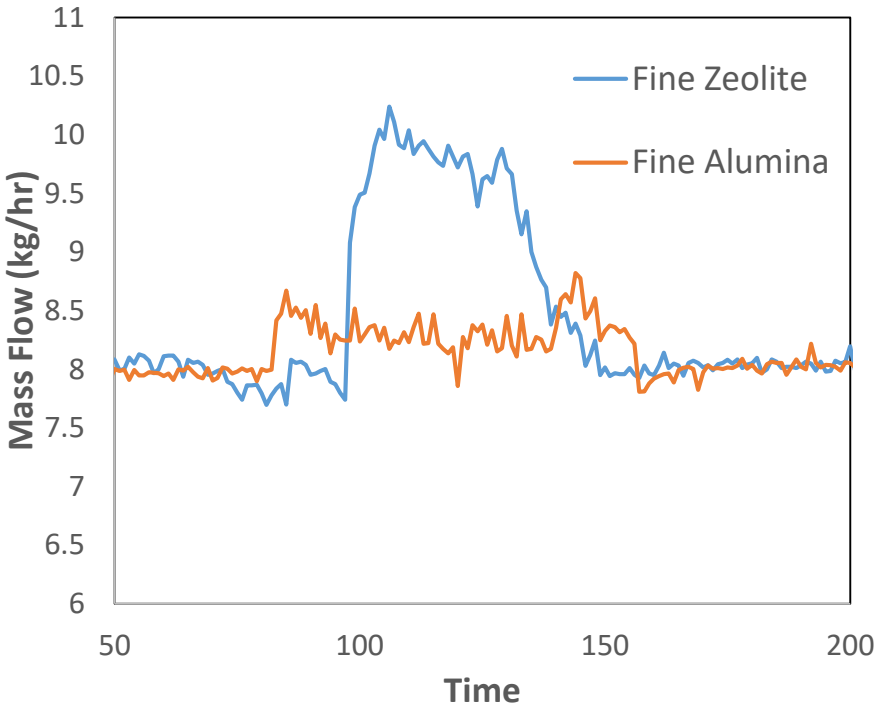
11
10.5
10
9.5
9
8.5
8
7.5
7
6.5
6
Mass Flow (kg/hr)
50
100
150
200
Time
Fine Zeolite
Fine Alumina

(b)

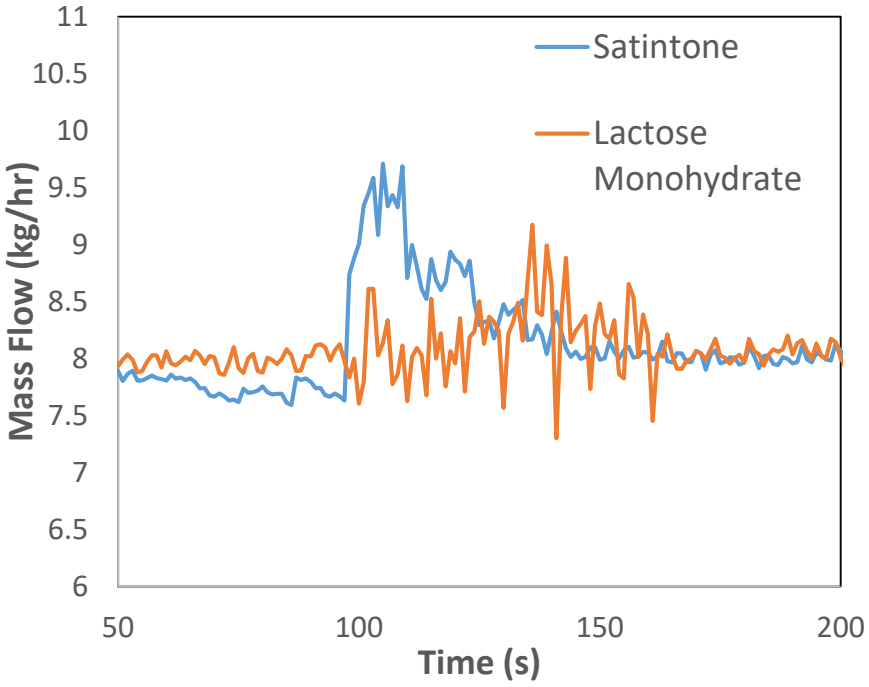
11
10.5
10
9.5
9
8.5
8
7.5
7
6.5
6
Mass Flow (kg/hr)
50
100
150
200
Time (s)
Satintone
Lactose Monohydrate

(c)

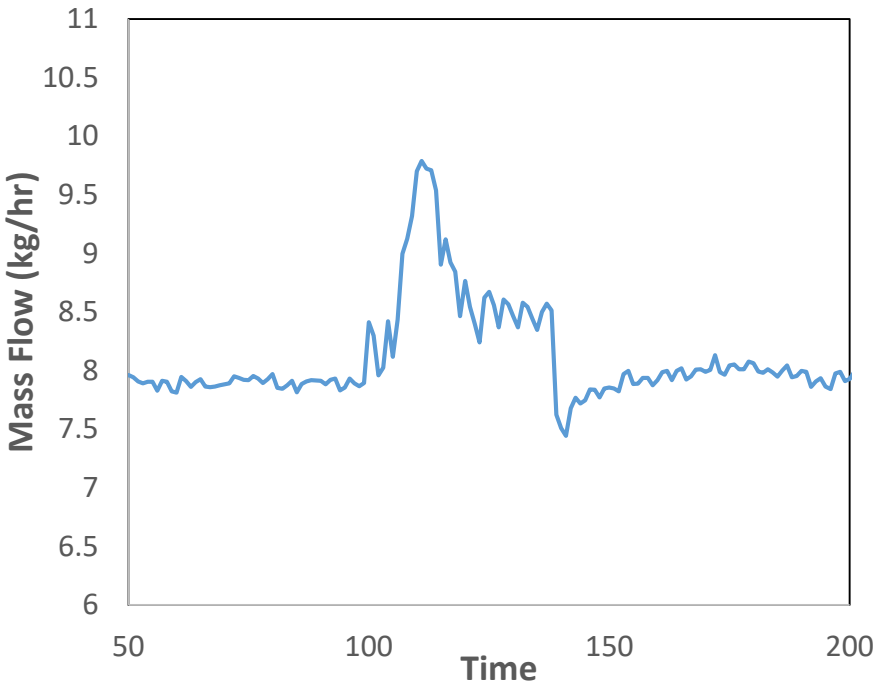
11
10.5
10
9.5
9
8.5
8
7.5
7
6.5
6
Mass Flow (kg/hr)
50
100
150
200
Time

(d)

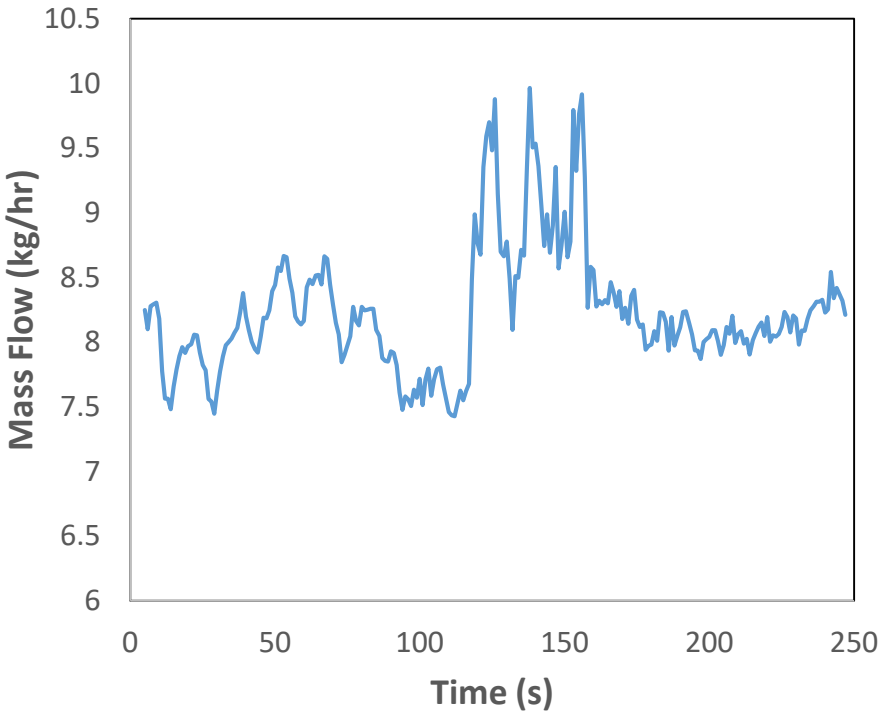
10.5
10
9.5
9
8.5
8
7.5
7
6.5
6
Mass Flow (kg/hr)
0
50
100
150
200
250
Time (s)

(e)

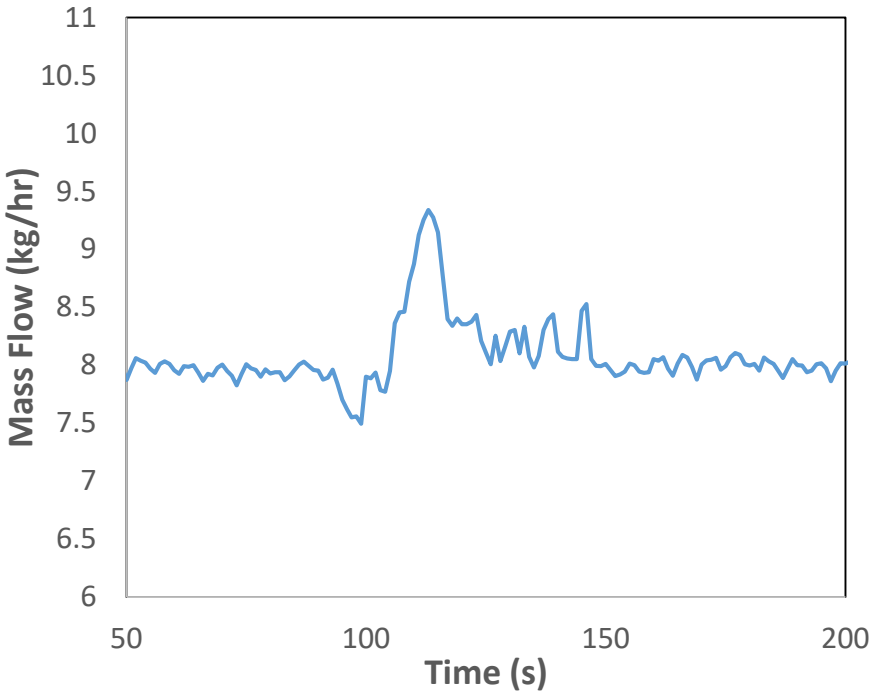

Figure 4. 5: The feed rate deviation of the feeder caused by hopper refill vs. time of (a) Fine alumina and Fine zeolite, (b) Lactose monohydrate and Satintone, (c) Zeolite, (d)Molybdenum Dioxide (e) Calcined zeolite Y655 (Material A).

(a)

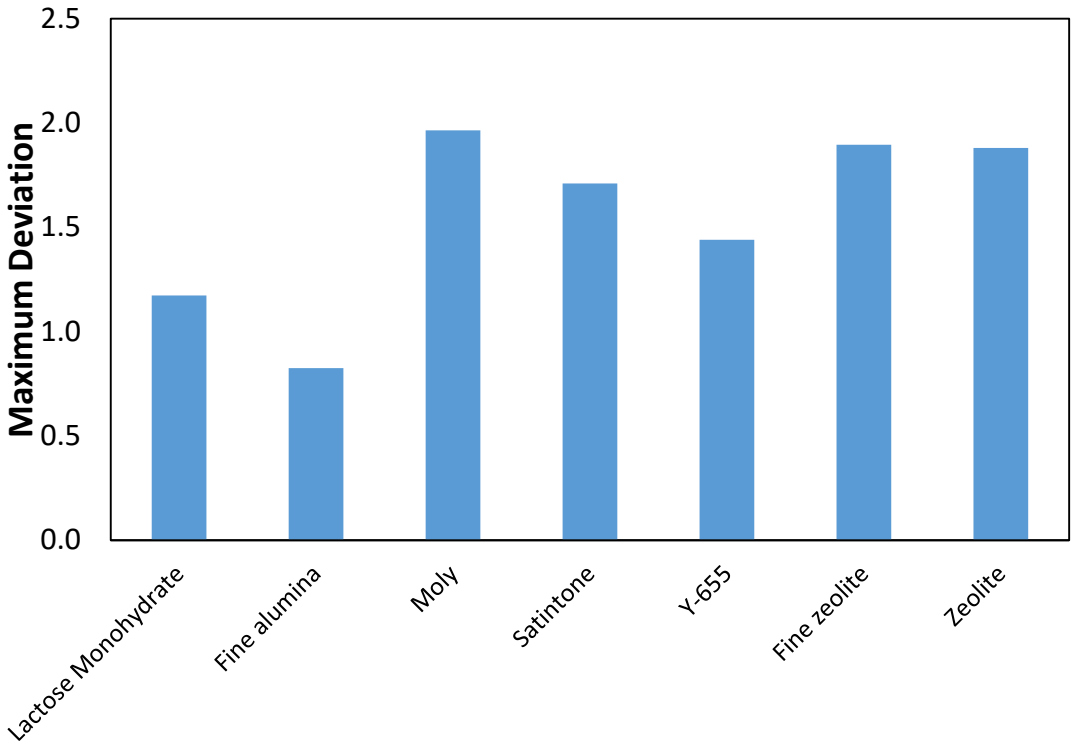
Maximum Deviation
2.5
2.0
1.5
1.0
0.5
0.0
Lactose Monohydrate
Fine alumina
Moly
Satintone
Y-655
Fine zeolite
Zeolite

(b)

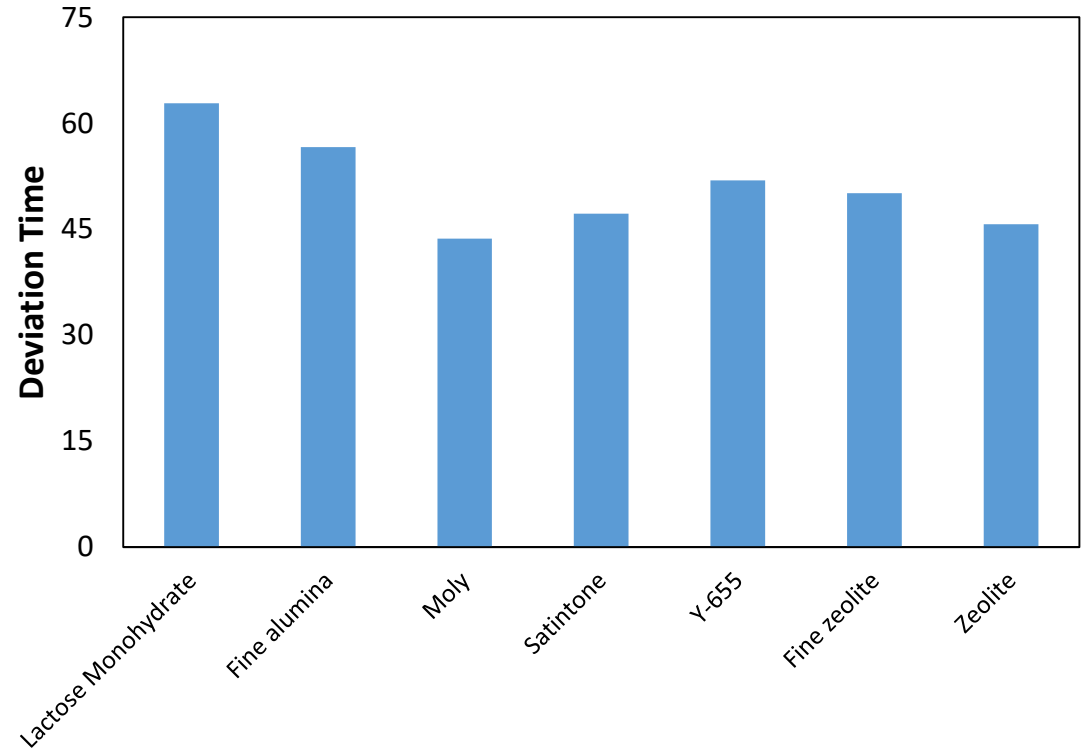
Deviation Time
75
60
45
30
15
0
Lactose Monohydrate
Fine alumina
Moly
Satintone
Y-655
Fine zeolite
Zeolite

(c)

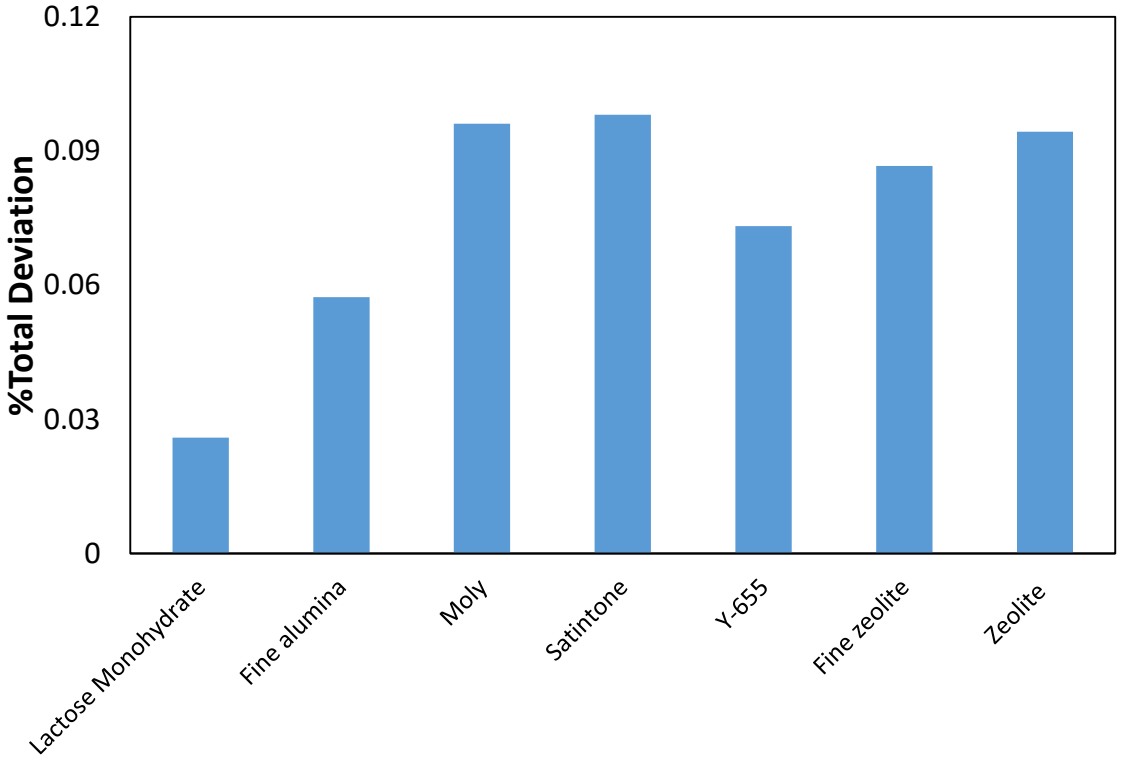

Figure 4. 6: **Measured (a) Maximum Deviation, (b) Deviation time, and (c) %Total Deviation of 7 characterized materials.**

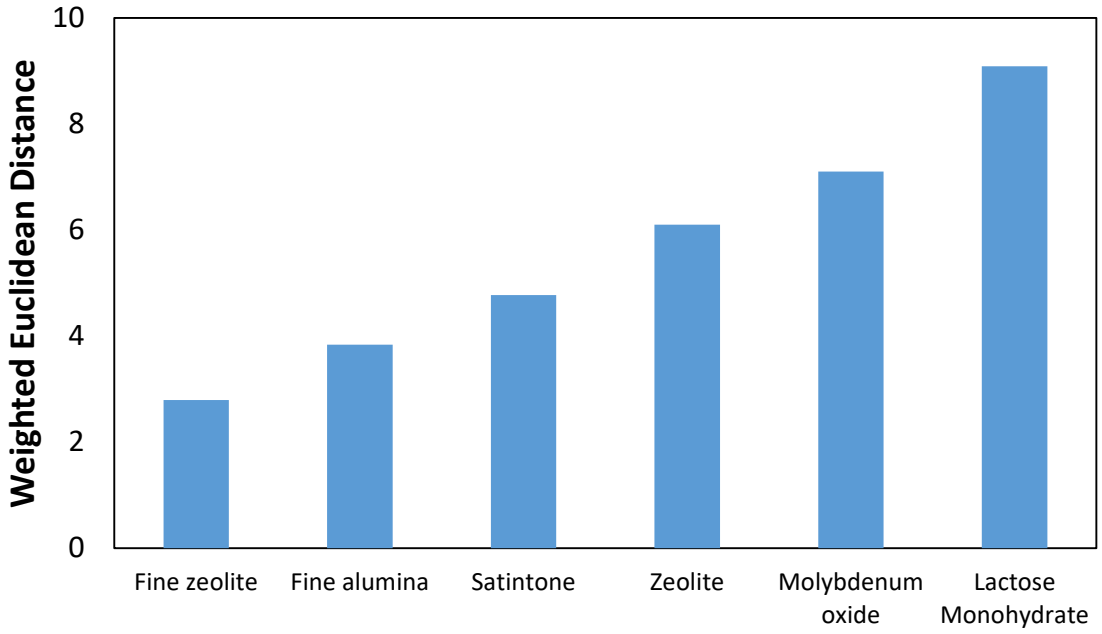

Figure 4. 7: **Weighted Euclidean distance between Y-655 (Material A) and other existing materials. Based on the concept of distance between objects in the reduced dimensions, Fine Zeolite was identified to be the most similar material to Material A.**

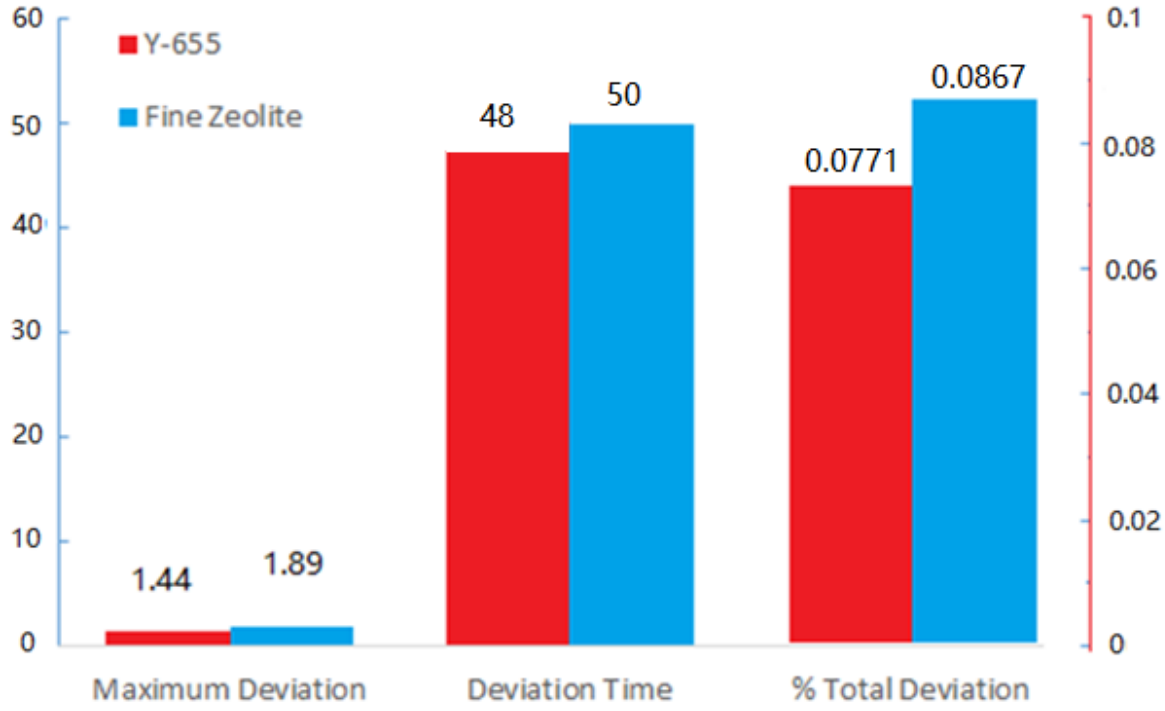

Figure 4. 8: **Comparison of Measured Maximum Deviation, Deviation Time and % Total Deviation between Y-655 and Fine Zeolite.**

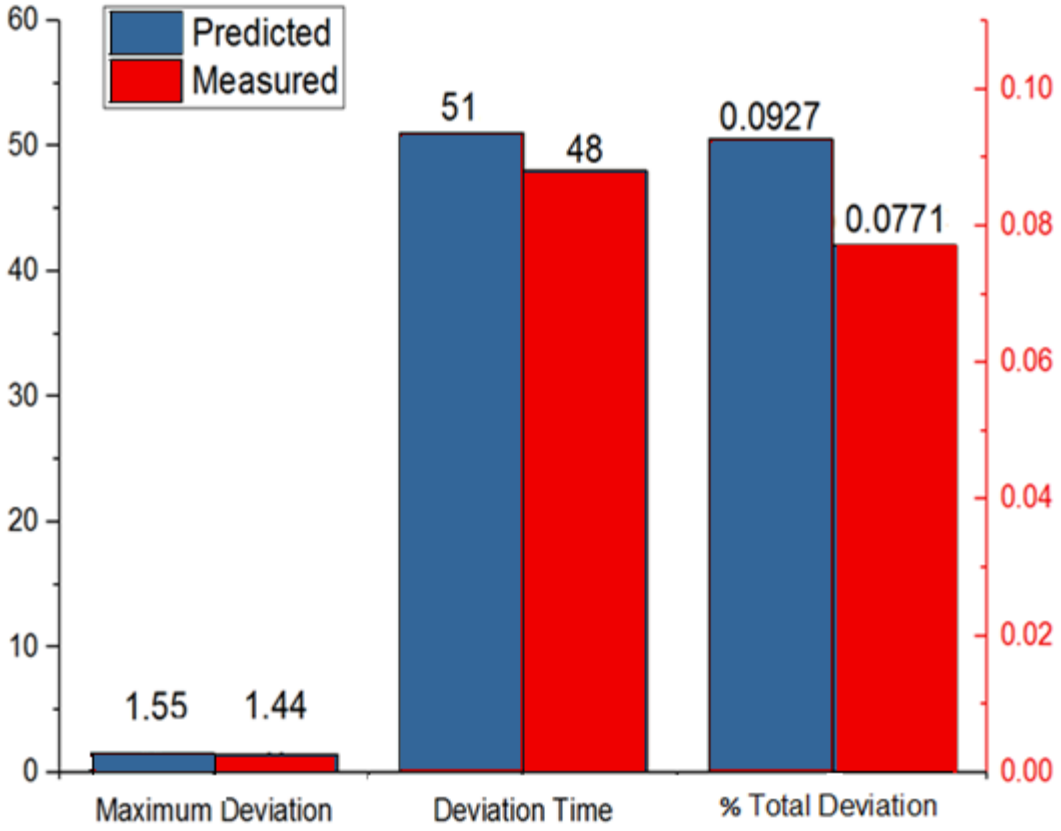

Figure 4. 9: **Comparison between predicted values and measured values of maximum deviation, deviation time and % total deviation based on PLSR model.**

(a)

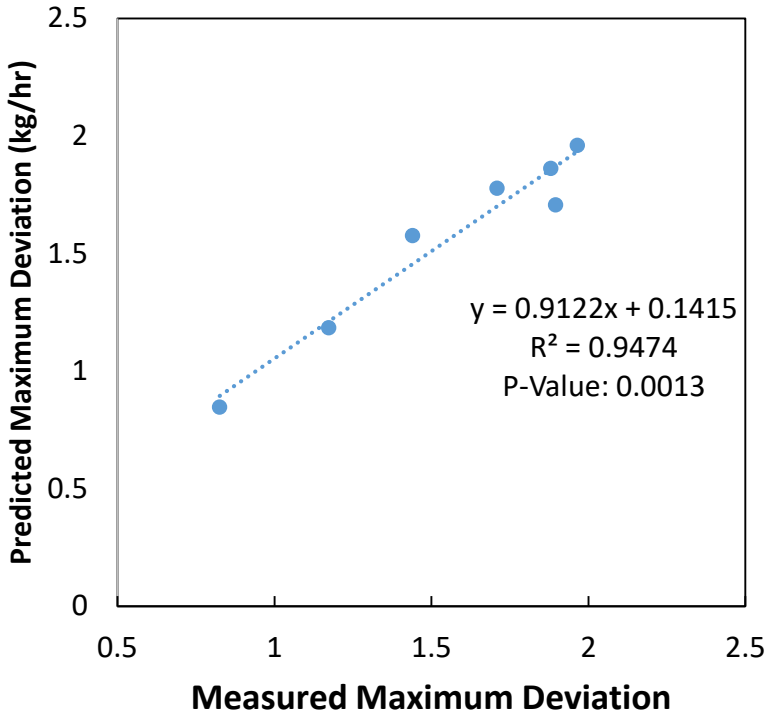
Predicted Maximum Deviation (kg/hr)
Measured Maximum Deviation
y = 0.9122x + 0.1415
R² = 0.9474
P-Value: 0.0013
0
0.5
1
1.5
2
2.5

(b)

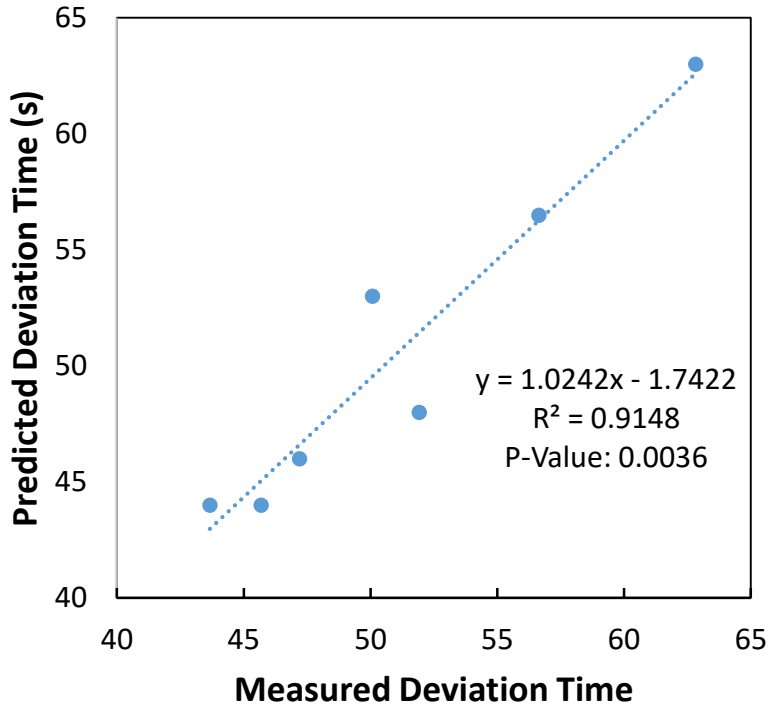
Predicted Deviation Time (s)
Measured Deviation Time
y = 1.0242x - 1.7422
R² = 0.9148
P-Value: 0.0036
40
45
50
55
60
65

(c)

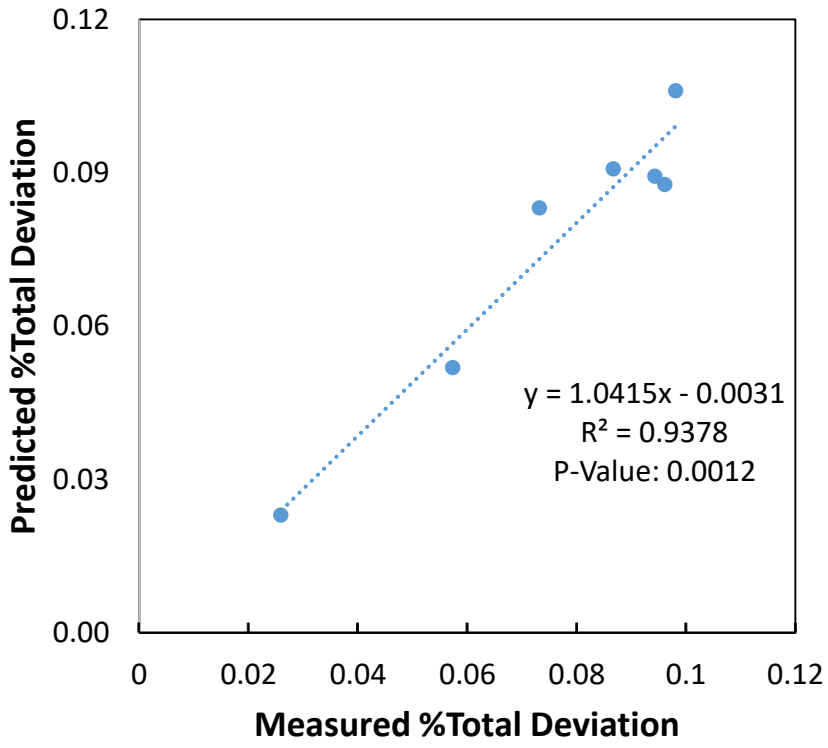

Figure 4. 10: **Predicted values versus measured values of (a) Maximum deviation, (b) Deviation time, and (c) % Total deviation of all the materials in the predictive library.**

(a)

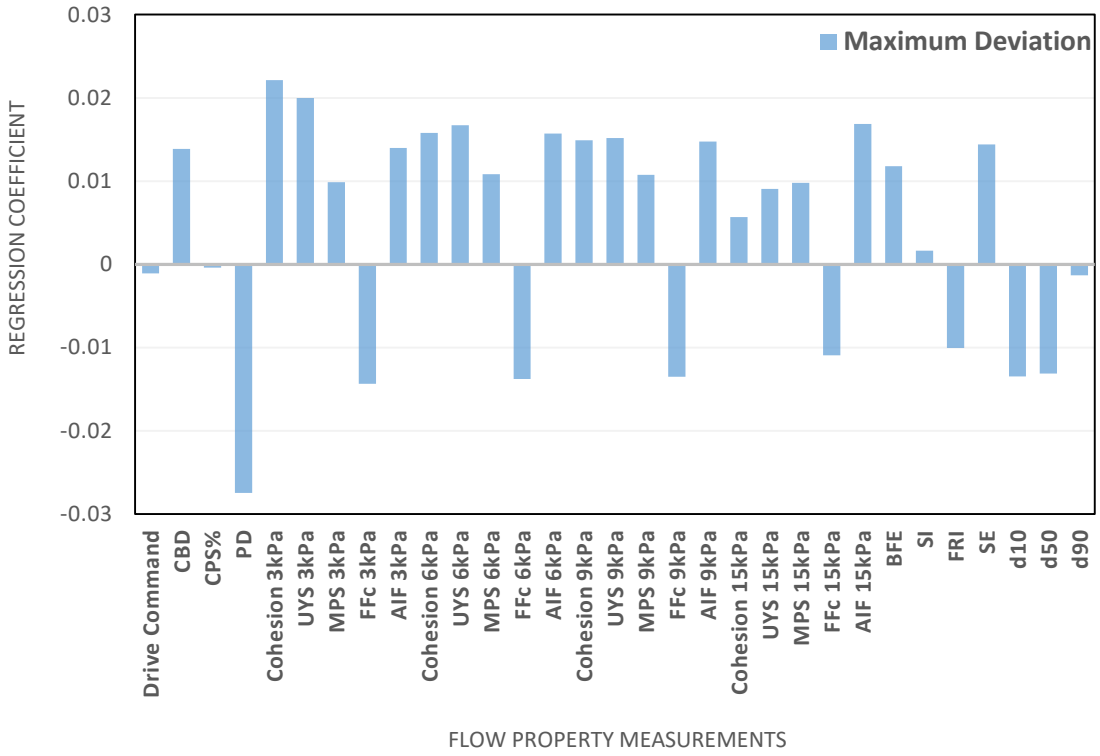
Maximum Deviation
REGRESSION COEFFICIENT
0.03
0.02
0.01
0
-0.01
-0.02
-0.03
Drive Command
CBD
CPS%
PD
Cohesion 3kPa
UYS 3kPa
MPS 3kPa
FFc 3kPa
AIF 3kPa
Cohesion 6kPa
UYS 6kPa
MPS 6kPa
FFc 6kPa
AIF 6kPa
Cohesion 9kPa
UYS 9kPa
MPS 9kPa
FFc 9kPa
AIF 9kPa
Cohesion 15kPa
UYS 15kPa
MPS 15kPa
FFc 15kPa
AIF 15kPa
BFE
SI
FRI
SE
d10
d50
d90
FLOW PROPERTY MEASUREMENTS

(b)

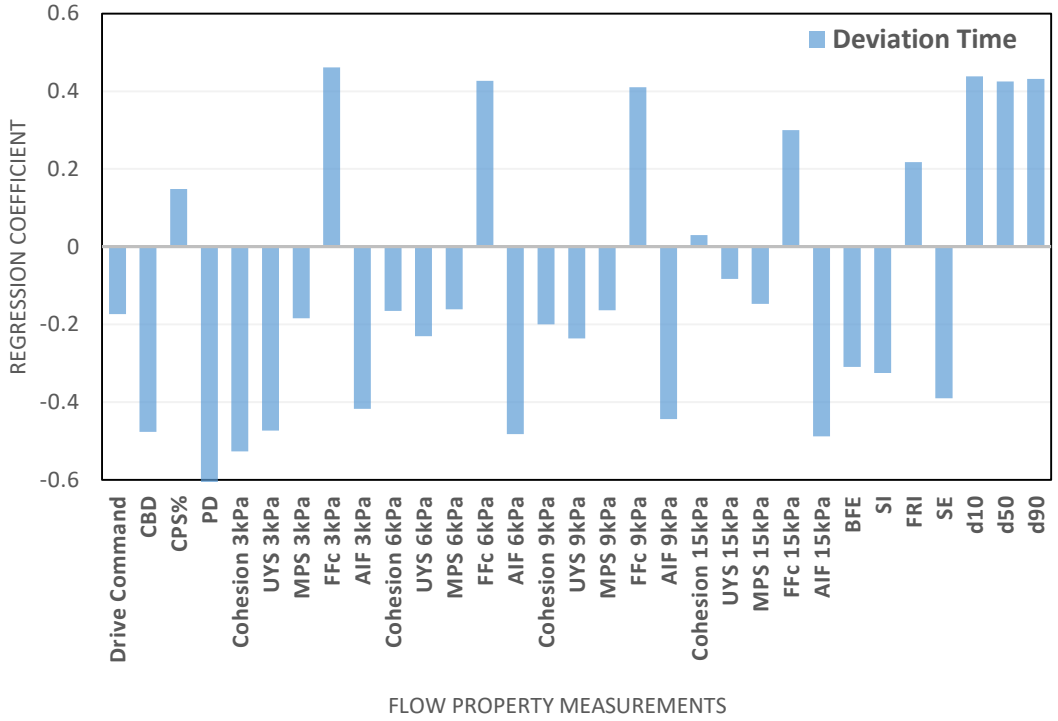
Deviation Time
REGRESSION COEFFICIENT
0.6
0.4
0.2
0
-0.2
-0.4
-0.6
Drive Command
CBD
CPS%
PD
Cohesion 3kPa
UYS 3kPa
MPS 3kPa
FFc 3kPa
AIF 3kPa
Cohesion 6kPa
UYS 6kPa
MPS 6kPa
FFc 6kPa
AIF 6kPa
Cohesion 9kPa
UYS 9kPa
MPS 9kPa
FFc 9kPa
AIF 9kPa
Cohesion 15kPa
UYS 15kPa
MPS 15kPa
FFc 15kPa
AIF 15kPa
BFE
SI
FRI
SE
d10
d50
d90
FLOW PROPERTY MEASUREMENTS

(c)

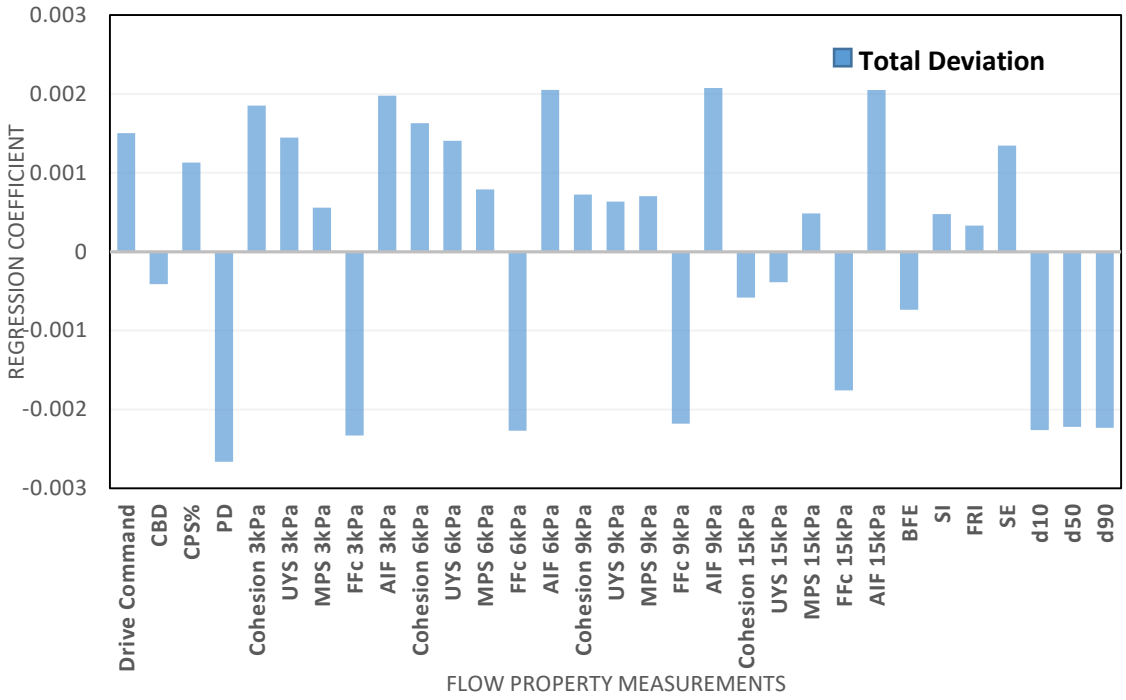

Figure 4. 11: **Regression Coefficient for each flow property variables for PLSR model of (a) Maximum Deviation, (b) Deviation Time, and (c) %Total Deviation prediction.**

Chapter 5. Dampening Effect on Feed Rate Variation from Downstream Unit Operations in Continuous Manufacturing

5.1. Introduction

Continuous manufacturing offers a number of economic and quality advantages over batch processing [6-9] including higher production capacity, smaller equipment, and the capability of implement of process analytical technology (PAT) and control system to monitor the critical quality attributes (CAQs) and critical process parameters (CPPs) in real time [10, 11]. Advancement in the development of equipment design, process analytical technology, control systems, and modeling tools has facilitated the growing interest in implementation of continuous manufacturing in major pharmaceutical companies around the world. A draft guidance for industry has been provided by FDA on the quality considerations for continuous manufacturing in 2019, and there are several FDA-and EMA-approved products on the market which were being manufactured by continuous manufacturing.

Loss-in-weight feeders are a vital component in manufacturing, as they are used to correctly meter a given weight of material per time. They serve as the top unit operations in the continuous manufacturing in order to maintain the target concentration of the API and the process stability, but they are also the first unit operations that introduce variability into the line due to material properties [21, 23, 72], design and operating conditions of the feeder[121, 140, 141], hopper refilling operations [107], and unexpected disturbance from the operating environment [24, 105]. Cohesive materials that tend to agglomerate, or entrap air within the powder bed, will have lower ranges in feed rate than easy flowing, well packing, material, per a given set up. Irregularity in bed density, due to entrapped air, can

result in unstable flow rate and variability. Another issue with powders are electrostatic effects, such as charge buildup, which can lead to material sticking to the exit of feeders, or on any exposed surface. Periodic hopper refill of the feeders can also lead to inconsistent and poor feeding performance[20]. These types variation in feed rates can then be transferred down to succeeding unit operations and affect the quality of the final products.

Fortunately, one of the major advantages of continuous manufacturing systems is that downstream equipment has been shown to be capable to filter the incoming variability in powder feed rates by providing back-mixing in the continuous blender and the feed frame in the tablet press, decreasing the risk of composition variation and improving content uniformity [37, 67, 142-148], which is one of the critical quality attributes of finished product. However, since as shown in the previous chapter composition variations from the feeders depend on material properties, content uniformity in the final product can also be affected by API flow properties, the design and operating conditions of the feeders and continuous blender, and the feed frame in the tablet press.

Another advantage of continuous manufacturing is that it enables the monitoring of API concentration during processing with suitable PAT implementation. Near infrared spectroscopy (NIR) is one of the most commonly used analytical techniques in continuous pharmaceutical manufacturing of solid oral dosage forms [149] and work have been performed to develop the use of NIR to determine the concentration of powder blends, drug content, hardness, moisture content in tablets and also dissolution profile[147, 150-155]. Typically, there are two locations have been reported to implement NIR to evaluate the powder blend uniformity in the continuous manufacturing, one is in the transition chute where the powder discharges from the continuous blender before entering the feed frame

[11, 150, 151, 156, 157], and the other is he feed frame in the tablet press before the blends enter the press dies [149, 158-160].

Previous work has examined the mixing effect from the blender and the feed frame and its effect on blend uniformity before and after these two processes. Dubey et al. identified the back mixing effect of the continuous blender due the backward facing blades and the impact of process parameters on critical attributes of a continuous blender [161]. Dalvi et al. studied the mixing effect of the feed frame by monitoring the Ibuprofen's concentration during and after tablet compression [162]. Simulation work on powder flowing in a lab-scale feed frame to investigate the design and operating parameters on measures of tablet quality has been performed by Ketterhagen [163]. Ward et al. performed a blend potency study in feed frame using NIR involving the study of mixing dynamics in the feed frame[164]. However, there is still a lack of work regarding how blend homogeneity measured at the inline monitoring point and final product quality react to different levels of disturbance from the feeders, and the effects of various process parameters such as blender speed and total throughput.

The work described in this chapter provides the comparison between the blend uniformity in the inline monitoring point (chute) and the content uniformity in the tablets when different levels of disturbance are applied to the API feed rate with two different formulations of low dosage and high dosage of API concentration. Effect from hopper refill operations on API and major excipient were also involved to mimic the perturbations that may occur during actual production. Moreover, the effect from different blender speeds and different total throughputs were also studied. The method and results of this work can

be applied to the optimization of PAT implementation and the risk assessment of continuous pharmaceutical manufacturing.

5.2. Materials and Methods

This work was performed in the continuous manufacturing platform of direct compaction (DC) at the Engineering Research Center for Structured Organic Particulate Systems (ERC-SOPS) laboratory. A schematic of the composition of the platform is shown in Figure 5-1.

5.2.1. Materials

5.2.1.1. High dosage formulation

A commercially available formulation was used for the study of high dosage formulation. The formulation consists of four materials including API X (Janssen Ortho LLC- Gurabo), Silicified MCC Prosolv 90 (JRS Pharma), Crospovione (Ashland) and Magnesium stearate (FMC Corporation). With a total throughput of 40 kilograms per hour, the detailed composition of the formulation and the target feed rate values for each raw material are shown in Table 5-1.

5.2.1.2. Low dosage formulation

For low dosage study, the formulation was designated with a commonly used API, Acetaminophen (Powder Grade APAP, Mallinckrodt Pharmaceuticals). The other three materials in the low dosage formulation are the same as those in high dosage, Silicified MCC Prosolv 90 (JRS Pharma), Crospovione (Ashland) and Magnesium stearate (FMC Corporation). A total throughput of 40 kilograms per hour was first evaluated and then a study of effect of throughput was conducted with two more throughputs, 20 kilograms per

hour and 30 kilograms per hour. A breakdown in drug composition and target value of feed rates are shown in Table 5-2.

5.2.2. Unit operations

The continuous manufacturing platform used in this work consists of three levels. Four twin screw loss-in-weight feeders including three KT20 and one KT35 (Coperion K-Tron Pitman, Inc. Sewell, NJ, USA) are located on the top level to feed 4 components in the formulation into the system. The numbers 20 and 35 indicate the diameter of a screw in millimeters. A larger diameter results in larger feeding capacity. The feeder delivers powder materials in gravimetric mode, which operates a gravimetric controller that acquires signals from the weighing platform as a function of time and screw speed. By calculating the weight loss reported by the weighing platform, the controller can determine the instantaneous feed rate, compare the calculated results to the target setpoint, and adjust the speed of the screw that dispenses the powder form the feeder to make the mass flow achieve the target setpoint. The feeders' control boxes were connected to a laptop, which was used to record multiple feeding performance parameters. Values recorded include time, setpoint, mass flow (the instantaneous feed rate calculated by the feeder's controlling system), initial feed factor (kg/h), average feed factor (kg/h), screw speed, drive command (the percentage of instantaneous screw speed compared to the maximum screw speed), net weight, and perturbation value. These feed streams are then connected to a continuous blender (Glatt GCG-70) on the middle level. The raw materials are continuously fed to the inlet port of the blender where they are mixed and discharged from the outlet port. The continuous blender is a single screw convection blender configured with multiple blades where the impeller is fitted with 24 evenly spaced blades. Eight blades (1/3rd) on both ends

of the impeller are angled forward, while the middle 1/3rd are alternated forward and backward to add back-mixing to the powder stream. The blends then flow through a vertical installed chute which consists of a stainless-steel pipe with a 3-inch internal diameter partially flattened to form a rectangular interface. A Near-infrared (NIR) spectroscopic probe Bruker Matrix (Brucker Corporation, Billerica, MA, USA) is positioned in a 3-inch diameter sensing interface on the chute for real time measurement of blend uniformity of the drug substance in the powder blend. Powder blend is then conveyed to a rotary tablet press FETTE 1200i (Fette Compacting America, NJ, USA) on the bottom level with a Fill-O-Matic three chamber and two-level feed frame. A feed frame is a mechanical device used to force-feed powders into tablet press dies which also provide back-mixing to the incoming powder blend to improve blends uniformity. The blend finally then fills in dies and is subsequently compressed to 600 mg tablets.

5.2.3. Multivariate analysis and model build-up

5.2.3.1. In-line NIR spectral acquisition

In-line NIR spectra were acquired using a Bruker Matrix spectrometer (Bruker corporation, Billerica, MA, USA). The probe of NIR spectrometers was attached on the chute which connected after the continuous blender and within tablet press feed frame. The probe was orthogonal to the powder flow to ensure scanning flowing powder as much as possible. The spectra were collected in reflectance mode under a spectral range of 4000-12000 cm^{-1} and resolution of 64 cm^{-1}. For each spectrum, a total of 32 scans were obtained and averaged. The acquisition time for this setting is approximately 5.0 s. The control software is Opus 7.2 and used for continuous spectral acquisition process.

5.2.3.2. Tablets NIR spectral acquisition

The transmission NIR spectra of tablets were obtained by using a Multipurpose Analyzer (MPA), Fourier Transform Near Infrared (FT-NIR) Spectrometer (Bruker Optics; Billerica, MA), which was equipped with an InGaAs-detector and tungsten light source. The setting of MPA was 32scans in range of 5800-12500 cm-1 at a resolution of 64 cm-1. The tablets were placed in the sample wheel for continuous analyzing by using OPUS-Lab tools which is one analyzing package from OPUS software. The spectra of tablets corresponded with the timeline of tablets manufactured. This helped to correlate In-line spectra and tablets spectra.

5.2.4. Experimental design

5.2.4.1. Residence time distribution (RTD)

The step change method (concentration vs. time) can be mathematically fit to a Taylor dispersion model to determine the RTD using a least squares approach. The functions for the Taylor dispersion model and those used to calculate the mean residence time (MRT or τ), mean centered variance (MCV or σ^2), and the standard deviation (SD or σ) for the residence time distribution are provided below.

$$C(\varepsilon,\theta) = \frac{C_0 Pe^{1/2}}{(4\pi\theta)^{1/2}} e^{-Pe(\varepsilon-\theta)^2/4\theta} \qquad \text{Taylor Dispersion Model}$$

Where C_0 is the initial concentration of the pulse, Pe is the Peclet number (ratio of convection to diffusion), ε is the relative location to the end of the mixer, and $\theta = \frac{t-t_0}{\tau}$, where t is time, t_0 is a time delay and τ is the Mean Residence Time. These quantities are defined by the following equations (insert references):

MRT $$\tau = \int_0^\infty tE(t)dt$$ Equation 5-1

MCV $$\sigma_\tau^2 = \int_0^\infty (t-\tau)^2 E(t)dt$$ Equation 5-2

SD $$\sigma_\tau = \sqrt{\sigma_\tau^2}$$ Equation 5-3

Using the residence time distribution, time of the step changes at the exit of the blender could be discovered. By knowing the time point and combining the feeder and NIR results, the concentration of API at the blender exit during the step changes can be monitored. Tablets were also collected every 5 second for each run, and off-line NIR analysis were performed on the tablets to further investigate RTD of the line, assuming the change in concentration is distinguishable from the normal noise of the line.

The experimental design used to determine the residence time distribution was based on the high dosage formulation. The design is based on 5 factors and 3 levels. The API and Prosolv particle size, blender rpm, feed frame rpm, and throughput were each varied based on a target, high, and low operation value. The experimental design contains 7 runs with coarse grade API, 6 runs with target grade API, and 7 runs with fine grade API. For the 14 runs that will be performed with either coarse or fine grade API, the step changes will be done as follows:

1. Each experimental run was start at 95% API concentration.
2. The concentration step change will be a step up for the API concentration, to 105%.

For the 6 runs that will be performed with target grade API, the step changes will be done as follows:

1. Each experimental run will start at 95% API concentration

2. The concentration step change will be a step up for the API concentration, to 105%
3. The concentration will be stepped down back to 95% API

The detailed design of experiments is shown in Table 5-3

5.2.4.1. Designated step changes

Loss-in-weight feeders' performance and consistency was first separately verified with each active and inactive material for both high and low dosage formulation. Off-line feeder experiments were performed using a dynamic catch scale which used an electronic balance positioned at the outlet of the feeder to measure mass change as a function of time. Initial relative standard deviations in normal gravimetric feeding (during steady state) for both APIs were obtained and applied to further in-line evaluation. After the offline feeder performance evaluation results were acquired, feeders were implemented into the continuous platform top level. Each individual material was loaded to and fed from an individual feeder with the selected optimal tooling, as shown in Table 5-4. Inline feed factor calibration was performed on each feeder before starting the line. Feeders were started at each target setpoint while blender running at the target speed to fill up the chute to a certain level, then the tablet press was started.

To simulate the situation when there is a significant perturbation to the feeder during continuous production, when loss-in-weight feeder is out of specification, step changes in API percentage, in this case - feeder's setpoint, were designated based on three levels of duration together with three levels of intensities while the line reaches steady state, which can be monitored by inline NIR and tablets' characteristics. Step changes with three levels of duration contain 30 second, 1 minute and 2 minutes of step-up in API setpoint for both low dosage and high dosage studies. Three levels of step-up intensities contain 5 %, 10%

and 15% for high dosage study and 10%, 15%, 20% for low dosage study. As shown in Figure 5-5, examples of step changes in high dosage API setpoint were demonstrated. The API feeder was first started with the target feed rate and after reaching the steady state of production, a 5 % step-up was performed for a 30 second duration and then step back down to the target feed rate, similar procedures were done for a 10 % step-up and a 15 % step up in Figure 5-5. Durations of 1 minute and 2 minutes also followed the same operation as for 30 second.

After a period of time (delay time), the deviated API percentage step-ups showed up in the blends after coming out of the continuous blender and reaching the chute, where the NIR probe is positioned and scanned every 4.5 second. To study the residence time distribution (RTD) study in this specific continuous manufacturing line, the probability distribution function that describes the length of time the materials spend in the system was developed with a delay time and new dose time. Delay time was defined as the time required for the concentration in the chute to start changing after feeder setpoint changes, and the new dose time was to analyze the time required for the step change to reach a steady state of production at the new concentration. Figure 5-6 shows the measurement of delay time and new dose time. Then, the perturbed powder blend continued to flow down to the feed frame, which provided back-mixing to filter the deviation in concentration and the powder blend was finally distributed to the dies in the tablet press and was compressed into tablets. Tablets were collected every 30 seconds until the steady state of production was reached and were then collected every 5 seconds until reaching steady state again or the termination of production. Off-line tablet content uniformity tests were performed using the MPA. Prediction models that converted spectra signal to API concentration for both in-line and

off-line NIR analysis were built prior to the step change tests, which is demonstrated in Section 2.3. By comparing the maximum deviation results (the point with the maximum deviation in API percentage to the target point) of predicted API concentration during step changes, the back-mixing ability and capacity of a continuous blender and a feed frame could be obtained.

5.2.4.2. Hopper refilling

Hopper refilling for feeders in the continuous manufacturing is inevitable. There are two modes of operation for loss-in-weight feeders: gravimetric (loss-in-weight) mode while feeding/dispensing and volumetric mode during the material hopper refill cycle. A refill to the feeder hopper is triggered when the amount of material left in the feeder hopper reaches the established minimum hopper refill setpoint. By the damping of powder into the feeder hopper when the feeder is running in volumetric model with no control system, a significant deviation in feed rate could appear, which is highly correlated to refill level, powder flow property and feed rate based on previous experience.

Similar to the step change study, API concentration deviation caused by rapid hopper refill was also studied in this work with the high dosage formulation. The hopper refilling study was evaluated at three different refill minimum levels for both API X and the major excipient, Silicified MCC. The maximum hopper capacities for both API X and Silicified MCC were first determined with filling in a full hopper of material with the maximum hopper weight recorded. Then, 20 %, 40%, 60 % and 80% of hopper level were determined based on the portion of the maximum hopper weight, each of which was then assigned as the minimum hopper refill setpoint. When hopper level reached the pre-set minimum setpoint during steady state of production, the feeder automatically switched to volumetric

mode and a manually pitch refill with a pre-weighted amount of material was performed within 10 seconds. Spectra scanning and tablet collecting strategy followed the same protocol as the study of designated step changes.

5.2.4.3. Blender speed and total throughput

Based on previous work, blender speed and total throughput of production also have critical impact on the residence time distribution of the powder flow in the continuous manufacturing line. Therefore, to obtain a more comprehensive idea of the filtering effect on feed rate deviation from downstream unit operations, three different blender speeds (150 rpm, 200 rpm, 250 rpm) and three total throughputs (20 kg/h, 30 kg/h and 40 kg/h) were also added to the study of low dosage formulation with the maximum combination of step changes: 20 % step-up and 2 min. This work also followed the same protocol as the step change and hopper refilling studies. In addition to compare the maximum deviation, deviation time (from the appearance of first deviated API concentration point to the end of deviation) was also added to the analysis for this study, since the residence time distribution had significant difference between different settings of blender speed and total throughputs.

5.3. Results and discussion

The initial point of this study was to characterize the off-line API's feeding performance as to be applied to the inline characterization. With the feeder, tooling and feed rate used in this work, API X in high dosage formulation has an original relative standard deviation (RSD) of 4.3% and powder APAP in low dosage formulation has a RSD of 4.0 %, which means that even if there is no perturbation or any designated disturbance to the feed rate, those RSD in feed rate would occur anyway mostly due to the material flow properties.

5.3.1. Development of NIR calibration models

The quantitative multivariate models for blends and tables were developed by using Unscrambler 10.4 (CAMO Analytics, NJ, USA). The basis for the development of a good model is the API homogeneity of the blends and tablets. To ensure all spectra used for the model development indicate the aimed API concentration, the following steps were applied: do the pretreatment for all calibration spectra, then a principal component analysis (PCA) was performed, and the central spectra of each API concentration were selected. The selected spectra were expected to represent the desired bulk API content. After picking out the spectra, a partial least squares (PLS) regression model was established to predict the API concentration.

The pretreatment methods for in-line blends were the first-order derivative with Savitzky-Golay smoothing (7598-5346 cm-1, second polynomial order, kernel: 5 points) followed by standard normal variate (SNV, 7598-5346 cm-1). A total of 200 in-line spectra were used to develop the calibration model, and 60 spectra (10 from each concentration level) were used to validate it. The PLS model was developed in the spectral ranges of 7598-5346 cm-1, within the API groups were well separated and equidistant (as shown in Figure 5-2). The model consisted of two latent factors which explained 98% of the X-Y correlation with an R^2 = 0.9727 for prediction, a root mean square error of cross validation RMSECV = 0.2236, and root mean square error of prediction RMSEP = 0.2645 (as shown in Figure 5-3).

The multivariate PLS model for tablets was developed by using a total 60 spectra (10 spectra per concentration level) and the combination pretreatment of firs-order derivative with Savitzky-Golay smoothing (9203-8601 cm-1. second polynomial order, kernel: 5

points) and SNV (9203-8601 cm-1). The Y-variance explained by the two PLS factor model was 98 % (as shown in Figure 5-4). Finally, the R2 for the tablet calibration model is 0.9744 and the RMSECV is 0.2158. The RMSEP calculated from 18 validation spectra (3 for each level) is 0.2128.

5.3.2. Delay time and new dose time

The delay time was collected from each of the 20 runs, and statistical analysis was performed on the data. The operational conditions and the recorded values of the delay times appear in Table 5-5.

ANOVA was performed on Table 5-5, and results appear in Table 5-6 and Figure 5-7. Chute step up delay time is independent of the feed frame speed; therefore, the feed frame speed parameter was eliminated from the statistical analysis. ANOVA results indicated that throughput had the highest effect on the delay time. As the throughput increases the delay time decreases linearly. This result is straightforward, as material passes faster through the system, the time the material passes through the blender would also be shorter. The blender speed is also a significant term in the model, the main effects plot shows a slight curvature, where the target blender speed, 150 RPM, had the smallest average delay time, and the 100RPM setting had the largest delay time. This result is intuitive, as the paddles of the blender move faster, the powder will be pushed through the blender faster, and the time will be shorter. The grade of the API X and the main excipient, Prosolv, did not have a significant effect on the delay time.

5.3.3. Designated Step Changes

As described in 5.2.4.1, three levels of step-up intensities and three levels of duration for each intensity were applied to both high dosage and low dosage studies. Figure 5-8 shows

the API concentration at the chute when blends coming out of the blender for the high dosage study. The concentration was predicted from the calibration model. Four different designated step changes are shown in the plot, including '5% 1min', '10 % 1min', '15 % 1min' and '15 % 2min'. A tolerance interval was designed as ±10 % of the target concentration which are the green and red lines. An example of the step-change from feed rate is colored in blue in the plot. As shown in Figure 5-8, only '5% 1min' has all its data points falling in between the tolerance interval, while all the other three designs have points locating outside the higher limit line. Table 5-7 shows the maximum deviation results to the target concentration for all the 9 (3*3) designated step changes. Results show that for a 5 % step-up with all the three durations, the maximum deviations fall into the tolerance limit, while for the other two intensities, none out of the 6 combination pass the qualification, which means in a real production line with only monitoring the API concentration at the point of chute, those six combinations will trigger the divert valve and all the blends/tablets, during this disturbed period or even longer, will be considered out-of-specification and sent to waste.

However, as mentioned above, there is another back-mixing point after the chute that will can help smoothen the deviation and improve the tablet uniformity, and that is the feed frame. Figure 5-9 shows the concentration of API in the tablets for the same four designated step changes. The target concentration in the prediction has a shift from 52.5 to 55.7 due to the error of the predicting model and the rejection limits were designated accordingly. Different from the 'Chute' results, the API concentration in all the tablets are within the tolerance limits, even for '15% 2min', which is the highest combination design. Table 5-8 shows the maximum deviation in API concentration in tablets for the 4 combinations. Since

the highest combination pass the tolerance qualification, and due to the unavailability of the MPA device, the author chose not to do the tablets uniformity tests for the remaining 5 combinations, which are marked as ‘N/A’ in the table.

A similar experimental design was applied to the low dosage study, to validate the filtering capacity of downstream units. The only difference is that 10 %, 15 % and 20 % were used for the three step-up levels, instead of 5 %, 10 %, 15 % for the high dosage study. Figure 5-10 shows the example of API concentration results for ’10 % 30s’, ’15 % 30s’, ’15 % 1min’ and ‘20%, 2min’ tested at the chute after the blends coming out of the blender, where 10 % concentration tolerance limits are marked in blue and green lines. Table 5-9 shows the maximum deviation results for all 9 (3*3) combinations. Results show that the maximum deviation ranges between 15.2 % and 29.4%, which means even for the lowest designated step change, the maximum deviation is around 5.2 % above the tolerance limit and for the highest step change, there is a nearly 30 % maximum deviation that can be observed at the chute monitoring point. Regarding tablet results, Figure 5-11 shows the API concentration in tablets based on the same step changes discussed in Figure 5-9. All data points fall within the tolerance limits, even for the highest step change. Table 5-10 shows the detailed results for all 9 combinations. Again, the maximum deviation in API concentration in tablets due to the designated step changes are all within the limits, which means they all pass the qualification.

The designated step change studies for both high dosage and low dosage formulations prove and validate that both continuous blender and feed frame has the ability to filter the API concentration variation due to perturbation or disturbance from feeder’s feed rate.

Surprisingly, the feed frame was found to have a better filtering capacity for variations and can efficiently maintain the tablet uniformity if there is disturbance in the production.

5.3.4. Hopper refill

Hopper refilling is a critical operation to continuous manufacturing, which could cause perturbations to feeder and lead to disturbance in feed rate. Therefore, the refilling strategy and the understanding of the disturbance it would bring to the downstream unit operations and final products is critical. Previous research has established a good understanding of the feed rate deviation caused by hopper refill. Refilling a feeder at a higher hopper level and at a higher feed rate may result in a lower deviation and shorter deviation time compare to refilling a feeder at a lower hopper level and at a lower feed rate. Also, materials with good flowability (i.e. high permeability, low cohesion) have better performance during hopper refill than poorly flowing ones.

Similar to designated step change studies, hopper refill work focuses on realistic and evitable perturbations during continuous production. This work used the high dosage formulation on the API X and one of the excipients, Silicified MCC. Three levels of hopper refill level were applied to both materials. Table 5-11 shows the maximum deviation results based on the inline NIR API concentration prediction at the chute according to API X and silicified MCC hopper refills. Hopper refills cause a period of increase in feed rate and as a result the refilling of Silicified MCC caused the API concentration to drop. Therefore, the numbers of API maximum deviation for Silicified MCC refilling are negative. Results show that the maximum deviation tested at the chute point follows the same trend as feeder offline refilling study: lower refilling level causes higher maximum deviation. For the case study examined here, hopper refilling of major excipients a has bigger impact on API

concentration than refilling of API, which caused a significant concentration drop in the blends coming out of the blender.

Table 5-12 shows that when the maximum deviation in API concentration occurred in tablets, the numbers do not strictly follow the trend since the deviation in tablets is small (all the numbers are below 3 %) and can be neglected. Therefore, although the refilling of both API and major excipients feeders caused disturbance in API concentration into the line, eventually the feed frame has the ability to filter the variation before it goes into the tablets. Figure 5-12 shows a comparison between all the hopper refills performed in this study, which shows that feed frame has a good filtering capacity to dampen the API concentration variation occurring in the line.

5.3.5. Blender speed and total throughput

Based on previous work, blender speed and total throughput have a major impact on the residence time distribution of the materials flowing in the line. Therefore, it is also important to include those factors in this work. This section of the work was performed with the low dosage formulation with three levels of blender speed: 150 RPM, 200 RPM, and 250 RPM and three levels of total throughput: 20 kg/h, 30 kg/h, and 40 kg/h. The step change method was used in this study with the highest combination of ’20%, 2min’.

Figure 5-13 shows the API concentration as monitored in real time at the chute point for three different blender speeds. Table 5-13 shows the results of maximum deviation and deviation time for API concentration at the chute. The results show that with higher blender speed, the maximum deviation is higher than that of lower blender speed; however, it required a longer time for the deviation to diminish. This is because that materials have higher mean residence time in the continuous blender with a lower blender speed, which

means the blender has a more sufficient time to back-mix and smoothen the deviated feeding. Figure 5-14 and Table 5-14 shows the API concentration during the blender speed study, and the results of maximum deviation and deviation time in the tablets were collected. Same trend can be observed as in the chute, while the feed frame again filtered the deviation to a lower level for all the three blender speeds. Figure 5-15 shows the combined results of both chute and feed frame in the tablets. A significantly higher maximum deviation was displayed in the chute results compared to the tablets, which again proves the feed frame's efficient effect to filter the deviation.

Figure 5-16 shows the API concentration monitored at the chute with three different total throughputs and Table 5-15 shows the results of maximum deviations and deviation time in API concentration. The results show that running with a higher throughput had a higher maximum deviation and lower deviation time than running at a lower throughput. Lower throughput gave materials more time to stay in the back-mixing zones and therefore results in a smoother but wider curve with a lower peak. Again, the same trend was observed in the tablets as shown in Figure 5-17 and Table 5-16. Figure 5-18 shows combined results of the maximum deviation and deviation time in API concentration for the total throughput study. Both the blender and the feed frame have good abilities to filter the variation from the feeder where the feed frame's filtering capacity is more substantial.

5.4. Conclusions

In this work, a continuous pharmaceutical manufacturing process of direct compaction was utilized to evaluate the dampening effect on feed rate deviation from the feeder by downstream unit operations. This work has determined that blender speed and total throughput are the major factors that have significant impact on the delay time on real time

monitoring point at the chute after the continuous blender when disturbances or changes in concentration occur on instantaneous mass flow rates due to feeder perturbations. Inline PLS offline PLS calibration models on two different formulations with two different API dosages have been developed and utilized to monitor the inline and offline API concentration.

Designated step changes on API feeder were used to mimic the unexpected disturbance on feeder. How disturbance from hopper refill process on both API feeder and major excipient feeder transferred to downstream and final products were also investigated in this work. In addition, the effect of different blender speeds and total throughput has also been added to fully evaluate the filtering ability from operational conditions.

The experimental results for both formulations have proved that both the continuous blender and the feed frame in the tablet press are able to filter the variation in feed rates and thus improve the content uniformity of final products, where the feed frame plays a more significant role on filtering the variation after the monitoring point at the chute after continuous blender. From the blender speed and total throughput study, the results demonstrated that higher blender speed and higher total throughput contributed to a lower residence time, which reduce the back-mixing time of the blends and resulted in a higher maximum deviation, compared to lower blender speed and lower total throughput, which allowed the powder blends stay in the downstream unit operations with a longer time. However, higher blender speed and total throughput has the ability to shorten the total disturbance time compared to lower blender speed and total throughput, which is because the mass of the powder blends were transferred faster in the downstream unit operations. The dampening ability from downstream unit operations depends on the design of each

unit operation and the whole manufacturing process. This work can provide a better knowledge of the interaction between feeder and downstream units which can be helpful with the design of feeder refill strategy, control strategy and alerting system of a specific design of the manufacturing process. Results reported in this work can help identify the best location for PAT implementation, which can help save a significant amount of materials. For example, placement of the NIR sensors in the chute would completely miss the beneficial effects of the feed frame on blend uniformity and could cause the line to trigger unwarranted alarms regarding non-existent failures. This work can also be applied to risk assessment during production.

5.5. Tables for Chapter 5

Table 5. 1: High Dosage Composition and Material Target Feed rates

Material Name	Composition (%)	Target Feed Rate (kg/h)
Silicified MCC	45.24	18.096
Magnesium Stearate	0.74	0.296
API X	52.02	20.808
Crospovidone	2.00	0.800
	Total Throughput	40.000

Table 5. 2: Low Dosage Composition and Material Target Feed rates (FR)

Material Name	Composition %	Target FR	Target FR	Target FR
Silicified MCC	92.00	18.400	27.600	36.800
Magnesium Stearate	1.00	0.200	0.300	0.400
API X	5.00	1.000	2.000	3.000
Crospovidone	2.00	0.400	0.600	0.800
Total Throughput		20.000	30.000	40.000

Table 5. 3: The designed experimental runs

Run Order	Prosolv PSD	Darunavir PSD	Throughput (kg/hr)	Blender Speed (RPM)	Feed Frame Speed (RPM)
1	0	0	0	0	0
2	-1	-1	1	1	1
3	-1	1	1	-1	0
4	1	-1	1	1	-1
5	1	1	-1	-1	-1
6	0	1	1	1	1
7	0	0	0	0	0
8	0	-1	-1	-1	-1
9	1	-1	-1	1	0
10	1	0	1	-1	1
11	-1	0	-1	1	-1
12	1	1	1	0	-1
13	0	0	0	0	0
14	-1	1	0	1	-1
15	-1	-1	-1	0	1
16	1	-1	0	-1	1
17	1	1	-1	1	1
18	-1	1	-1	-1	1
19	-1	-1	1	-1	-1
20	0	0	0	0	0

Table 5. 4: Feeder and Tooling for Each Component

Material Name	Loss-in-weight Feeder	Tooling
API X	KT-20 Type B gear-box	Coarse Concave Screws
Magnesium Stearate	KT-20 Type C gear-box	Fince Concave Screws
Silicified MCC	KT-35 Type C gear-box	Coarse Concave Screws
Crospovidone	KT-20 Type C gear-box	Fine Concave Screws
Acetaminophen	KT-20 Type C gear-box	Fine Concave Screws

Table 5. 5: Operating Conditions and Delay times for each of the 20-point DoE runs.

	Operating Conditions - Inputs					**Responses - CHUTE**
Run #	**Throughput**	**Blender RPM**	**Feed Frame RPM**	**Darunavir grade**	**Prosolv Grade**	**Delay Time (seconds)**
1	0	0	0	0	0	34
2	1	1	1	-1	-1	25
3	1	-1	0	1	-1	50
4	1	1	-1	-1	1	22
5	-1	-1	-1	1	1	67
6	1	1	1	1	0	18
7	0	0	0	0	0	37
8	-1	-1	-1	-1	0	61
9	0	1	0	-1	1	52
10	1	-1	1	0	1	47
11	-1	1	-1	0	-1	52
12	-1	0	-1	1	1	31
13	0	0	0	0	0	33
14	0	1	-1	1	-1	52
15	-1	0	1	-1	-1	58
16	0	-1	1	-1	1	55
17	-1	1	1	1	1	45
18	-1	-1	1	1	-1	59
19	1	-1	-1	-1	-1	25
20	0	0	0	0	0	30

Table 5. 6: Response Surface Regression: Delay Time (seconds) in Chute versus Process Parameters and Material Properties

Analysis of Variance

Source	DF	Adj SS	Adj MS	F-Value	P-Value
Model	7	3217.81	459.69	6.41	0.003
Linear	4	2732.05	683.01	9.52	0.001
Throughput	1	2039.02	2039.02	28.43	0.000
Blender RPM	1	450.39	450.39	6.28	0.028
Darunavir grade	1	10.26	10.26	0.14	0.712
Prosolv Grade	1	0.38	0.38	0.01	0.944
Square	1	564.15	564.15	7.87	0.016
Blender RPM*Blender RPM	1	564.15	564.15	7.87	0.016
2-Way Interaction	2	409.02	204.51	2.85	0.097
Throughput*Darunavir grade	1	164.84	164.84	2.30	0.155
Darunavir grade*Prosolv Grade	1	112.56	112.56	1.57	0.234
Error	12	860.74	71.73		
Lack-of-Fit	9	835.74	92.86	11.14	0.036
Pure Error	3	25.00	8.33		
Total	19	4078.55			

Model Summary

S	R-sq	R-sq(adj)	R-sq(pred)
8.46927	78.90%	66.59%	22.20%

Coded Coefficients

Term	Coef	SE Coef	T-Value	P-Value	VIF
Constant	33.78	3.64	9.29	0.000	
Throughput	-13.59	2.55	-5.33	0.000	1.17
Blender RPM	-5.71	2.28	-2.51	0.028	1.02
Darunavir grade	-0.88	2.34	-0.38	0.712	1.07
Prosolv Grade	-0.17	2.35	-0.07	0.944	1.08
Blender RPM*Blender RPM	12.64	4.51	2.80	0.016	1.19
Throughput*Darunavir grade	4.40	2.90	1.52	0.155	1.24
Darunavir grade*Prosolv Grade	-3.44	2.75	-1.25	0.234	1.26

Regression Equation in Uncoded Units

Delay Time (seconds) = 33.78 - 13.59 Throughput - 5.71 Blender RPM - 0.88 Darunavir grade - 0.17 Prosolv Grade + 12.64 Blender RPM*Blender RPM + 4.40 Throughput*Darunavir grade - 3.44 Darunavir grade*Prosolv Grade

Fits and Diagnostics for Unusual Observations

Obs	Delay Time (seconds)	Fit	Resid	Std Resid	
6	18.00	30.64	-12.64	-2.23	R

Magnitude of the effects

Term	T-Value
Throughput	-5.33
Blender RPM*Blender RPM	2.8
Blender RPM	-2.51
Throughput*Darunavir	1.52
Darunavir grade*Prosolv Grade	-1.25
Darunavir	-0.38
Prosolv Grade	-0.07

Table 5. 7: Maximum Deviation in API Concentration Results in the Chute According to Feeder Step Changes for High Dosage Step Change Study

	30s	1min	2min
5%	7.5	8.4	9.2
10%	11.7	13.1	13.9
15%	13.7	14.9	16.1

Table 5. 8: Maximum Deviation in API Concentration Results in Tablets According to Feeder Step Changes for High Dosage Study

	30s	1min	2min
5%	N/A	2.3	N/A
10%	N/A	13.1	N/A
15%	N/A	7.5	8.7

Table 5. 9: Maximum Deviation in API Concentration Results in the Chute According to Feeder Step Changes for Low Dosage Step Change Study

	30s	1min	2min
10%	15.2	17.4	17.5
15%	16.4	22.2	26.6
20%	18.2	27.5	29.4

Table 5. 10: Maximum Deviation in API Concentration Results in Tablets According to Feeder Step Changes for High Dosage Study

	30s	1min	2min
10%	1.2	2.0	3.4
15%	4.4	6.4	7.5
20%	5.5	5.7	9.2

Table 5. 11: Maximum Deviation in API Concentration Results in Chute According to Hopper Refill for High Dosage Study

	60%-80%	40%-80%	20%-80%
API X	3.5	5.5	5.4
Silicified MCC	-6.1	-6.9	-9.2

Table 5. 12: Maximum Deviation in API Concentration Results in Tablets According to Hopper Refill for High Dosage Study

	60%-80%	40%-80%	20%-80%
API X	1.1	1.8	1.2
Silicified MCC	-1.5	-2.5	-1.8

Table 5. 13: Maximum Deviation and Deviation Time in API Concentration Results in Chute According to 20% deviation in feed rate for 2 minutes with different blender speeds.

	150 RPM	200 RPM	250 RPM
Maximum Deviation (%)	29.4	30.3	36.4
Deviation Time (s)	126	117	99

Table 5. 14: Maximum Deviation and Deviation Time in API Concentration Results in Tablets According to 20% deviation in feed rate for 2 minutes with different blender speeds.

	150 RPM	200 RPM	250 RPM
Maximum Deviation (%)	9.2	12.0	14.0
Deviation Time (s)	70	50	50

Table 5. 15: Maximum Deviation and Deviation Time in API Concentration Results in Chute According to 20% deviation in feed rate for 2 minutes with different total throughputs.

	20kg/h	30kg/h	40kg/h
Maximum Deviation (%)	15.9	20.2	29.4
Deviation Time (s)	180	144	126

Table 5. 16: Maximum Deviation and Deviation Time in API Concentration Results in Tablets According to 20% deviation in feed rate for 2 minutes with different total throughputs.

	20kg/h	30kg/h	40kg/h
Maximum Deviation (%)	3.4	5.6	9.2
Deviation Time (s)	130	90	70

5.6. Figures for Chapter 5

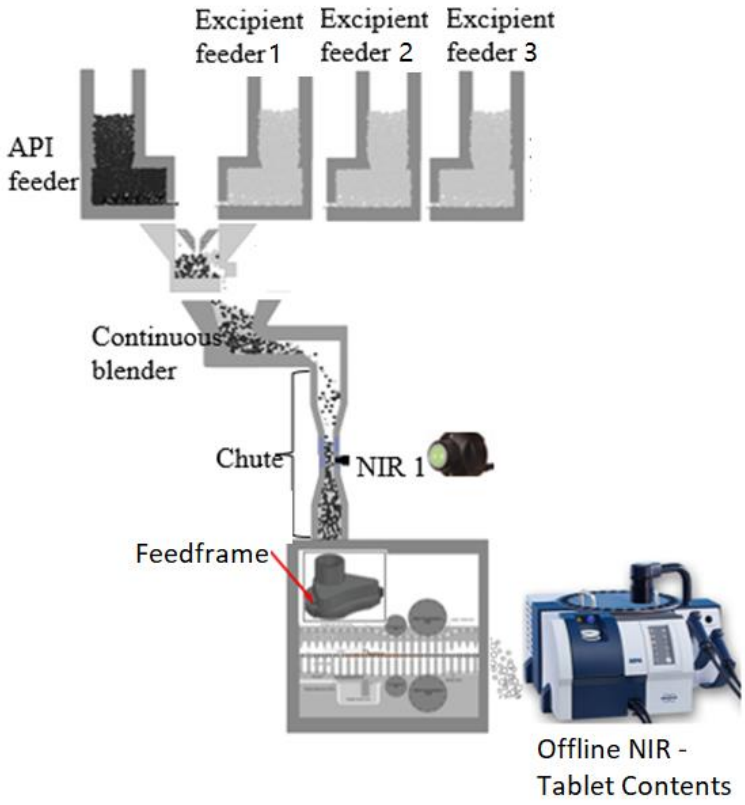

Figure 5. 1: Schematic of the continuous manufacturing design of direct compaction used in this work.

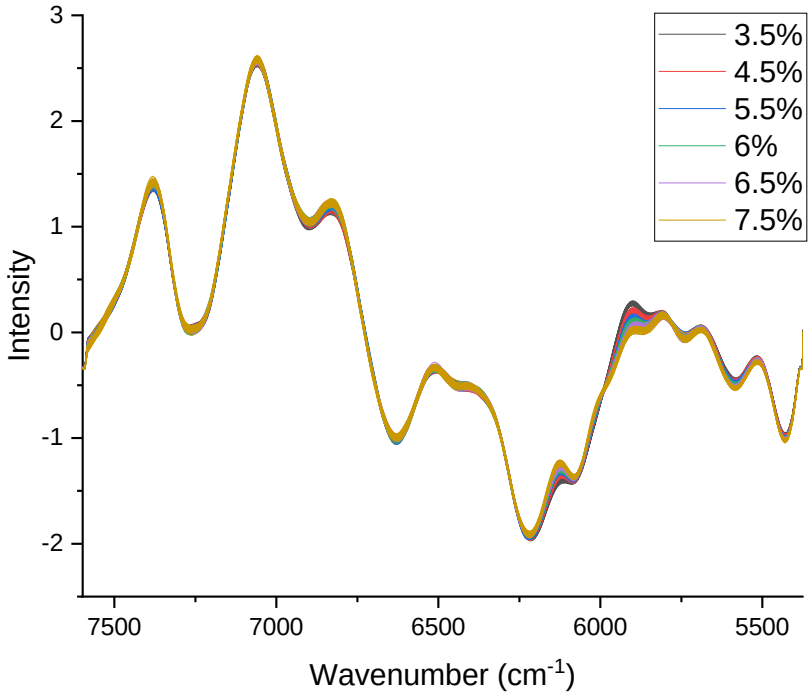

Figure 5. 2: In-line blends calibration model spectra after pre-treatment: second-order derivative with Savitzky-Golay smoothing.

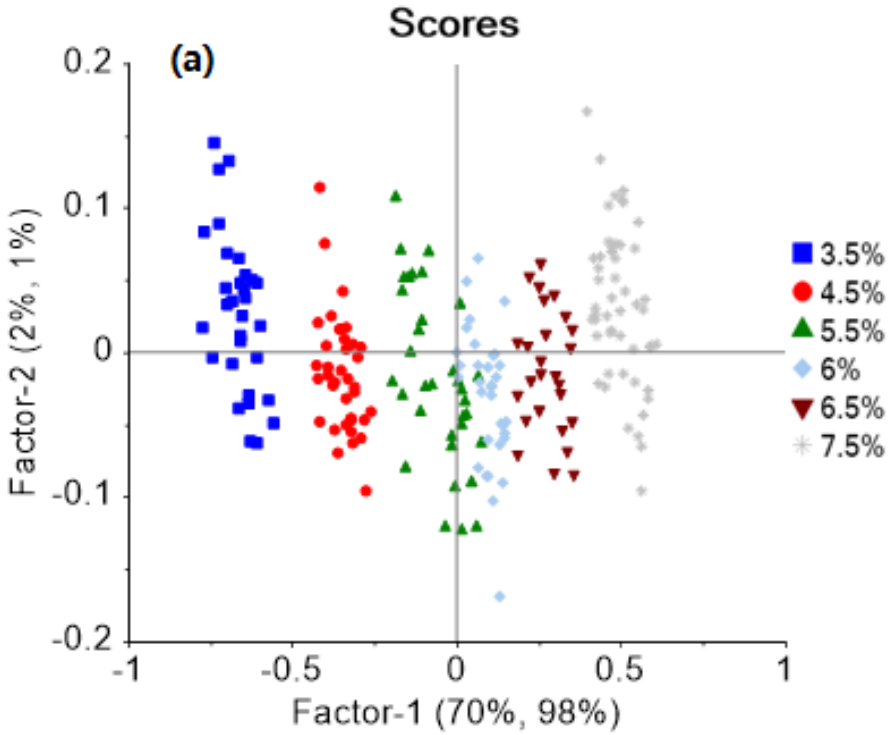

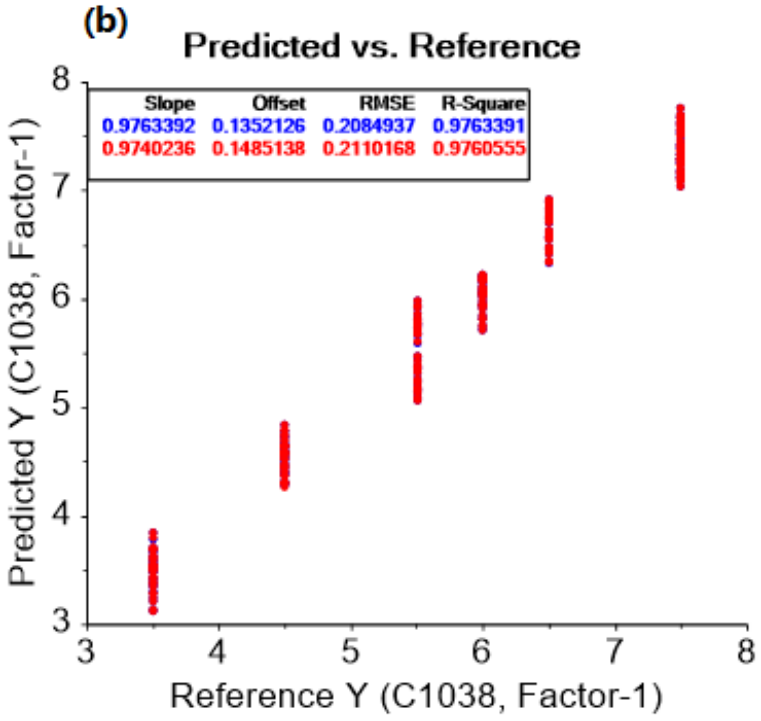

Figure 5. 3: (a) PLS score plot for in-line blends calibration model, (b) Predicted vs reference plot for in-line blends (blue for calibration set and red for cross validation set)

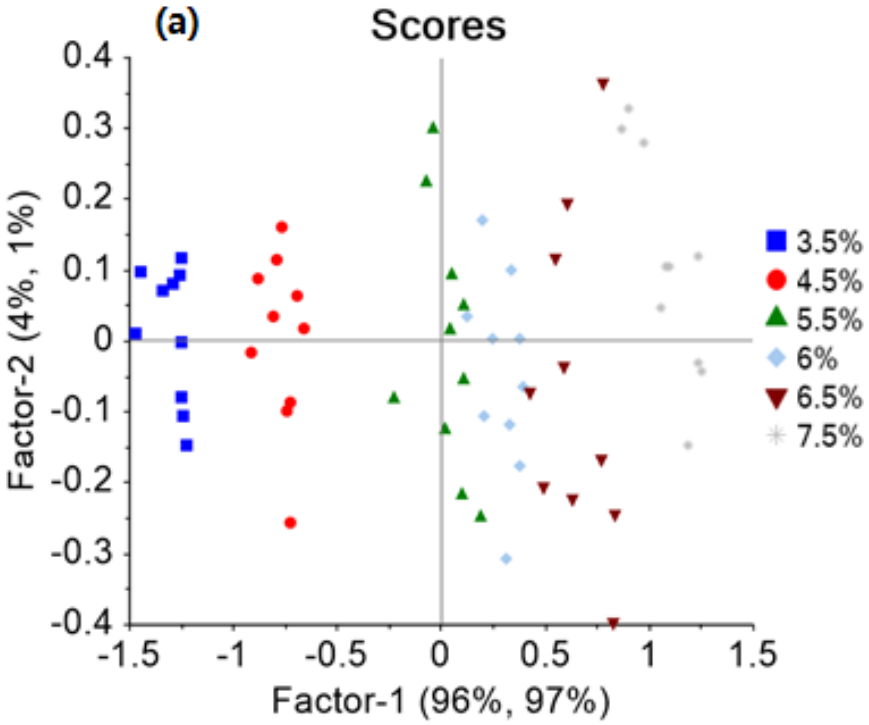

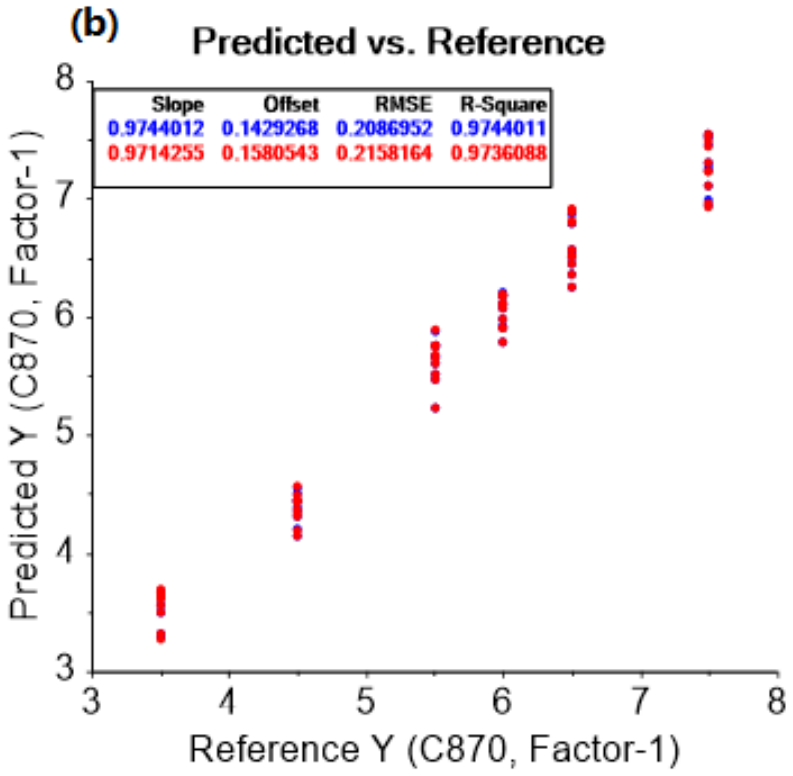

Figure 5. 4: (a) PLS score plot for tablet calibration model, (b) Predicted vs reference plot for tablet (blue for calibration set and red for cross validation set).

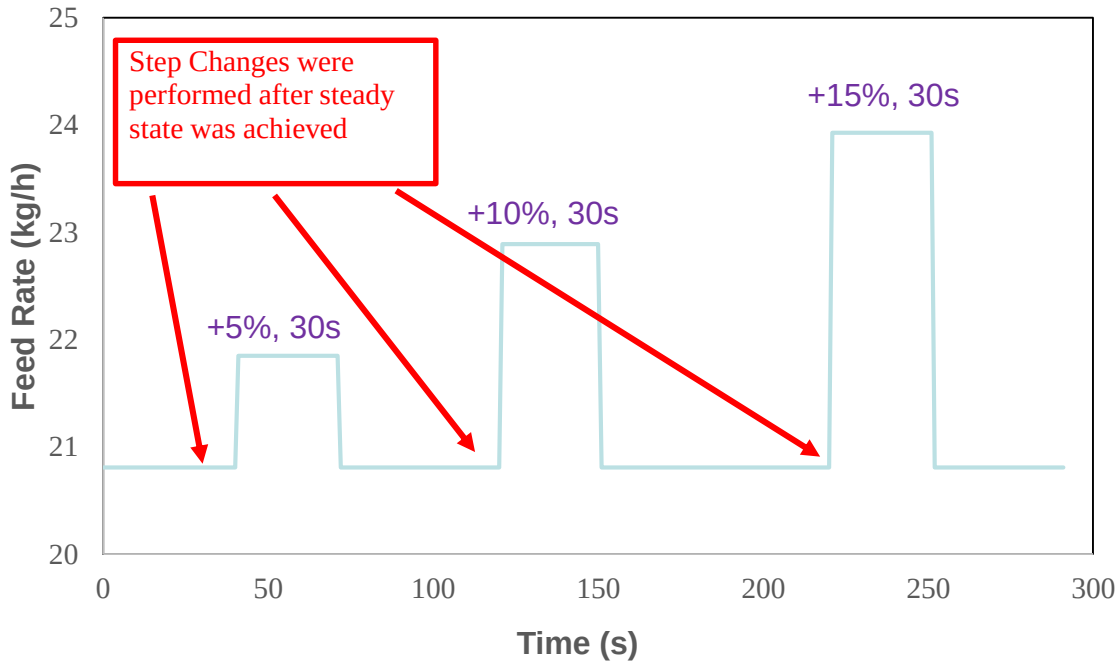

Figure 5. 5: Example of designated step changes on feeder set points.

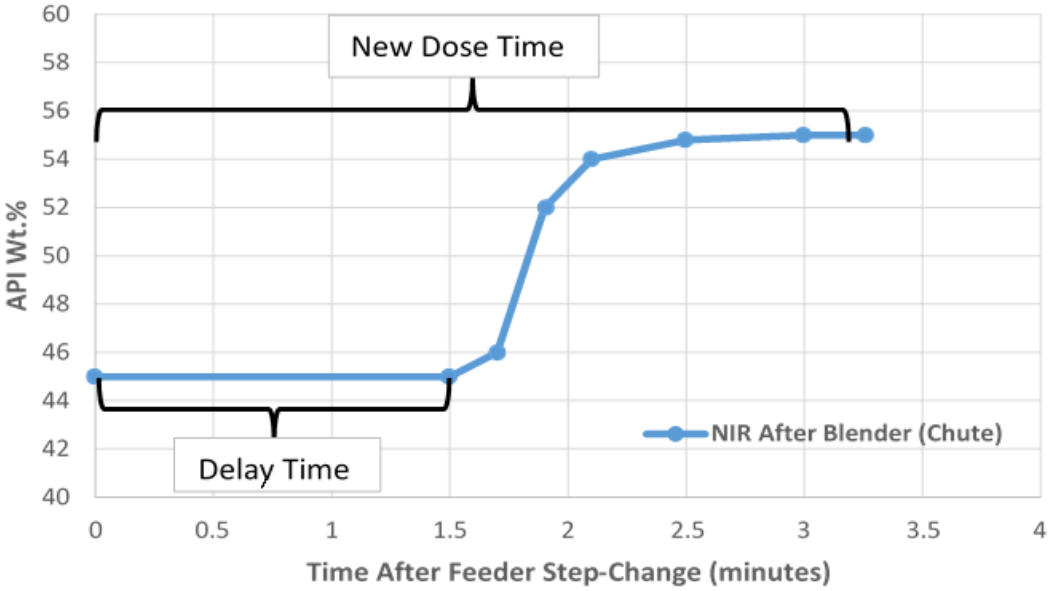

Figure 5. 6: Delay time and new dose time between feeder step changes and signal received at chute.

(a)

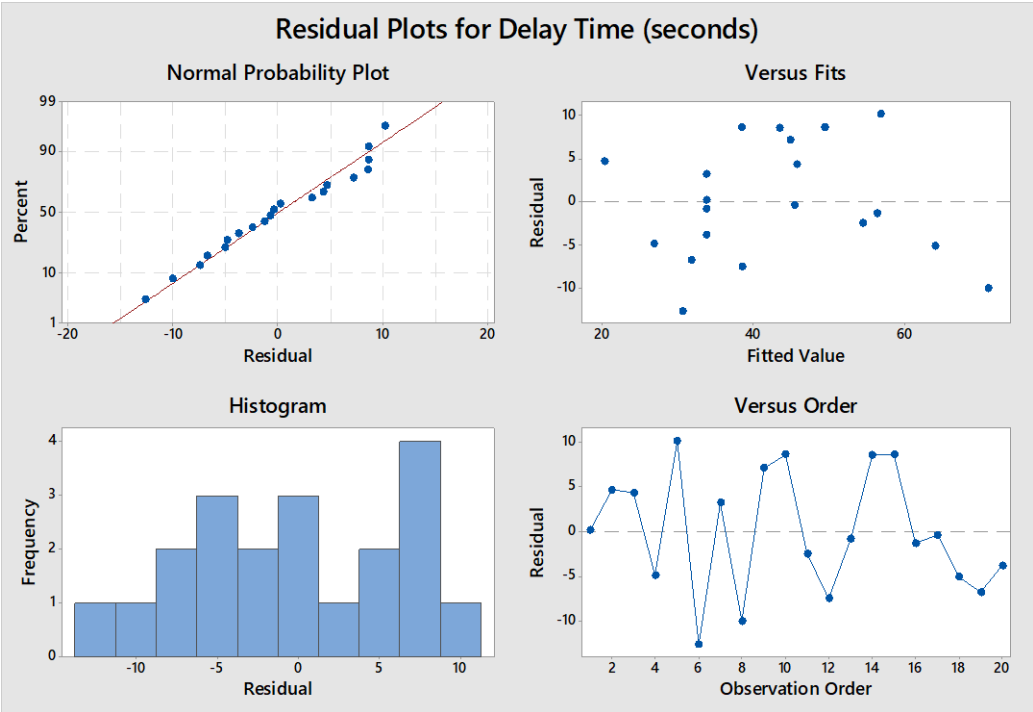

(b)

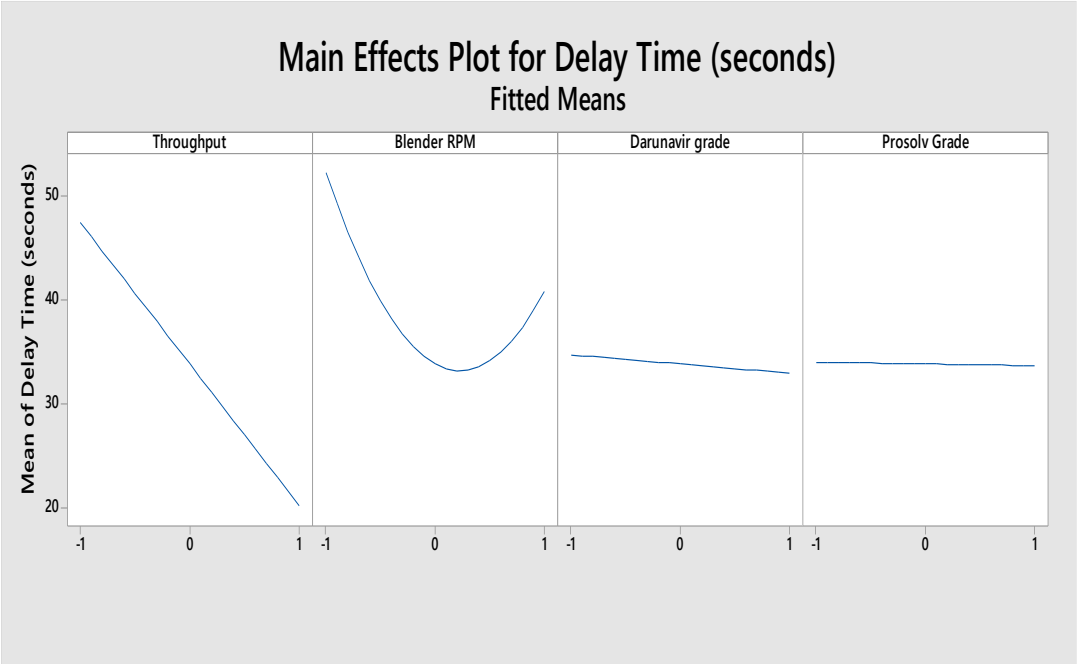

(c)

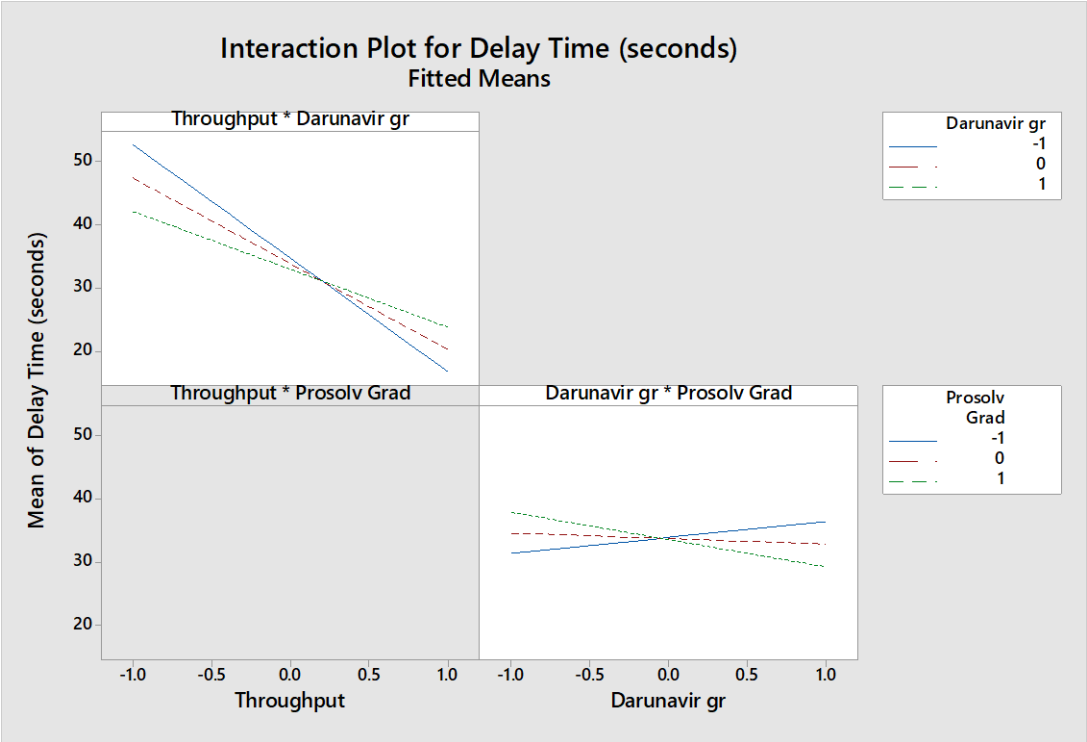

Figure 5. 7: (a) Residual plots, (b) Main effects plots (c) Interaction plots for delay time through the blender.

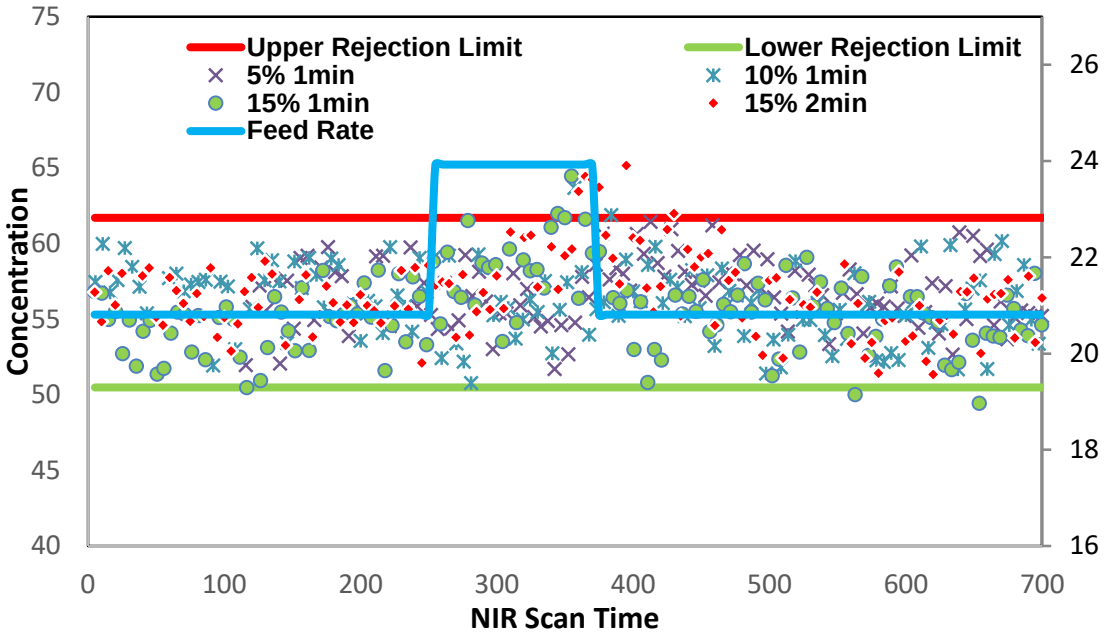

Figure 5. 8: API concentration in the chute according to step changes for high dosage study.

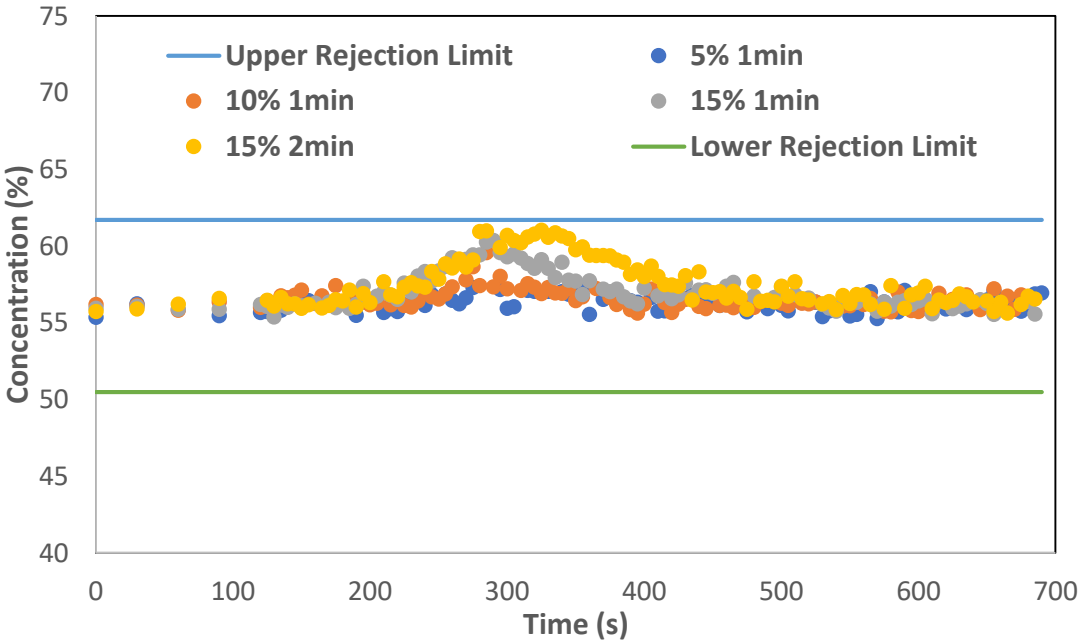

Figure 5. 9: API concentration in the tablets according to step changes for high dosage study.

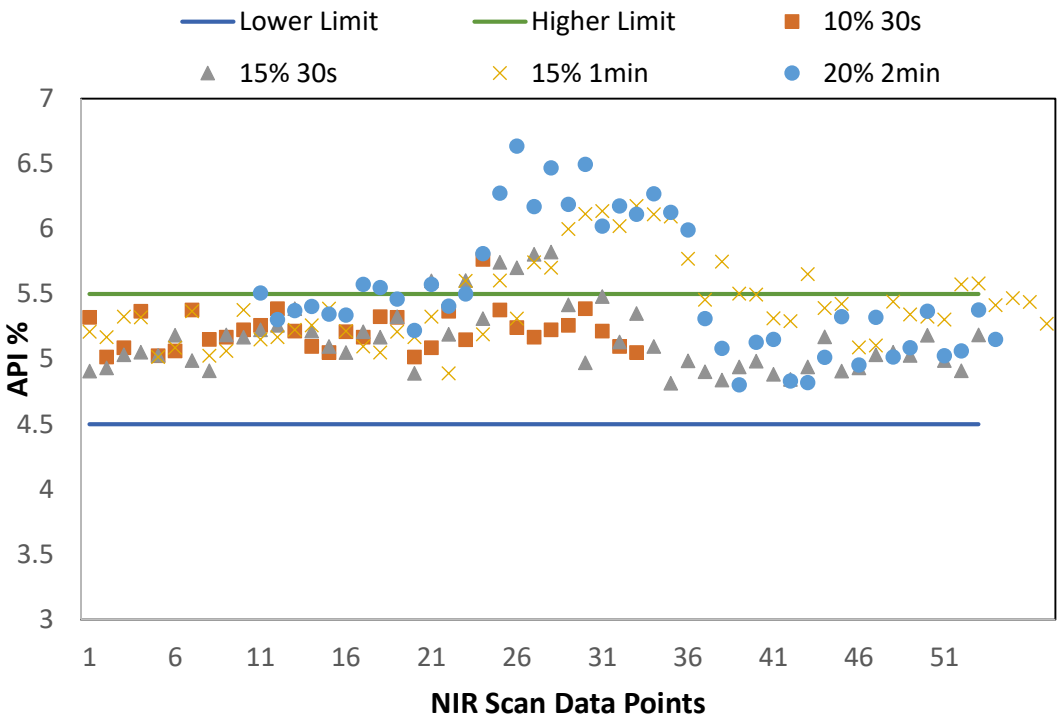

Figure 5. 10: API concentration in the chute according to step changes for low dosage study.

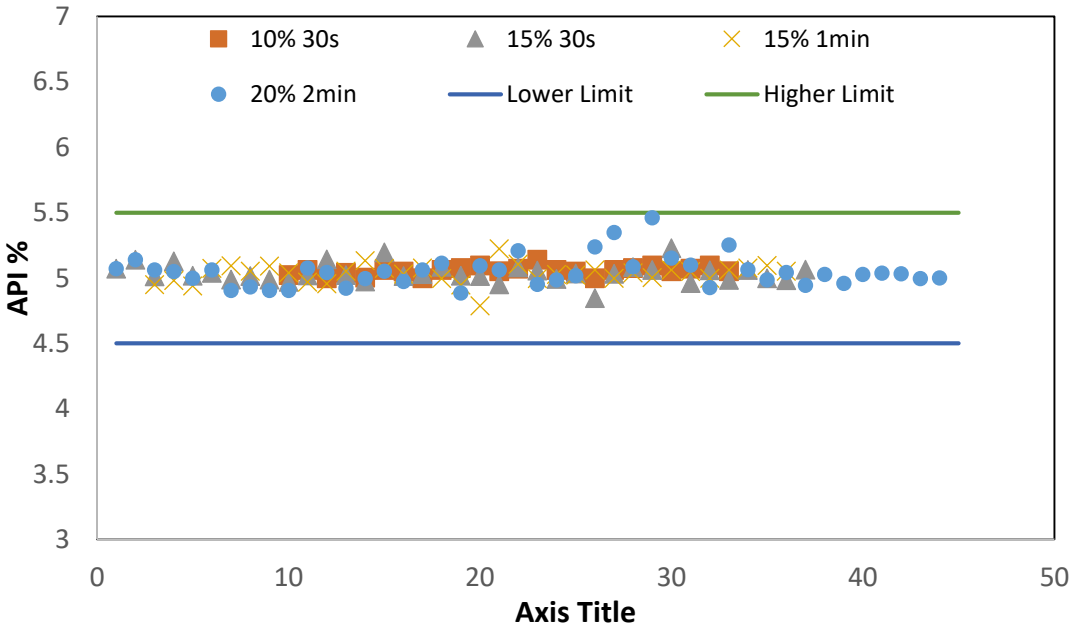

Figure 5. 11: API concentration in the tablets according to step changes for low dosage study.

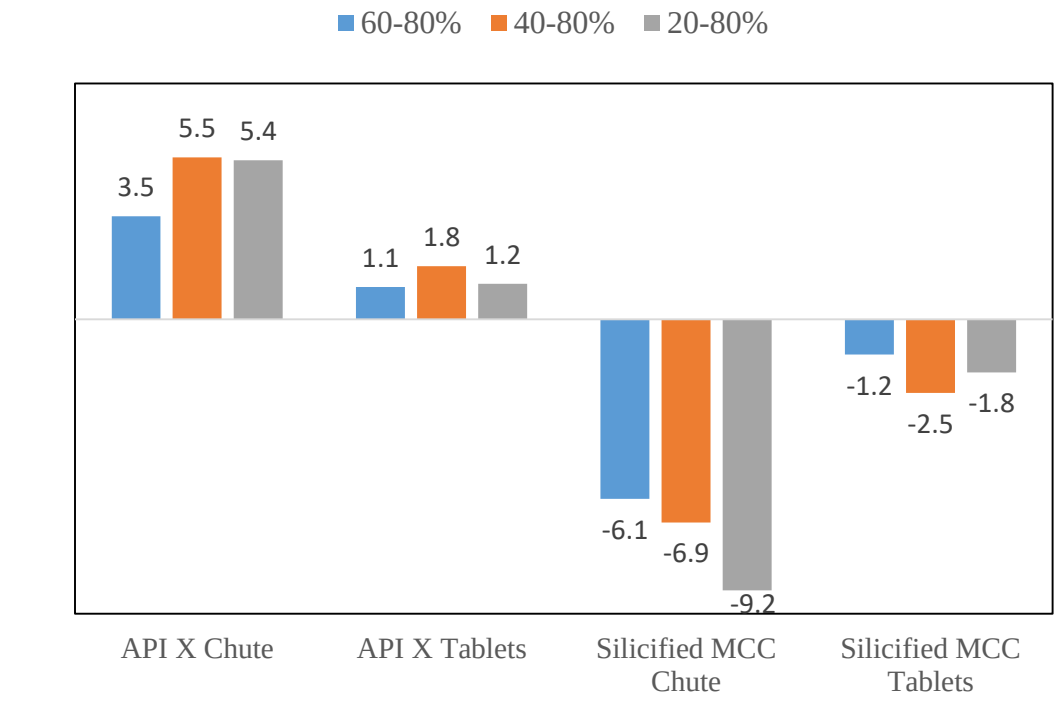

Figure 5. 12: Maximum deviation in API concentration results in chute and tablets according to API and major excipient hopper refill for high dosage study

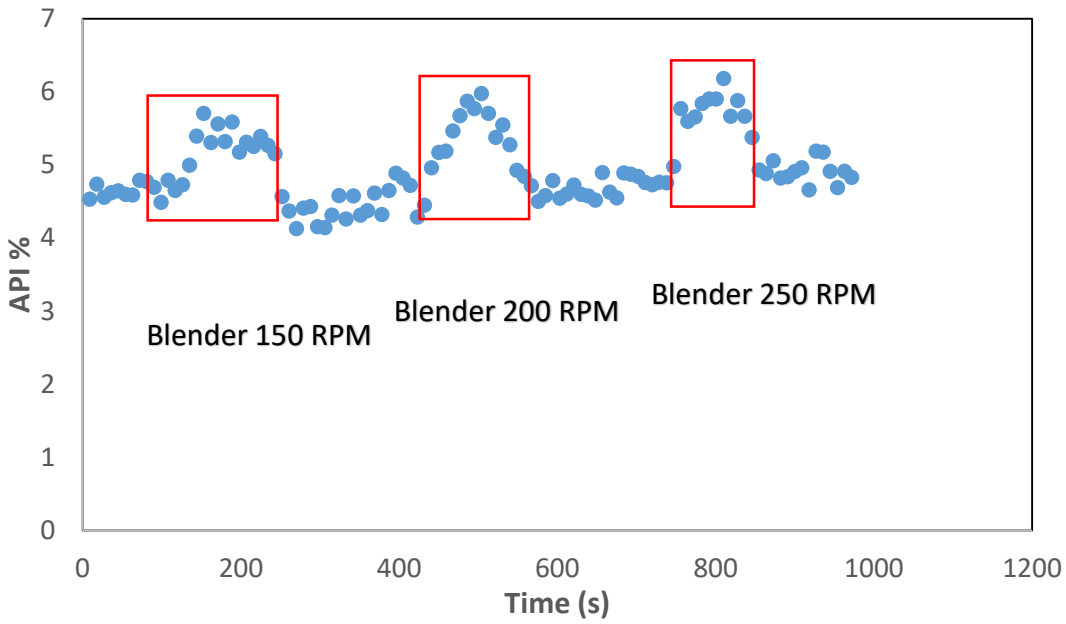

Figure 5. 13: API concentration in the chute according to 20% deviation in feed rate for 2 minutes with different blender speeds.

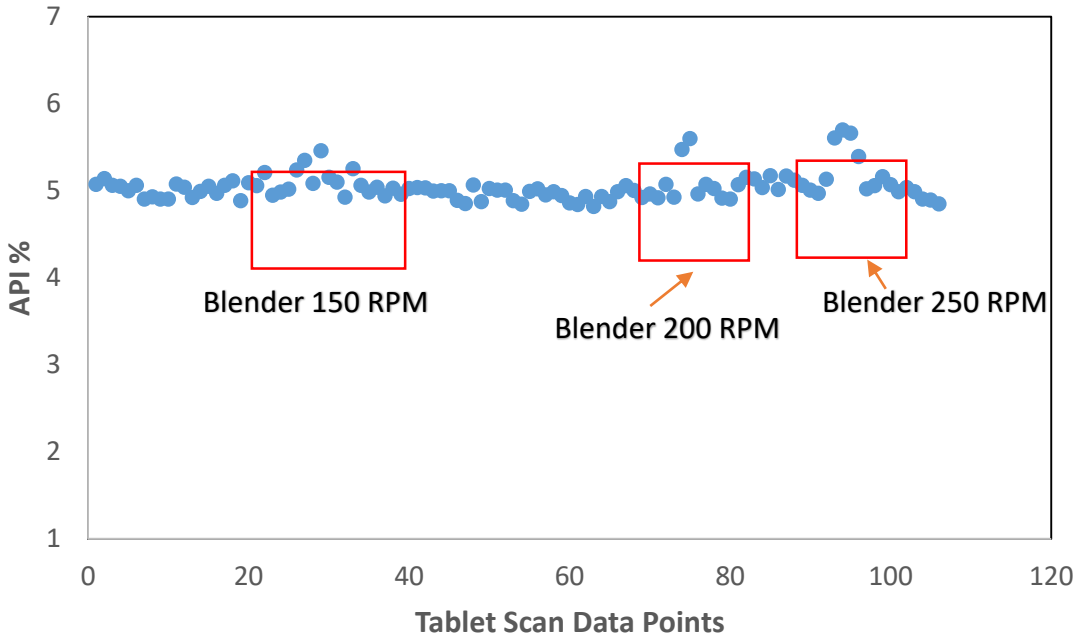

Figure 5. 14: API concentration in tablets according to 20% deviation in feed rate for 2 minutes with different blender speeds.

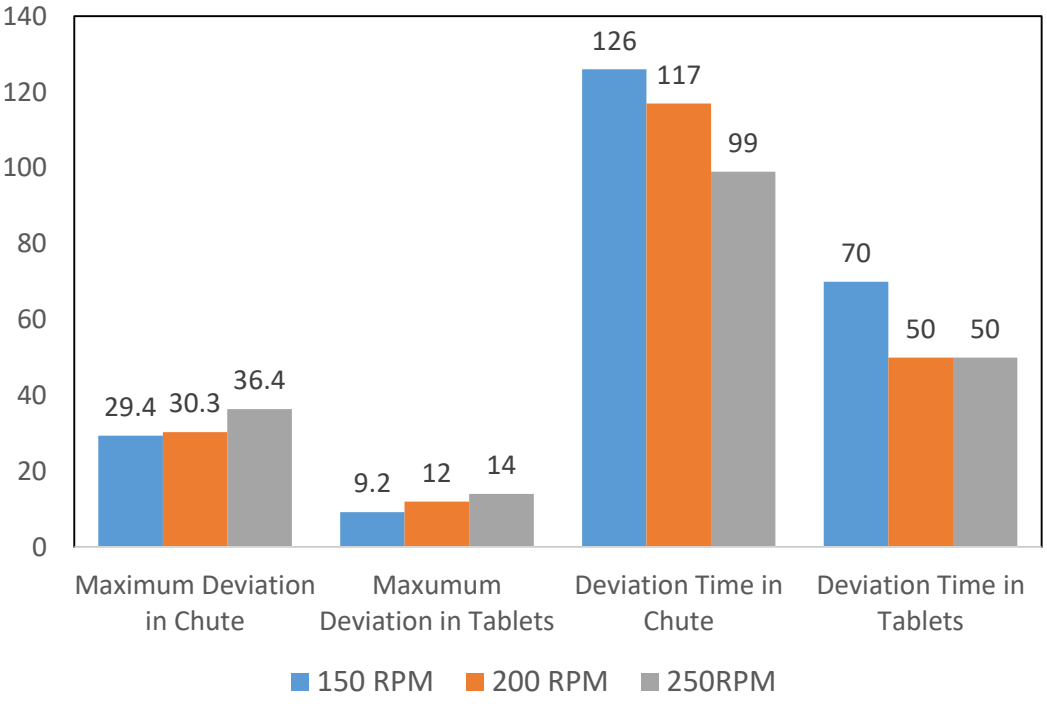

Figure 5. 15: Maximum Deviation and Deviation Time in API Concentration Results in Chute and Tablets According to 20% deviation in feed rate for 2 minutes with different blender speeds.

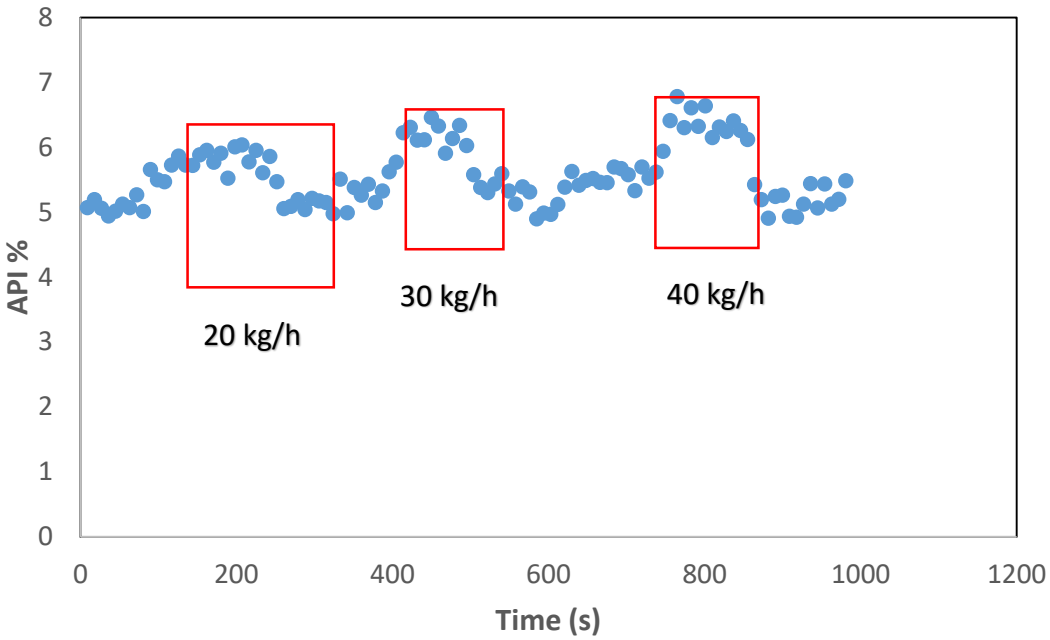

Figure 5. 16: API concentration in the chute according to 20% deviation in feed rate for 2 minutes with different total throughputs.

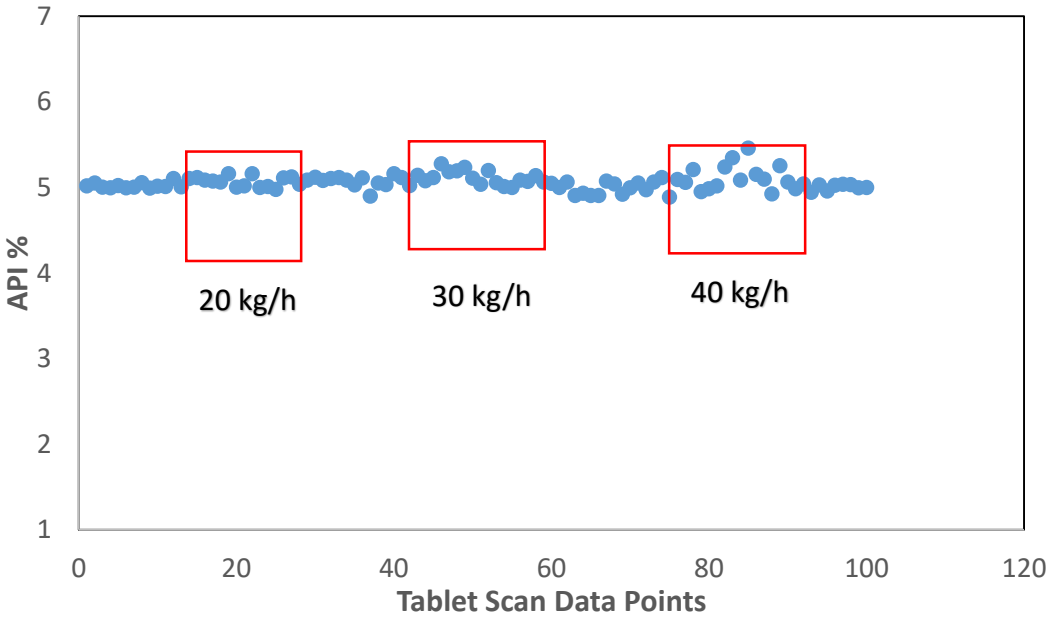

Figure 5. 17: API concentration in tablets according to 20% deviation in feed rate for 2 minutes with different total throughputs.

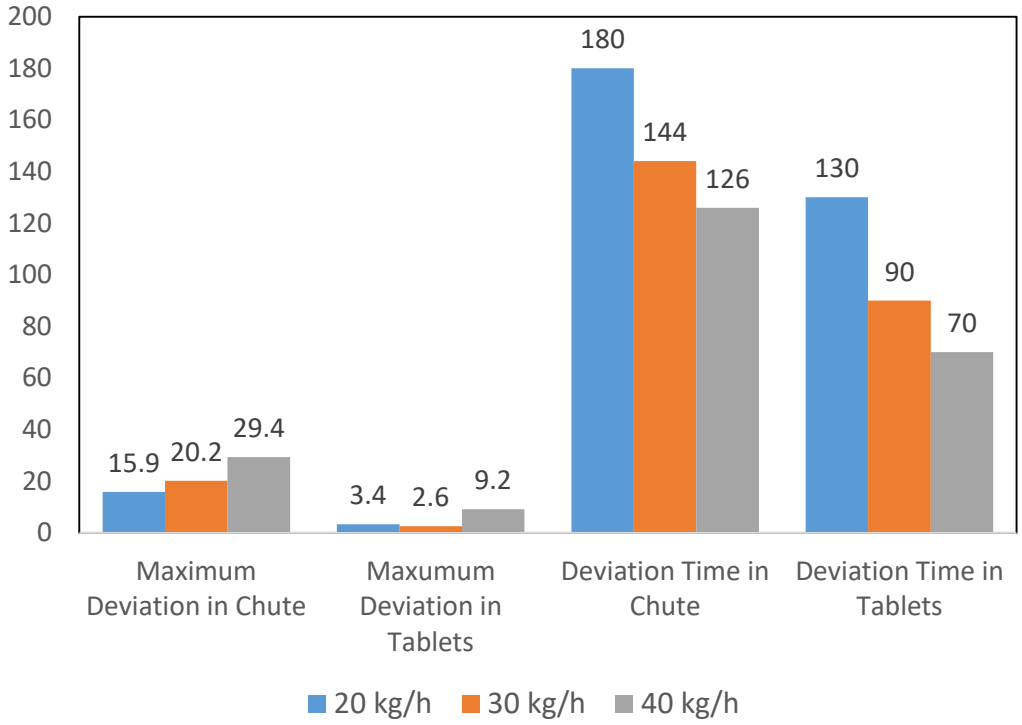

Figure 5. 18: Maximum Deviation and Deviation Time in API Concentration Results in Chute and Tablets According to 20% deviation in feed rate for 2 minutes with different total throughputs.

Chapter 6. Conclusions and Recommendations

The work presented in this dissertation focused on predicting the performance of loss-in-weight feeders, including identifying a feeder's design space, correlating feed rate deviations caused by hopper refill with material properties using a multivariate analysis method, and how downstream unit operations react and help filter disturbances in feed rates. To reach the goal of this dissertation, a principal component analysis (PCA) method was utilized to build a material database of raw material properties and identify and distinguish the similarity between raw materials, and a partial least squares regression (PLSR) method was introduced to build up a prediction model between process performance and material flow properties. This chapter summarizes the work presented in this dissertation and outlines recommendations for future work.

6.1. Conclusions

The first specific aim focused on a QbD approach that identifies a maximum powder and screw throughput (feed factor) from conditioned bulk density. Chapter 2 of the dissertation details the material properties characterization, loss-in-weight feeder characterization, and how different material properties impact on process performance. Chapter 3 couples the correlation to feed factor with the identified design space for a K-Tron feeder, defining the operational throughput for a given material and screw combination, as predicted by the material's conditioned bulk density. By feeding 14 materials at different six levels of drive commands, the effective range of operation was located by calculating the relative standard deviation, the relative deviation from the mean, and identifying a region of minimum v in both deviations. Values of 20% and 90% were determined as the lower and upper limit of

drive command for suitable operational range for fine concave, coarse concave, and coarse auger screws with KT20 C-gear box, while the suitable range for fine auger screws was between 40% and 90% drive command. These observations were confirmed for materials ranging from freely flowing to cohesive. In addition to the operational range for the feeder, a linear correlation between conditioned bulk density and feed factor was identified. With the two identified phenomena, the K-Tron KT-20 C-gearbox feeding capacity, for each of the different types of screws, can be predicted by the conditioned bulk density of the material.

In specific aim 2 (Chapter 4), two methodologies, PCA and PLSR, were utilized to develop predictive correlations between material flow properties and the perturbations to mass flow experienced in loss-in-weight feeders due to a hopper refill. For PCA-SS, the approach was based on weighted Euclidean distances, calculated after performing the principal component analysis on the entire data set. The bulk properties of the material that had the shortest distance, in the PCA scores plot, to the "material of interest", calcined zeolite, was compared to and then confirmed to have similar flow behavior to each other. The PLSR approach further quantified the correlation between material properties and the deviations caused by hopper refill. This study showed that the feed rate deviations caused by the refill of the feeder hopper were highly correlated and predictable with bulk material properties. The predicted mass flow deviation results were, in general, in good agreement with the experimental results. The work presented here has shown an efficient approach to correlate material properties with process performance using multivariate analysis. Moreover, this study also identifies the significant material flow properties for each type of deviation during hopper refill. Therefore, potential mass flow deviations due to feeder refills can be

predicted, based on the materials bulk properties performed at a state that lessens the impact on the mass flow.

In specific aim 3 (Chapter 5), a continuous pharmaceutical manufacturing process of direct compaction was utilized to evaluate the dampening effect on feed rate deviation from feeder level from downstream unit operations. This work has determined that blender speed and total throughput are the major factors that have significant impact on the delay time on real time monitoring point at the chute after the continuous blender when disturbances or changes in concentration occur on feeders' feed rates. The development of inline PLS calibration models and offline PLS calibration models on two different formulations with two different API dosages have been developed and utilized to monitor the inline and offline API concentration.

Designed step changes on API feeder were used to mimic the unexpected disturbance on feeder. How disturbances from hopper refill process on both API feeder and major excipient feeder transferred to downstream and final products were also investigated in this work. In addition, effects from different blender speeds and total throughput has also been added to fully evaluate the filtering ability from operational conditions. The experimental results for both formulations have proved that both a continuous blender and a feed frame in the tablet press have good abilities to filter short-lived variations in feed rates and thus improve the content uniformity of final products, where the feed frame has played a more significant role on filtering the variation after the monitoring point at the chute located after the continuous blender. From the blender speed and total throughput study, results demonstrated that higher blender speed and higher total throughput contributed to a lower residence time, which reduce the back-mixing time of the blends and resulted in a higher

maximum deviation, as compared to lower blender speed and lower total throughput, which allowed the powder blends stay in the downstream unit operations with a longer time. However, higher blender speed and total throughput has showed an ability to shorten the total disturbance time compared to lower blender speed and total throughput, which is because the mass of the powder blends were transferred faster in the downstream unit operations. The dampening ability from downstream unit operations really depend on the design of each unit operation and the whole manufacturing process.

6.2. Recommendations for future work

Based on the work presented in this dissertation, there are several potential areas of future study. Two specific directions are detailed here.

6.2.1. Using residence time distribution to understand powder behavior in loss-in-weight feeders

Residence time distribution models are essential to understand process dynamics and support process monitoring and control. In a continuous flow system, the residence time distribution is defined as the probability distribution of time that solid or liquid materials stay inside one or more unit operations [165-168]. A residence time distribution based control system for continuous pharmaceutical manufacturing has been developed in 2019[169]. Several studies pursuing an improved understanding of the residence time distribution in blending, extruding, dry granulation, capsule filling and fluidized bed operations have been published recently [170-180]. There is limited knowledge of the material dynamics inside loss-in-weight feeders with a vertical agitation system, which is a critical index in understand the material flow profile in loss-in-weight feeders.

Future work should focus on the residence time distribution in a loss-in-weight feeder, the K-Tron KT20, whose major components is shown in **Figure 6-1**. A KT20 loss-in-weight feeder has a flow aid system, which is a vertical-spinning agitator inside the feeder hopper, as marked in blue box. The agitator is also connected to a gear box, which rotates at a certain ratio of the screw speed, in this case, 12.5%. The vertical agitating applies a breaking force to the materials in the hopper in case there is any bridging between the particles and blockage from material flowing in the hopper. Moreover, due to the agitating, the agitator will also perform motion to the materials in the hopper from different levels, which will result in mixing of materials if there is more than one material in the hopper.

Given the presence of the conveying element inside the hopper, this work will start with studying the residence time distribution for a single component by introducing an impulse amount of tracer in the unit via the layering strategy. The next step will be to study multiple components, with similar properties, by layering one material on top of another. The location of the split between materials could be varied to determine if location within the hopper has an effect on the RTD. The work can not only identify RTD within the hopper, but also can identify a refill strategy that can be utilized to minimize back-mixing within the feeder.

The residence time distribution study inside the feeder hopper can be evaluated using a loss-in-weight feeder K-Tron KT20, a conveyer belt, a catch scale and near infrared spectral acquisition unit. **Figure 6-2** shows a schematic of the experimental setup used to perform the feeder experiments, where the NIR instrument used in this work is a Matrix F FT NIR from Bruker (Billerica, MA USA). The KT20 hopper has the same shape as the

KT35, and therefore, the knowledge obtained with the T20 can be utilized for the T35 as well.

For the single component RTD study, six impulse RTD experiments should be performed using three materials at two different flow rates. Using PCA, materials will be identified with significantly different properties and used for the experiments. Tracers should be identified based on similarity to the material of interest as well as chemical detectability.

The tracer should be added at location based on possible refill strategies for a feeder while it is in operation. For each of the three materials tested, the feed factor would be calibrated with base material. Then, the feeder would be set to the target mass flow rate and started. The speed of conveyer belts is adjusted to ensure the material does not accumulate on the belt. The feeder will then be stopped, and the pulse sample will be layered in the hopper at various levels based on possible refill strategies. The test will then be started, and spectra collected. The powder will then flow from the conveyer belt to the catch scale to determine if the mass flow rate matches to the set point of the feeder

The RTD study can be performed to investigate the flow and mixing dynamic for multiple components inside the hopper of loss-in-weight feeder KT20. The experimental setup is similar to that for a single component; however, different materials should be used in this study with a change of location at different levels inside the feeder hopper. The proposed experimental designs of powder layers inside the feeder hopper are show in **Figure 6-3**.

A preliminary study was performed with two granular materials. Material A was Metformin granules (98.5%, w/w of metformin and 1.5% w/w of hypromellose (HPMC)), while Material B is a blend of Metformin granules with Avicel 200, resulting in a blend

with 70% Metformin. The Metformin granules were provided by Janssen Ortho LLC-Gurabo, while material B was prepared by blending the two components in a V-blender. Experiments a) and b) were carried out when materials A and B each contribute to half of the weight percentage of the whole hopper. Preliminary results appear in **Figure 6-4**. The results show a transition from one concentration to the second concentration (either the step up to 98.5% or the step down to 70%). The predicted spectra have a wide deviation, showing that there is some blending during this phase of feeding. Then, approximately when half the hopper is filled, the concentration trend reverts back to the first material in the hopper. This second change in concentration is likely due to a dead-zone in the hopper, where the material at the bottom of the hopper gets segregated and does not reach the screws.

For the multiple component RTD study, the NIR models for each combination of material will first be developed based on the proposed materials and experimental setup. Similar to the tracer approach, a feed rate will first be selected based on the material properties and feeder's design space work. Experiments for residence time distribution for multiple components are remaining to be finished. Six proposed material layering methods will be studied

For experiment a) and b), material A and B will both fill half of the hopper volume with reversed position, while for experiment c) and d), material A and B will each capture 70% and 30% of the hopper volume in order to study the mixing effect of the agitating system to the material's traceability in the hopper. Experiment e) and f) will be performed with three layers of materials containing the same material on the top and bottom but different material in the middle layer to investigate the dead zone in the KT20 loss-in-weight feeder.

Near-infrared spectra will be used to analyze the concentration of the materials coming out of the feeder over time to obtain the residence time of each component inside the feeder.

The developed RTD model from this feeder study can facilitate material traceability in the hopper of a loss-in-weight feeder along with the mixing effect from the vertical agitating system inside a loss-in-weight feeder. In addition, a RTD model for feeding multiple components could be developed based on this RTD study that will also distinguish if material properties play a significant role in the back-mixing and the dissipation of the apparent dead-zone in the hopper. This work can be applied to the industrial research and development of the pharmaceutical continuous manufacturing, specifically to the risk assessment of material adjustment in a post-approval amendment (PAAs) stage.

6.2.2. Predicting loss-in-weight feeder's performance based on a reduced set of measurements

The predictive model that correlated feeder's feed rate deviation caused by hopper refill with material flow properties was developed with 30 material flow properties. However, based on the prediction results of the identified major material flow properties that contribute to the model and previous knowledge of the similarity between material flow properties, the prediction model can be further improved with a reduced set of material properties measurement, which can save a significant amount of time for material characterization tests.

This work can start with the comparison between the material database built by PCA with different sets of measurements. The first step would be to reduce the material property measurements to a set with compressibility, permeability, shear cell test at 6 KPa and particle size distribution. After that, a further reduced set could perhaps remove the particle

size distribution. Hierarchical clustering analysis can be used to compare the clusters' composition and also materials' location in each cluster. In addition, feeder performance with different types of screws can be used to compare the prediction results by performing the PLSR analysis with different sets of measurements.

With this work, half of the time and materials can be saved from material characterization tests. Moreover, a deeper understanding between material properties and their correlation with feeding performance can be established.

6.3 Figures for Chapter 6

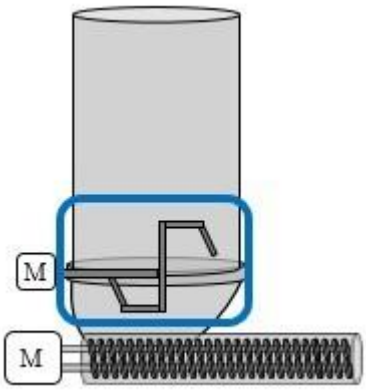

Figure 6. 1: K-Tron KT20 loss-in-weight feeder with its major components symbolized. The flow aid system, the bridge breaker, is marked in the blue box, where M represents the points where the motor is connected.

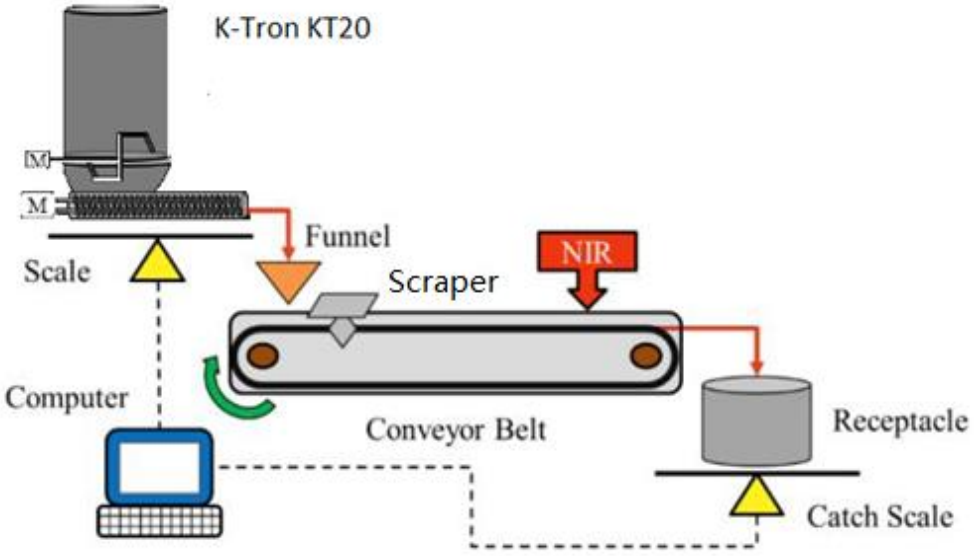

Figure 6. 2: Schematic of the experimental setup of the RTD study.

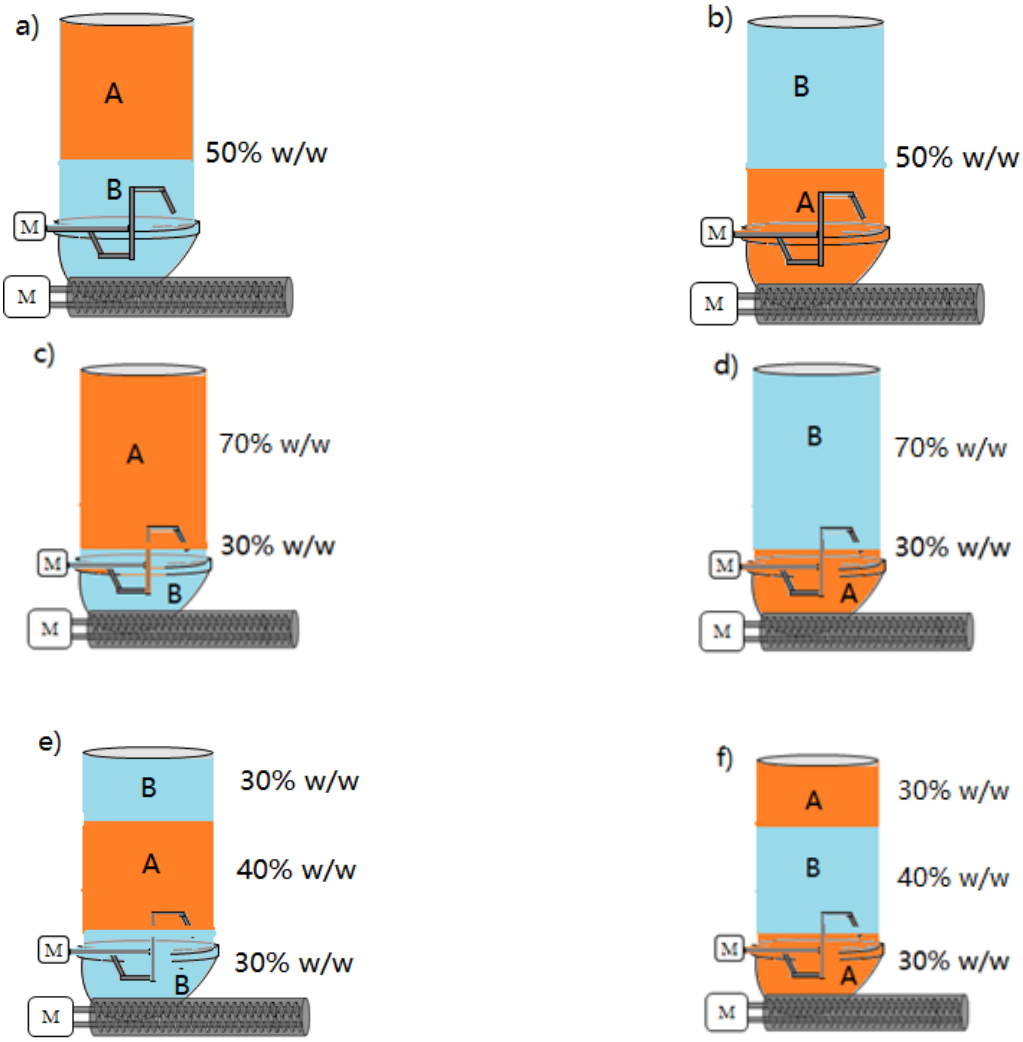

Figure 6. 3: Design of experiment of the RTD study with multiple components, A and B, inside the feeder hopper.

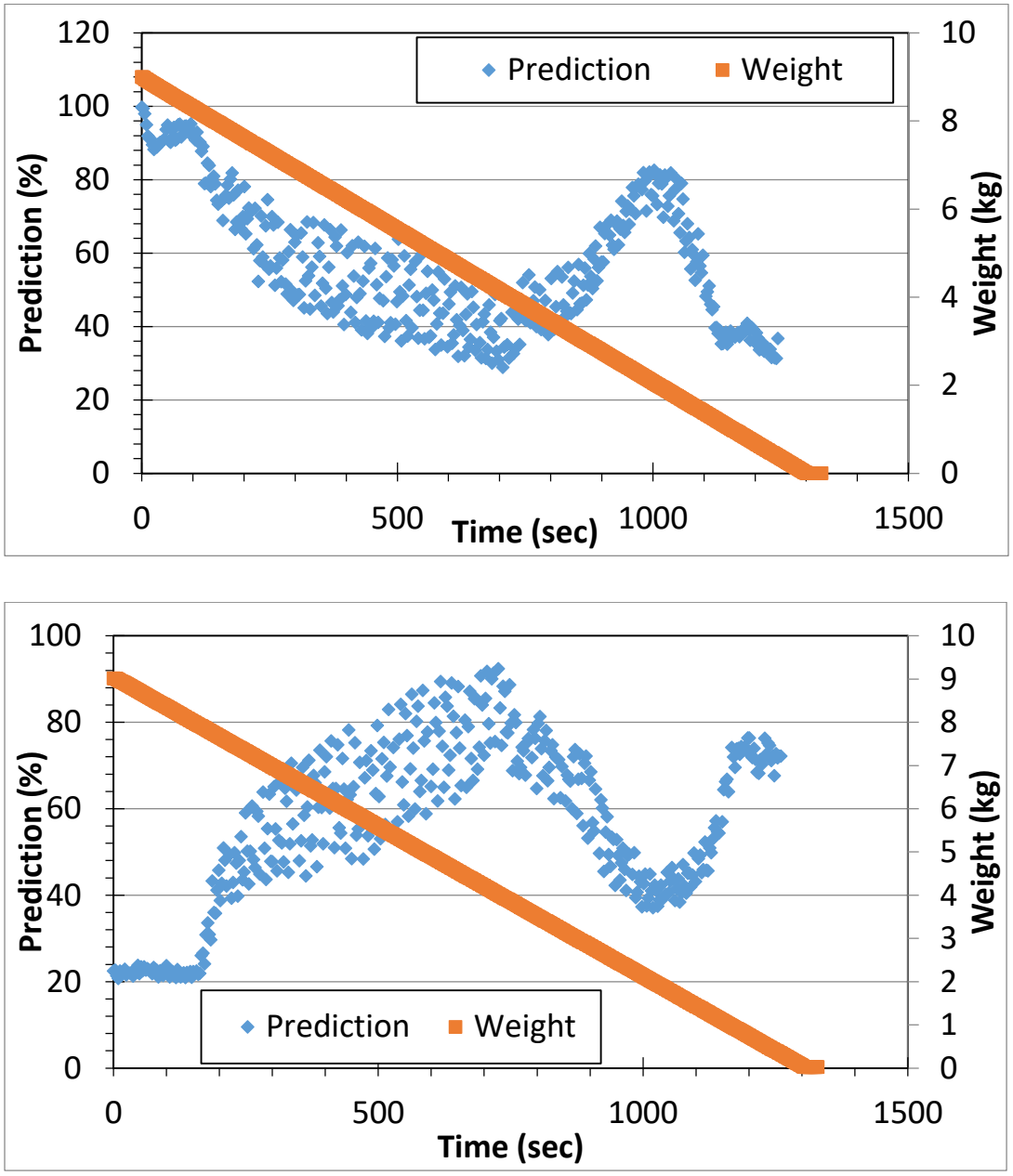

Figure 6. 4: Concentration step changes from 98.5% down to 70% (top) and 70% up to 98.5% metformin for experimental set ups of (a) and (b) from Figure 18.

References

[1] M. Ierapetritou, F. Muzzio, G. Reklaitis, Perspectives on the continuous manufacturing of powder‐based pharmaceutical processes, AIChE Journal 62 (2016) 1846-1862.
[2] S. Mascia, P.L. Heider, H. Zhang, R. Lakerveld, B. Benyahia, P.I. Barton, R.D. Braatz, C.L. Cooney, J.M. Evans, T.F. Jamison, End ‐ to ‐ end continuous manufacturing of pharmaceuticals: integrated synthesis, purification, and final dosage formation, Angewandte Chemie 125 (2013) 12585-12589.
[3] I. Khanna, Drug discovery in pharmaceutical industry: productivity challenges and trends, Drug discovery today 17 (2012) 1088-1102.
[4] H. Leuenberger, New trends in the production of pharmaceutical granules: batch versus continuous processing, European journal of pharmaceutics and biopharmaceutics 52 (2001) 289-296.
[5] J. Markarian, Modernizing Pharma Manufacturing, (2018).
[6] S.L. Lee, T.F. O'Connor, X. Yang, C.N. Cruz, S. Chatterjee, R.D. Madurawe, C.M. Moore, X.Y. Lawrence, J. Woodcock, Modernizing pharmaceutical manufacturing: from batch to continuous production, Journal of Pharmaceutical Innovation 10 (2015) 191-199.
[7] J.G. Osorio, F.J. Muzzio, Effects of processing parameters and blade patterns on continuous pharmaceutical powder mixing, Chemical Engineering and Processing-Process Intensification 109 (2016) 59-67.
[8] R. Hernandez, Continuous manufacturing: a changing processing paradigm, (2015).
[9] S. Lee, Current FDA perspective for continuous manufacturing, 2nd International Symposium on Continuous Manufacturing of Pharmaceuticals, Cambridge, Vereinigte Staaten von Amerika, 2016.
[10] E.M. Hetrick, Z. Shi, L.E. Barnes, A.W. Garrett, R.G. Rupard, T.T. Kramer, T.M. Cooper, D.P. Myers, B.C. Castle, Development of near infrared spectroscopy-based process monitoring methodology for pharmaceutical continuous manufacturing using an offline calibration approach, Analytical chemistry 89 (2017) 9175-9183.
[11] A.U. Vanarase, M. Järvinen, J. Paaso, F.J. Muzzio, Development of a methodology to estimate error in the on-line measurements of blend uniformity in a continuous powder mixing process, Powder technology 241 (2013) 263-271.
[12] F.a.D.A. U.S. Department of Health and Human Services, Center for Drug Evaluation and Research (CDER), Quality Considerations for Continuous Manufacturing Guidance for Industry, (2019).
[13] T. O'Connor, S. Lee, Emerging Technology for Modernizing Pharmaceutical Production: Continuous Manufacturing, Developing Solid Oral Dosage Forms (Second Edition), Elsevier2017, pp. 1031-1046.
[14] T. Garcia, G. Cook, R. Nosal, PQLI key topics-criticality, design space, and control strategy, Journal of Pharmaceutical Innovation 3 (2008) 60-68.
[15] R.A. Lionberger, S.L. Lee, L. Lee, A. Raw, X.Y. Lawrence, Quality by design: concepts for ANDAs, The AAPS journal 10 (2008) 268-276.

[16] R. Nosal, T. Schultz, PQLI definition of criticality, Journal of Pharmaceutical Innovation 3 (2008) 69-78.
[17] S. Challa, R. Potumarthi, Chemometrics-based process analytical technology (PAT) tools: applications and adaptation in pharmaceutical and biopharmaceutical industries, Applied biochemistry and biotechnology 169 (2013) 66-76.
[18] C. Moore, Continuous Manufacturing - FDA Perspective on Submissions and Implementation," presented at the PQRI Workshop on Sample Sizes for Decision Making in New Manufacturing Paradigms, (2011).
[19] P.L. Heider, S.C. Born, S. Basak, B. Benyahia, R. Lakerveld, H. Zhang, R. Hogan, L. Buchbinder, A. Wolfe, S. Mascia, Development of a multi-step synthesis and workup sequence for an integrated, continuous manufacturing process of a pharmaceutical, Organic Process Research & Development 18 (2014) 402-409.
[20] W.E. Engisch, F.J. Muzzio, Feedrate deviations caused by hopper refill of loss-in-weight feeders, Powder Technology 283 (2015) 389-400.
[21] W.E. Engisch, F.J. Muzzio, Method for characterization of loss-in-weight feeder equipment, Powder technology 228 (2012) 395-403.
[22] D.H.W.a.J.M. Loe, Apparatus and method for improving the accuracy of a loss-in-weight feeding system, (1985).
[23] Y. Wang, T. Li, F.J. Muzzio, B.J. Glasser, Predicting feeder performance based on material flow properties, Powder Technology 308 (2017) 135-148.
[24] M. Hopkins, Loss in weight feeder systems, Measurement and Control 39 (2006) 237-240.
[25] W.E. Engisch Jr, Loss-in-weight feeding in continuous powder manufacturing, Rutgers The State University of New Jersey-New Brunswick2014.
[26] C.A. Blackshields, A.M. Crean, Continuous powder feeding for pharmaceutical solid dosage form manufacture: a short review, Pharmaceutical development and technology 23 (2018) 554-560.
[27] M.S. Escotet-Espinoza, S. Moghtadernejad, S. Oka, Z. Wang, Y. Wang, A. Roman-Ospino, E. Schäfer, P. Cappuyns, I. Van Assche, M. Futran, Effect of material properties on the residence time distribution (RTD) characterization of powder blending unit operations. Part II of II: Application of models, Powder Technology 344 (2019) 525-544.
[28] M.S. Escotet-Espinoza, S. Moghtadernejad, S. Oka, Y. Wang, A. Roman-Ospino, E. Schäfer, P. Cappuyns, I. Van Assche, M. Futran, M. Ierapetritou, Effect of tracer material properties on the residence time distribution (RTD) of continuous powder blending operations. Part I of II: Experimental evaluation, Powder Technology 342 (2019) 744-763.
[29] W. Engisch, F. Muzzio, Using residence time distributions (RTDs) to address the traceability of raw materials in continuous pharmaceutical manufacturing, Journal of pharmaceutical innovation 11 (2016) 64-81.
[30] M.J. Rhodes, Principles of powder technology, (1990).
[31] J.F. Jenck, F. Agterberg, M.J. Droescher, Products and processes for a sustainable chemical industry: a review of achievements and prospects, Green Chemistry 6 (2004) 544-556.

[32] J. Bridgwater, The dynamics of granular materials–towards grasping the fundamentals, Granular Matter 4 (2003) 175-181.
[33] M. Poux, P. Fayolle, J. Bertrand, D. Bridoux, J. Bousquet, Powder mixing: some practical rules applied to agitated systems, Powder Technology 68 (1991) 213-234.
[34] S. Radl, E. Kalvoda, B.J. Glasser, J.G. Khinast, Mixing characteristics of wet granular matter in a bladed mixer, Powder Technology 200 (2010) 171-189.
[35] B. Remy, B.J. Glasser, J.G. Khinast, The effect of mixer properties and fill level on granular flow in a bladed mixer, AIChE journal 56 (2010) 336-353.
[36] D. Mateo-Ortiz, F.J. Muzzio, R. Méndez, Particle size segregation promoted by powder flow in confined space: The die filling process case, Powder technology 262 (2014) 215-222.
[37] S. Oka, A. Sahay, W. Meng, F. Muzzio, Diminished segregation in continuous powder mixing, Powder Technology 309 (2017) 79-88.
[38] K. To, P.-Y. Lai, H. Pak, Jamming of granular flow in a two-dimensional hopper, Physical review letters 86 (2001) 71.
[39] J. Tang, R. Behringer, How granular materials jam in a hopper, Chaos: An Interdisciplinary Journal of Nonlinear Science 21 (2011) 041107.
[40] T. Baxter, J. Prescott, Process development, optimization, and scale-up: powder handling and segregation concerns, Developing solid oral dosage forms, Elsevier2009, pp. 637-665.
[41] T.A. Bell, Challenges in the scale-up of particulate processes—an industrial perspective, Powder Technology 150 (2005) 60-71.
[42] A.C.-Y. Wong, Use of angle of repose and bulk densities for powder characterization and the prediction of minimum fluidization and minimum bubbling velocities, Chemical engineering science 57 (2002) 2635-2640.
[43] A.S. El-Hagrasy, J.K. Drennen III, A process analytical technology approach to near-infrared process control of pharmaceutical powder blending. Part III: Quantitative near-infrared calibration for prediction of blend homogeneity and characterization of powder mixing kinetics, Journal of pharmaceutical sciences 95 (2006) 422-434.
[44] S. Koynov, Using statistical methods to optimize powder flow measurements and to predict powder processing performance, Rutgers University-Graduate School-New Brunswick, 2015.
[45] V.R. Nalluri, M. Kuentz, Flowability characterisation of drug–excipient blends using a novel powder avalanching method, European Journal of Pharmaceutics and Biopharmaceutics 74 (2010) 388-396.
[46] V. Jaggi, M.C. Leaper, A. Ingham, Measuring the flow properties of small powder samples using an avalanche tester, Drying Technology 34 (2016) 723-728.
[47] S. Nakamura, N. Otsuka, Y. Yoshino, T. Sakamoto, H. Yuasa, Predicting the occurrence of sticking during tablet production by shear testing of a pharmaceutical powder, Chemical and Pharmaceutical Bulletin 64 (2016) 512-516.
[48] S. Savage, M. Sayed, Stresses developed by dry cohesionless granular materials sheared in an annular shear cell, Journal of Fluid Mechanics 142 (1984) 391-430.

[49] M. Ghadiri, Z. Ning, S. Kenter, E. Puik, Attrition of granular solids in a shear cell, Chemical Engineering Science 55 (2000) 5445-5456.
[50] M. Krantz, H. Zhang, J. Zhu, Characterization of powder flow: Static and dynamic testing, Powder Technology 194 (2009) 239-245.
[51] D. Geldart, E. Abdullah, A. Hassanpour, L. Nwoke, I. Wouters, Characterization of powder flowability using measurement of angle of repose, China Particuology 4 (2006) 104-107.
[52] Z. Chik, L.E. Vallejo, Characterization of the angle of repose of binary granular materials, Canadian Geotechnical Journal 42 (2005) 683-692.
[53] K. Rietema, Powders, what are they, Powder Technology 37 (1984).
[54] D. Schulze, Powders and bulk solids: Behavior, characterization, storage and flow. 2008, Springer, 2003.
[55] E.L. Paul, V.A. Atiemo-Obeng, S.M. Kresta, Handbook of industrial mixing: science and practice, John Wiley & Sons2004.
[56] R. Mendez, F.J. Muzzio, C. Velazquez, Powder hydrophobicity and flow properties: effect of feed frame design and operating parameters, AIChE journal 58 (2012) 697-706.
[57] M. Llusa, M. Levin, R.D. Snee, F.J. Muzzio, Measuring the hydrophobicity of lubricated blends of pharmaceutical excipients, Powder technology 198 (2010) 101-107.
[58] J. Peart, Powder electrostatics: theory, techniques and applications, KONA Powder and Particle Journal 19 (2001) 34-45.
[59] S. Matsusaka, H. Masuda, Electrostatics of particles, Advanced Powder Technology 14 (2003) 143-166.
[60] H.L. Bennett, Device for measuring the friability of particulate solid materials, Google Patents, 1972.
[61] Q. Li, V. Rudolph, B. Weigl, A. Earl, Interparticle van der Waals force in powder flowability and compactibility, International journal of pharmaceutics 280 (2004) 77-93.
[62] K.C. Pingali, S.V. Hammond, F.J. Muzzio, T. Shinbrot, Use of a static eliminator to improve powder flow, International journal of pharmaceutics 369 (2009) 2-4.
[63] K.C. Pingali, K. Saranteas, R. Foroughi, F.J. Muzzio, Practical methods for improving flow properties of active pharmaceutical ingredients, Drug development and industrial pharmacy 35 (2009) 1460-1469.
[64] J.L. Orband, D. Geldart, The use of an antistatic agent to improve powder flowability, Particle & particle systems characterization 12 (1995) 204-206.
[65] M.P. Mullarney, L.E. Beach, R.N. Davé, B.A. Langdon, M. Polizzi, D.O. Blackwood, Applying dry powder coatings to pharmaceutical powders using a comil for improving powder flow and bulk density, Powder technology 212 (2011) 397-402.
[66] L. Liu, I. Marziano, A. Bentham, J. Litster, E. White, T. Howes, Effect of particle properties on the flowability of ibuprofen powders, International journal of pharmaceutics 362 (2008) 109-117.
[67] A.U. Vanarase, J.G. Osorio, F.J. Muzzio, Effects of powder flow properties and shear environment on the performance of continuous mixing of pharmaceutical powders, Powder technology 246 (2013) 63-72.

[68] J. Bouffard, A. Cabana, J. Chaouki, F. Bertrand, Experimental investigation of the effect of particle cohesion on the flow dynamics in a spheronizer, AIChE Journal 59 (2013) 1491-1501.
[69] R. Mendez, F. Muzzio, C. Velazquez, Study of the effects of feed frames on powder blend properties during the filling of tablet press dies, Powder Technology 200 (2010) 105-116.
[70] A.M.N. Faqih, A. Mehrotra, S.V. Hammond, F.J. Muzzio, Effect of moisture and magnesium stearate concentration on flow properties of cohesive granular materials, International journal of pharmaceutics 336 (2007) 338-345.
[71] A.N. Faqih, A.W. Alexander, F.J. Muzzio, M.S. Tomassone, A method for predicting hopper flow characteristics of pharmaceutical powders, Chemical Engineering Science 62 (2007) 1536-1542.
[72] Y. Wang, T. O'Connor, T. Li, M. Ashraf, C.N. Cruz, Development and applications of a material library for pharmaceutical continuous manufacturing of solid dosage forms, International journal of pharmaceutics 569 (2019) 118551.
[73] A.T. Sutton, C.S. Kriewall, M.C. Leu, J.W. Newkirk, Powder characterisation techniques and effects of powder characteristics on part properties in powder-bed fusion processes, Virtual and physical prototyping 12 (2017) 3-29.
[74] J.K. Prescott, R.A. Barnum, On powder flowability, Pharmaceutical technology 24 (2000) 60-85.
[75] A. Vasilenko, B.J. Glasser, F.J. Muzzio, Shear and flow behavior of pharmaceutical blends—Method comparison study, Powder Technology 208 (2011) 628-636.
[76] R.S. Tump, Loss-in-weight feeder system, Google Patents, 1989.
[77] N. Bostijn, J. Dhondt, A. Ryckaert, E. Szabó, W. Dhondt, B. Van Snick, V. Vanhoorne, C. Vervaet, T. De Beer, A multivariate approach to predict the volumetric and gravimetric feeding behavior of a low feed rate feeder based on raw material properties, International journal of pharmaceutics 557 (2019) 342-353.
[78] S.N. Bhattachar, D.B. Hedden, A.M. Olsofsky, X. Qu, W.-Y. Hsieh, K.G. Canter, Evaluation of the vibratory feeder method for assessment of powder flow properties, International journal of pharmaceutics 269 (2004) 385-392.
[79] B. Van Snick, A. Kumar, M. Verstraeten, K. Pandelaere, J. Dhondt, G. Di Pretoro, T. De Beer, C. Vervaet, V. Vanhoorne, Impact of material properties and process variables on the residence time distribution in twin screw feeding equipment, International journal of pharmaceutics 556 (2019) 200-216.
[80] J. Hanson, Control of a system of loss-in-weight feeders for drug product continuous manufacturing, Powder Technology 331 (2018) 236-243.
[81] X. Fu, D. Huck, L. Makein, B. Armstrong, U. Willen, T. Freeman, Effect of particle shape and size on flow properties of lactose powders, Particuology 10 (2012) 203-208.
[82] R. Bharadwaj, W.R. Ketterhagen, B.C. Hancock, Discrete element simulation study of a Freeman powder rheometer, Chemical Engineering Science 65 (2010) 5747-5756.
[83] E. Cordts, H. Steckel, Capabilities and limitations of using powder rheology and permeability to predict dry powder inhaler performance, European journal of pharmaceutics and biopharmaceutics 82 (2012) 417-423.

[84] R. Freeman, Measuring the flow properties of consolidated, conditioned and aerated powders—a comparative study using a powder rheometer and a rotational shear cell, Powder Technology 174 (2007) 25-33.
[85] R. Freeman, X. Fu, Characterisation of powder bulk, dynamic flow and shear properties in relation to die filling, Powder Metallurgy 51 (2008) 196-201.
[86] J.W. Carson, H. Wilms, Development of an international standard for shear testing, Powder technology 167 (2006) 1-9.
[87] J. Carr, D. Walker, An annular shear cell for granular materials, Powder Technology 1 (1968) 369-373.
[88] A.S. Çağli, B.N. Deveci, C.H. Okutan, D. Sirkeci, E. Teoman, Flow property measurement using Jenike shear cell for 7 different bulk solids, Proceedings of European Congress of Chemical Engineering (ECCE-6), Copenhagen, 2007, pp. 16-20.
[89] Q.T. Zhou, L. Qu, I. Larson, P.J. Stewart, D.A. Morton, Effect of mechanical dry particle coating on the improvement of powder flowability for lactose monohydrate: A model cohesive pharmaceutical powder, Powder technology 207 (2011) 414-421.
[90] T. Horio, M. Yasuda, S. Matsusaka, Effect of particle shape on powder flowability of microcrystalline cellulose as determined using the vibration shear tube method, International journal of pharmaceutics 473 (2014) 572-578.
[91] J.R. Pillai, M. Bradley, R. Berry, Comparison between the angles of wall friction measured on an on-line wall friction tester and the Jenike wall friction tester, Powder technology 174 (2007) 64-70.
[92] Y. Wang, S. Koynov, B.J. Glasser, F.J. Muzzio, A method to analyze shear cell data of powders measured under different initial consolidation stresses, Powder Technology 294 (2016) 105-112.
[93] L. Pordesimo, C. Onwulata, Food powder delivery through a feeder system: effect of physico-chemical properties, 2007 ASAE Annual Meeting, American Society of Agricultural and Biological Engineers, 2007, pp. 1.
[94] M.S. Escotet-Espinoza, J.V. Scicolone, S. Moghtadernejad, E. Sanchez, P. Cappuyns, I. Van Assche, G. Di Pretoro, M. Ierapetritou, F.J. Muzzio, Improving Feedability of Highly Adhesive Active Pharmaceutical Ingredients by Silication, JOURNAL OF PHARMACEUTICAL INNOVATION (2020).
[95] F. Tahir, J. Palmer, J. Khoo, J. Holman, I.K. Yadav, G. Reynolds, E. Meehan, A. Mitchell, G. Bajwa, Development of feed factor prediction models for loss-in-weight powder feeders, Powder Technology (2019).
[96] H. Toyota, M. Iwanaga, Powder feeding apparatus, electrostatic powder coating apparatus and powder flow-rate measuring apparatus, Google Patents, 1996.
[97] E.A. Wahl, Powder-feeding apparatus, Google Patents, 1957.
[98] T. Yokoi, H. Kuragairi, S. Nakamura, T. Kato, K. Umemura, H. Yamanaka, Apparatus for feeding recording medium, having means for easy handling of jamming trouble, Google Patents, 1990.
[99] D.F. Morrison, Multivariate analysis, overview, Encyclopedia of Biostatistics 5 (2005).
[100] A.P. Dempster, An overview of multivariate data analysis, Journal of Multivariate Analysis 1 (1971) 316-346.

[101] W. Revelle, How to: Use the psych package for factor analysis and data reduction, Evanston, IL: Northwestern University, Department of Psychology (2016).
[102] S. Tobias, J.E. Carlson, Brief report: Bartlett's test of sphericity and chance findings in factor analysis, Multivariate Behavioral Research 4 (1969) 375-377.
[103] J.P. Azevedo, FACTORTEST: Stata module to perform tests for appropriateness of factor analysis, (2006).
[104] J.R. Reddon, D.N. Jackson, A note on testing the sphericity hypothesis with Bartlett's test, (1984).
[105] D.H. Wilson, K.W. Bullivant, Loss-in-weight gravimetric feeder, Google Patents, 1986.
[106] R. Weinekötter, L. Reh, Continuous mixing of fine particles, Particle & particle systems characterization 12 (1995) 46-53.
[107] W. Engisch, M. Ierapetritou, F. Muzzio, Hopper refill of loss-in-weight feeding equipment, Proceedings of the 2010 AIChE Annual Meeting, Salt Lake City, UT, USA, 2010.
[108] K. Plumb, Continuous processing in the pharmaceutical industry: changing the mind set, Chemical Engineering Research and Design 83 (2005) 730-738.
[109] S.D. Schaber, D.I. Gerogiorgis, R. Ramachandran, J.M. Evans, P.I. Barton, B.L. Trout, Economic analysis of integrated continuous and batch pharmaceutical manufacturing: a case study, Industrial & Engineering Chemistry Research 50 (2011) 10083-10092.
[110] D.M. Roberge, B. Zimmermann, F. Rainone, M. Gottsponer, M. Eyholzer, N. Kockmann, Microreactor technology and continuous processes in the fine chemical and pharmaceutical industry: is the revolution underway?, Organic Process Research & Development 12 (2008) 905-910.
[111] P.T. Editors, FDA Approves Tablet Production on Janssen Continuous Manufacturing Line, PharmTech.com (2016).
[112] Food, D. Administration, Guidance for industry: PAT—A framework for innovative pharmaceutical development, manufacturing, and quality assurance, DHHS, Rockville, MD (2004).
[113] X.Y. Lawrence, Pharmaceutical quality by design: product and process development, understanding, and control, Pharmaceutical research 25 (2008) 781-791.
[114] A.S. Rathore, Roadmap for implementation of quality by design (QbD) for biotechnology products, Trends in biotechnology 27 (2009) 546-553.
[115] L. Urquhart, Regulatory watch: FDA new drug approvals in Q1 2018, Nature Publishing Group, 2018.
[116] N. Walker, EMA Approves Continuous Manufacture of Prezista, Pharma's almanac PAO-M07-17-NI-002 (2017).
[117] 2016 ISPE Continous Manufacturing Conference Summary, (2017).
[118] N.R. Johnson, System for precisely controlling discharge rates of loss-in-weight feeder systems, Google Patents, 1992.
[119] P. Aalto, J.-P. Björklund, Loss-in-weight feeder control, Google Patents, 2002.
[120] V. Kehlenbeck, K. Sommer, Possibilities to improve the short-term dosing constancy of volumetric feeders, Powder technology 138 (2003) 51-56.

[121] G.I. Tardos, Q. Lu, Precision dosing of powders by vibratory and screw feeders: an experimental study, Advanced Powder Technology 7 (1996) 51-58.
[122] Z. Huang, J.V. Scicolone, L. Gurumuthy, R.N. Davé, Flow and bulk density enhancements of pharmaceutical powders using a conical screen mill: A continuous dry coating device, Chemical Engineering Science 125 (2015) 209-224.
[123] Z. Huang, J.V. Scicolone, X. Han, R.N. Davé, Improved blend and tablet properties of fine pharmaceutical powders via dry particle coating, International Journal of Pharmaceutics 478 (2015) 447-455.
[124] J.V. Scicolone, M. Metzger, S. Koynov, K. Anderson, P. Takhistov, B.J. Glasser, F.J. Muzzio, Effect of liquid addition on the bulk and flow properties of fine and coarse glass beads, AIChE Journal 62 (2016) 648-658.
[125] R. Freeman, Measuring the flow properties of consolidated, conditioned and aerated powders—a comparative study using a powder rheometer and a rotational shear cell, Powder Technology 174 (2007) 25-33.
[126] I. Peschl, NEW ROTATIONAL SHEAR-TESTING TECHNIQUE, J. Powder Bulk Solids Technol. 1 (1977) 55.
[127] J. Schwedes, D. Schulze, Measurement of flow properties of bulk solids, Powder Technology 61 (1990) 59-68.
[128] R. Schmitt, H. Feise, Influence of tester geometry, speed and procedure on the results from a ring shear tester, Particle & Particle Systems Characterization: Measurement and Description of Particle Properties and Behavior in Powders and Other Disperse Systems 21 (2004) 403-410.
[129] F.a.D.A. U.S. Department of Health and Human Services, Center for Drug Evaluation and Research (CDER), Quality Considerations for Continuous Manufacturing Guidance for Industry, February 2019.
[130] T. Fahlenbock, Design Considerations for Refilling and Venting Continuous Loss-in-Weight Feeders, Brabender Technologie Inc (2008).
[131] D.H. Wilson, J.M. Loe, Apparatus and method for improving the accuracy of a loss-in-weight feeding system, Google Patents, 1985.
[132] I. Ghebre-Sellassie, C. Martin, Pharmaceutical Extrusion Technology 2003, Marcel Dekker, New York.
[133] W.a. Loe, Apparatus and method for improving the accuracy of a loss-in-weight feeding system, US Patent 4,524,886 (1982).
[134] W.a. Bullivant, Loss-in-weight gravimetric feeder, US Patent 4,579,252 (1983).
[135] T. Li, J.V. Scicolone, E. Sanchez, F.J. Muzzio, Identifying a Loss-in-Weight Feeder Design Space Based on Performance and Material Properties, Journal of Pharmaceutical Innovation (2019) 1-14.
[136] A. Rogers, M. Ierapetritou, Challenges and opportunities in modeling pharmaceutical manufacturing processes, Computers & Chemical Engineering 81 (2015) 32-39.
[137] I. Jolliffe, Principal component analysis, Springer2011.
[138] T. Davies, Multivariate Analysis in Practice, a Training Package, SAGE Publications Sage UK: London, England, 1996.

[139] P. Geladi, B.R. Kowalski, Partial least-squares regression: a tutorial, Analytica chimica acta 185 (1986) 1-17.
[140] T. Li, J.V. Scicolone, E. Sanchez, F.J. Muzzio, Identifying a Loss-in-Weight Feeder Design Space Based on Performance and Material Properties, Journal of Pharmaceutical Innovation 1-14.
[141] W.-K. Hsiao, T.R. Hörmann, P. Toson, A. Paudel, P. Ghiotti, F. Staufer, F. Bauer, S. Lakio, O. Behrend, R. Maurer, Feeding of particle-based materials in continuous solid dosage manufacturing: a material science perspective, Drug Discovery Today (2020).
[142] J.N. Staniforth, Relationship between particle packing and the physical stability of powder mixes, Journal of pharmacy and pharmacology 37 (1985) 692-697.
[143] E.D. Liss, S.L. Conway, J.A. Zega, B.J. Glasser, Segregation of powders during gravity flow through vertical pipes, Pharmaceutical technology 28 (2004) 78-97.
[144] M. Teżyk, E. Jakubowska, K. Milczewska, B. Milanowski, A. Voelkel, J. Lulek, The influence of direct compression powder blend transfer method from the container to the tablet press on product critical quality attributes: a case study, Drug development and industrial pharmacy 43 (2017) 911-916.
[145] H. Berthiaux, K. Marikh, C. Gatumel, Continuous mixing of powder mixtures with pharmaceutical process constraints, Chemical Engineering and Processing: Process Intensification 47 (2008) 2315-2322.
[146] A.U. Vanarase, F.J. Muzzio, Effect of operating conditions and design parameters in a continuous powder mixer, Powder Technology 208 (2011) 26-36.
[147] P. Pawar, Y. Wang, G. Keyvan, G. Callegari, A. Cuitino, F. Muzzio, Enabling real time release testing by NIR prediction of dissolution of tablets made by continuous direct compression (CDC), International journal of pharmaceutics 512 (2016) 96-107.
[148] N.O. Sierra-Vega, A. Román-Ospino, J. Scicolone, F.J. Muzzio, R.J. Romañach, R. Méndez, Assessment of blend uniformity in a continuous tablet manufacturing process, International journal of pharmaceutics 560 (2019) 322-333.
[149] P.R. Wahl, G. Fruhmann, S. Sacher, G. Straka, S. Sowinski, J.G. Khinast, PAT for tableting: inline monitoring of API and excipients via NIR spectroscopy, European journal of pharmaceutics and biopharmaceutics 87 (2014) 271-278.
[150] Y.M. Colón, M.A. Florian, D. Acevedo, R. Méndez, R.J. Romañach, Near infrared method development for a continuous manufacturing blending process, Journal of Pharmaceutical Innovation 9 (2014) 291-301.
[151] J.M. Vargas, S. Nielsen, V. Cárdenas, A. Gonzalez, E.Y. Aymat, E. Almodovar, G. Classe, Y. Colón, E. Sanchez, R.J. Romañach, Process analytical technology in continuous manufacturing of a commercial pharmaceutical product, International journal of pharmaceutics 538 (2018) 167-178.
[152] M. Alcalà, J. León, J. Ropero, M. Blanco, R.J. Romañach, Analysis of low content drug tablets by transmission near infrared spectroscopy: selection of calibration ranges according to multivariate detection and quantitation limits of PLS models, Journal of pharmaceutical sciences 97 (2008) 5318-5327.

[153] M. Blanco, M. Alcalá, Content uniformity and tablet hardness testing of intact pharmaceutical tablets by near infrared spectroscopy: a contribution to process analytical technologies, Analytica chimica acta 557 (2006) 353-359.
[154] D. Mainali, J. Li, P. Yehl, N. Chetwyn, Development of a comprehensive near infrared spectroscopy calibration model for rapid measurements of moisture content in multiple pharmaceutical products, Journal of pharmaceutical and biomedical analysis 95 (2014) 169-175.
[155] E. Hernandez, P. Pawar, G. Keyvan, Y. Wang, N. Velez, G. Callegari, A. Cuitino, B. Michniak-Kohn, F.J. Muzzio, R.J. Romañach, Prediction of dissolution profiles by non-destructive near infrared spectroscopy in tablets subjected to different levels of strain, Journal of pharmaceutical and biomedical analysis 117 (2016) 568-576.
[156] A.U. Vanarase, M. Alcalà, J.I.J. Rozo, F.J. Muzzio, R.J. Romañach, Real-time monitoring of drug concentration in a continuous powder mixing process using NIR spectroscopy, Chemical Engineering Science 65 (2010) 5728-5733.
[157] J.M. Vargas, A.D. Roman-Ospino, E. Sanchez, R.J. Romañach, Evaluation of analytical and sampling errors in the prediction of the active pharmaceutical ingredient concentration in blends from a continuous manufacturing process, Journal of Pharmaceutical Innovation 12 (2017) 155-167.
[158] F. De Leersnyder, E. Peeters, H. Djalabi, V. Vanhoorne, B. Van Snick, K. Hong, S. Hammond, A.Y. Liu, E. Ziemons, C. Vervaet, Development and validation of an in-line NIR spectroscopic method for continuous blend potency determination in the feed frame of a tablet press, Journal of pharmaceutical and biomedical analysis 151 (2018) 274-283.
[159] D. Mateo-Ortiz, Y. Colon, R.J. Romañach, R. Méndez, Analysis of powder phenomena inside a Fette 3090 feed frame using in-line NIR spectroscopy, Journal of pharmaceutical and biomedical analysis 100 (2014) 40-49.
[160] Z. Shi, K.C. McGhehey, I.M. Leavesley, L.F. Manley, On-line monitoring of blend uniformity in continuous drug product manufacturing process—the impact of powder flow rate and the choice of spectrometer: dispersive vs. FT, Journal of pharmaceutical and biomedical analysis 118 (2016) 259-266.
[161] A. Dubey, A.U. Vanarase, F.J. Muzzio, Impact of process parameters on critical performance attributes of a continuous blender—A DEM-based study, AIChE journal 58 (2012) 3676-3684.
[162] H. Dalvi, A. Langlet, M.-J. Colbert, A. Cournoyer, J.-M. Guay, N. Abatzoglou, R. Gosselin, In-line monitoring of Ibuprofen during and after tablet compression using near-infrared spectroscopy, Talanta 195 (2019) 87-96.
[163] W.R. Ketterhagen, Simulation of powder flow in a lab-scale tablet press feed frame: effects of design and operating parameters on measures of tablet quality, Powder Technology 275 (2015) 361-374.
[164] H.W. Ward, D.O. Blackwood, M. Polizzi, H. Clarke, Monitoring blend potency in a tablet press feed frame using near infrared spectroscopy, Journal of pharmaceutical and biomedical analysis 80 (2013) 18-23.

[165] Y. Gao, A. Vanarase, F. Muzzio, M. Ierapetritou, Characterizing continuous powder mixing using residence time distribution, Chemical Engineering Science 66 (2011) 417-425.
[166] Y. Gao, B.J. Glasser, M.G. Ierapetritou, A. Cuitino, F.J. Muzzio, J.W. Beeckman, N.A. Fassbender, W.G. Borghard, Measurement of residence time distribution in a rotary calciner, AIChE Journal 59 (2013) 4068-4076.
[167] Y. Gao, F. Muzzio, M. Ierapetritou, Characterization of feeder effects on continuous solid mixing using fourier series analysis, AIChE Journal 57 (2011) 1144-1153.
[168] Y. Gao, M. Ierapetritou, F. Muzzio, Periodic section modeling of convective continuous powder mixing processes, AIChE Journal 58 (2012) 69-78.
[169] A. Bhaskar, R. Singh, Residence time distribution (RTD)-based control system for continuous pharmaceutical manufacturing process, Journal of Pharmaceutical Innovation 14 (2019) 316-331.
[170] A.D. Román-Ospino, R. Singh, M. Ierapetritou, R. Ramachandran, R. Méndez, C. Ortega-Zuñiga, F.J. Muzzio, R.J. Romañach, Near infrared spectroscopic calibration models for real time monitoring of powder density, International journal of pharmaceutics 512 (2016) 61-74.
[171] G. Hu, J. Chen, B. Jian, H. Wan, L. Liu, Modeling and simulation of transportation system of screw conveyors by the discrete element method, Mechanic Automation and Control Engineering (MACE), 2010 International Conference on, IEEE, 2010, pp. 927-930.
[172] D. Mateo-Ortiz, R. Méndez, Relationship between residence time distribution and forces applied by paddles on powder attrition during the die filling process, Powder Technology 278 (2015) 111-117.
[173] A. Kumar, J. Vercruysse, V. Vanhoorne, M. Toiviainen, P.-E. Panouillot, M. Juuti, C. Vervaet, J.P. Remon, K.V. Gernaey, T. De Beer, Conceptual framework for model-based analysis of residence time distribution in twin-screw granulation, European Journal of Pharmaceutical Sciences 71 (2015) 25-34.
[174] E. Reitz, H. Podhaisky, D. Ely, M. Thommes, Residence time modeling of hot melt extrusion processes, European Journal of Pharmaceutics and Biopharmaceutics 85 (2013) 1200-1205.
[175] J. Wesholowski, H. Podhaisky, M. Thommes, Comparison of residence time models for pharmaceutical twin-screw-extrusion processes, Powder Technology 341 (2019) 85-93.
[176] J. Kruisz, E. Faulhammer, J. Rehrl, O. Scheibelhofer, A. Witschnigg, J.G. Khinast, Residence time distribution of a continuously-operated capsule filling machine: Development of a measurement technique and comparison of three volume-reducing inserts, International journal of pharmaceutics 550 (2018) 180-189.
[177] H. Mangal, P. Kleinebudde, Experimental determination of residence time distribution in continuous dry granulation, International journal of pharmaceutics 524 (2017) 91-100.
[178] J. Wesholowski, A. Berghaus, M. Thommes, Investigations Concerning the Residence Time Distribution of Twin-Screw-Extrusion Processes as Indicator for Inherent Mixing, Pharmaceutics 10 (2018) 207.

[179] J. Wesholowski, A. Berghaus, M. Thommes, Inline determination of residence time distribution in hot-melt-extrusion, Pharmaceutics 10 (2018) 49.
[180] G. Tian, S.L. Lee, X. Yang, M.S. Hong, Z. Gu, S. Li, R. Fisher, T.F. O'Connor, A dimensionless analysis of residence time distributions for continuous powder mixing, Powder technology 315 (2017) 332-338.